ABSTRACT

Title of dissertation: COMPRESSIVE QUANTIZATION FOR SCALABLE CLOUD RADIO ACCESS NETWORKS

Hang Ma, Doctor of Philosophy, 2016

Dissertation directed by: Professor K. J. Ray Liu
Department of Electrical and Computer Engineering

With the proliferation of new mobile devices and applications, the demand for ubiquitous wireless services has increased dramatically in recent years. The explosive growth in the wireless traffic requires the wireless networks to be scalable so that they can be efficiently extended to meet the wireless communication demands.

In a wireless network, the interference power typically grows with the number of devices without necessary coordination among them. On the other hand, large scale coordination is always difficult due to the low-bandwidth and high-latency interfaces between access points (APs) in traditional wireless networks. To address this challenge, cloud radio access network (C-RAN) has been proposed, where a pool of base band units (BBUs) are connected to the distributed remote radio heads (RRHs) via high bandwidth and low latency links (i.e., the front-haul) and are responsible for all the baseband processing. But the insufficient front-haul link capacity may limit the scale of C-RAN and prevent it from fully utilizing the benefits made possible by the centralized baseband processing. As a result, the front-haul

link capacity becomes a bottleneck in the scalability of C-RAN. In this dissertation, we explore the scalable C-RAN in the effort of tackling this challenge.

In the first aspect of this dissertation, we investigate the scalability issues in the existing wireless networks and propose a novel time-reversal (TR) based scalable wireless network in which the interference power is naturally mitigated by the focusing effects of TR communications without coordination among APs or terminal devices (TDs). Due to this nice feature, it is shown that the system can be easily extended to serve more TDs.

Motivated by the nice properties of TR communications in providing scalable wireless networking solutions, in the second aspect of this dissertation, we apply the TR based communications to the C-RAN and discover the TR tunneling effects which alleviate the traffic load in the front-haul links caused by the increment of TDs. We further design waveforming schemes to optimize the downlink and uplink transmissions in the TR based C-RAN, which are shown to improve the downlink and uplink transmission accuracies. Consequently, the traffic load in the front-haul links is further alleviated by the reducing re-transmissions caused by transmission errors. Moreover, inspired by the TR-based C-RAN, we propose the compressive quantization scheme which applies to the uplink of multi-antenna C-RAN so that more antennas can be utilized with the limited front-haul capacity, which provide rich spatial diversity such that the massive TDs can be served more efficiently.

COMPRESSIVE QUANTIZATION FOR SCALABLE CLOUD RADIO ACCESS NETWORKS

by

Hang Ma

Dissertation submitted to the Faculty of the Graduate School of the
University of Maryland, College Park in partial fulfillment
of the requirements for the degree of
Doctor of Philosophy
2016

Advisory Committee:
Professor K. J. Ray Liu, Chair/Advisor
Professor Min Wu
Professor Gang Qu
Dr. Zoltan Safar
Dr. Beibei Wang
Professor Lawrence C. Washington

Dedication

To my wife and my parents.

Acknowledgments

I would like to express my deepest gratitude to my advisor, Professor. K. J. Ray Liu for his guidance and support throughout my graduate study, without which this dissertation would not have been possible. I appreciate his constant involvement in my research work where he always thinks bigger than I do and leads me to see a larger picture. He has been putting confidence in me for me to try bold ideas, and providing timely suggestions as well as corrections along the way. I have also been influenced by his enthusiasm, devotion and desire to excel, which he has shown me time after time by examples. He has played a significant role in my professional and personal development during my graduate study.

I would like to thank other members on my dissertation committee. Special thanks are due to Dr. Beibei Wang and Dr. Zoltan Safar for their collaboration and enormous help and support that led to fruitful research results. I am also grateful to Professor Min Wu, Professor Gang Qu and Professor Lawrence C. Washington for their precious time and effort serving on my committee.

I would like to thank all the members (and some alumni whom I interacted with) in our Signals and Information Group for collaboration, friendship, encouragement, and help. Special thanks go to Dr. Yan Chen, Dr. Feng Han and Dr. Yu-Han Yang, Dr. Chunxiao Jiang, Mr. Yi Han and Mr. Zhung-Han Wu for our inspiring research discussions, through which I learned a lot.

I would like to thank ECE staff Ms. Melanie Prange and Mr. Bill Churma for their very kind help and advice regarding the departmental graduate study affairs.

I also want to thank the financial support of China Scholarship Council (CSC).

Finally, I would like to thank my wife and my parents, for their unconditional love, understanding, and endless support. I dedicate this dissertation to them.

Table of Contents

List of Tables

List of Figures

Chapter 1: Introduction

1.1 Motivation

With the proliferation of new mobile devices and applications, the demand for ubiquitous wireless services has increased dramatically in recent years. It has been projected that by the year 2020, the volume of the wireless traffic will rise to about 1000 times that of the year 2010 [1]. Moreover, unlike the wired devices which are usually hard to move, most wireless devices are small and portable. As a result, the number of wireless devices in one particular area can change dramatically from time to time, and sometimes is hard to predict. These changes in the wireless communications require the wireless networks to be scalable so that they can be efficiently extended to meet the wireless communication demand in a particular area.

To accommodate the massive wireless devices, one promising solution is to add more access points (APs) so that the wireless traffic is offloaded to the wired back-haul. However, with more and more APs in a certain region, some of them will work in the same band and create strong interference to each other without necessary coordination. The interference power increases with the scale of the network, which will dominate the useful signal and the information can not be efficiently delivered

in the network. In other words, interference is a main obstacle in the scalability of wireless networks.

Some coordinations are necessary to mitigate the interference so that multiple APs can work together efficiently to accommodate the massive devices. However, in the traditional wireless networks, the communication overhead caused by the coordination will grow with the number of APs, which makes large scale coordination very difficult and even impossible over the high-latency and low-bandwidth interface between APs. In summary, the difficulty in large scale coordination is another factor limiting the scalability of wireless networks.

To address the aforementioned challenges, cloud radio access network (C-RAN) has been recently proposed as a viable solution [2–5]. It is a novel type of radio access network (RAN) architecture, where a pool of base band units (BBUs) are connected to the distributed remote radio heads (RRHs) via high bandwidth and low latency links. The BBUs are responsible for all the baseband processing through high performance computing. In this centralized structure, many coordinated communication schemes become possible or more efficient, and can be utilized to mitigate the interference. For example, the coordinated multiple-point process (CoMP) in the LTE-A standard [6] can be implemented in the C-RAN to improve network capacity and energy efficiency [7]. In addition, by moving the baseband processing to the cloud, the RRHs need only support the basic transmission/reception functionalities, which further reduces their energy consumption and deployment cost.

Nevertheless, the limited front-haul link capacity [8] between the BBU and the RRH may prevent the C-RAN from scaling up and fully utilizing the benefits

made possible by concentrating the processing intelligence. In most of the current C-RAN structures, the data transmitted in the front-haul is the concatenation of the baseband signals of all the terminal devices (TDs) [9, 10]. As a result, the front-haul link capacity becomes a bottleneck when there are massive TDs in the network. To tackle this challenge, several solutions have been proposed. One of them is to use compression where the baseband signal is compressed before the front-haul transmission and then de-compressed after the front-haul transmission [11–13]. Although signal compression can alleviate the traffic in the front-haul under certain cases, it introduces extra computation complexity at the RRH side, which makes this approach less cost effective. An alternative solution is the sparse beamforming [9,10,14] where each TD is associated with a cluster of APs. However, the data rate in the front-haul link is related to the cluster size, and a larger cluster requires a higher front-haul link capacity [9]. As a result, the limited front-haul link capacity makes it impossible to fully take advantage of the available spatial diversity, which is one of the main benefits of the C-RAN structure.

In seeking of solutions to this front-haul link capacity challenge, we discovered that the time-reversal (TR) based communications [15] can be utilized to provide a scalable wireless networking scheme, where all the TDs are naturally separated by the location-specific signatures in both downlink [16] and uplink [17]. Due to this fact, we apply the TR based communications to the C-RAN and discover a "tunneling effects" to alleviate the traffic load in the front-haul link of C-RAN.

In fact, it is the natural location-specific signatures inherent in the TR communications that make the "tunneling effects" happen. Inspired by this fact, we

propose the compressive quantization scheme for the multi-antenna C-RAN where similar signatures are also available.

1.2 Dissertation Outline and Contributions

From the discussion above, we can clearly see the necessity and difficulty in exploring the scalable C-RAN. This dissertation contributes to this topic by utilizing the unique temporal and spatial focusing effects of TR based communications and generalizing the results to apply to the MIMO as well as OFDM based C-RANs. The rest of the dissertation is organized as follows.

1.2.1 Scalable Time-Reversal Self-Organizing Wireless Network (Chapter 2)

In this chapter, we first show the scalability issues in the existing wireless networks. Then, we propose a novel time-reversal (TR) based scalable wireless network for the broadband downlink transmission. Due to the unique spatial and temporal focusing effects of TR communications, the interference to the unintended receiver is automatically mitigated with no need for cooperation among APs or TDs in the transmission phase. We analyze the performance of the proposed system under both open and closed access models, using both simulated channels and channels measured in a real world environment. It is shown that under the open access model, the proposed system can be easily extended to support more TDs and/or higher data rate. Under the closed access model, it is shown that the system is less

prone to the failure caused by the interference from neighboring devices. It is also shown that the proposed system has less packet delay than the IEEE 802.11 (WiFi) based system.

1.2.2 Time-Reversal Tunneling Effect For Cloud Radio Access Network (Chapter 3)

In this chapter, we apply the time-reversal (TR) communication to both the downlink and uplink of cloud radio access network (C-RAN) to alleviate the traffic load in the front-haul links. Owing to the unique spatial and temporal focusing effects, the baseband signals from multiple users can be more efficiently combined and transmitted, which in essence creates "tunneling effects" in the front-haul links. As a result, the traffic load in the front-haul link keeps almost constant when more TDs need to be served. The tunneling effects are illustrated through numerical results based on channels measured in a real world environment. This feature significantly alleviates the limitation of the cloud radio access network in serving massive devices.

1.2.3 Waveforming for Time-Reversal Cloud Radio Access Network (Chapter 4)

In this chapter, we go one step further in optimizing the downlink and uplink transmissions of the time-reversal (TR) based cloud radio access network (C-RAN). In the downlink, we propose content based waveforming such that both the channel information and the content information are utilized to improve the accuracy of the

detection. In the uplink, we propose the waveforming scheme so that the BBUs can better detect the symbols transmitted by the TDs. By the proposed waveforming techniques, the accuracy of the transmissions is improved, which reduces the necessity of re-transmissions of baseband signal in the case of error. The traffic loads in the front-haul links of C-RAN are further reduced.

1.2.4 Compressive Quantization For Multi-Antenna Cloud Radio Access Network (Chapter 5)

In this chapter, we continue to look at the cloud radio access network (C-RAN). In the literature of C-RAN, the RRH always uses a single antenna since the traffic load in the front-haul link increases with the number of antennas, and multiple antennas can not be supported by the front-haul links with limited capacity. As a result, the total number of antennas that can be utilized are limited. In this chapter, we discover the underlying compressive quantization that enables the "tunneling effects" in the TR based C-RAN proposed in Chapter 3, and generalize it to the uplink of a multi-antenna C-RAN where each RRH uses multiple antennas. The compressive quantization scheme is tailored for the C-RAN architecture in that the complexity at the RRH side is low so that the low deployment cost feature of C-RAN is preserved. Weight vectors and parallel interference cancellation schemes are designed in the BBU side to detect the symbols from the compressive quantized baseband signal. Numerical results show the effectiveness of the compressive quantization scheme in tackling the front-haul capacity deficit challenge. We also apply

the proposed scheme to the OFDM base multi-antenna C-RAN and the numerical results show that the compressive quantization can facilitate the OFDM based C-RAN utilize larger bandwidth. With the proposed scheme, the C-RAN can utilize more antennas and/or larger bandwidth so that the massive TDs can be efficiently served.

Chapter 2: Scalable Time-Reversal Self-Organizing Wireless Network

As introduced in Chapter 1, although using more access points (APs) is a promising solution to accommodate massive devices, the extra APs do not help unconditionally. Some coordination is needed such that the multiplexing gain provided by extra antennas is effective and higher data rate can be achieved. However, the difficulty to enable the coordination may limit the scalability of the system as well as the potential applications.

In recent years, time-reversal (TR) communications have been widely investigated. In [15], it was shown that the TR communications have the features of spatial and temporal focusing such that the signal power can be naturally focused at the intended receiver while creating little leakage to the surroundings even with single transmitting and receiving antennas. Motivated by these features, a Time-Reversal division multiple access (TRDMA) scheme was proposed in [16] to deliver the downlink data to multiple terminal devices simultaneously. To make it a complete system, the uplink architecture for the TRDMA system was proposed in [17]. The TR technique was also shown to create little interference to other users due to the focusing effects [18]. All the works above used the natural signatures for multiple users, where the environment serves as the matched filter to perform perfect

deconvolution, resulting in the benefit of low computational complexity. In [19], algorithms were proposed to further improve the achievable data rate of the TRDMA downlink system by the optimal design of the user signatures. Due to the ability to naturally separate multiple devices in both uplink and downlink, TR technique was shown to be ideal paradigms for the internet of things [20].

The existing works showed that TR communications have the unique focusing effects such that the signal is focused at the intended location with little interference to other locations, even when the unintended receiver is close to the transmitter. Such a focusing effect is in essence a resonating phenomenon of the multi-path environment that is more location sensitive instead of distance-based. In other words, the "near-far" effect plays a much less important role in TR communications and the interference power is automatically mitigated and full spectrum reuse can be efficiently achieved, i.e., the TR-based schemes have excellent self-organizing feature [21]. Motivated by this observation, in this chapter, we propose a TR-based self-organing network.

The proposed system leverages the spatial focusing feature of TR communications to deliver data to massive devices. It is able to achieve full spectrum reuse even with single transmitting/receiving antennas and no cooperation between APs or terminal devices (TDs) is needed in the transmission phase. This self-organizing feature makes the system easy to set up and the scale of the system is not constrained by the difficulty of coordination. We investigate the system in two access models: the open access model where an AP is open to all the terminal devices (TDs), and the closed access model where an AP is only open to specific TDs. We

analyze the achievable data rate of the proposed system using the Poisson Point Process (PPP) location model to characterize the chaotic and nomadic deployment of the APs and TDs. We evaluate the performance of the proposed system using simulation based on existing channel model as well as real-world measured channels where single transmitting and receiving antennas are used. We show that in the open access case, the proposed system can be easily extended to serve higher user density and/or higher data rate by adding extra APs independently. On the other hand, in the closed access case, each TD suffers less from neighboring APs since each link does not require exclusive use of the channel, and the interference power is automatically mitigated.

The chapter is organized as follows. In section 2.1, we illustrate the scalability issues in the existing wireless networks. The TR based communications are briefly introduced in section 2.2. The system model is introduced in section 2.3. In section 2.4, we theoretically analyze the proposed system. The advantages of the proposed system in accommodating massive devices are shown through simulation and experimental results in section 2.5 and section 2.6, respectively. Finally, we draw conclusions in section 2.7.

2.1 Scalability Issues in Existing Wireless Network

In this section, we will use the IEEE 802.11 (WiFi) wireless network as an example to illustrate the scalability issues in the existing wireless networks via both experiment and modeling.

With 802.11 technology, we first consider the single AP case. We conduct an experiment in an office environment for the downlink case where there are 1 AP and 14 TDs indexed from 1 to 14, all of which are equipped with IEEE 802.11n air interface. We utilize TCP connections between the AP and TDs enabled by Iperf [22]. The floor plan and the locations of the AP and the TDs are shown in Fig. 2.1.

Table 2.1: all the testing cases in the experiment

case ID	active TDs' IDs
a	1,7,9
b	1,2,5,7,9,10
c	1,2,3,5,6,7,8,9,10
d	1,2,3,4,5,6,7,8,9,10,11
e	1,2,3,4,5,6,7,8,9,10,11,12,13,14

The 5 experiment settings are shown in Table 2.1. As shown in Fig. 2.2, the sum throughput keeps almost constant regardless of the number of active devices. In other words, when there are more TDs served by the AP, they have to share the limited throughput. This result coincides with that shown in Fig. 7(c) in [23] where the total throughput remains almost the same when the number of TDs ranges between 1 and 127. This observation is further illustrated in Fig. 2.3 where the average throughput of each user is inversely proportional to the number of users n, i.e., each user approximately shares $\frac{1}{n}$ of the total throughput. Therefore, when there are many users in the system, the throughput for each user will be very small,

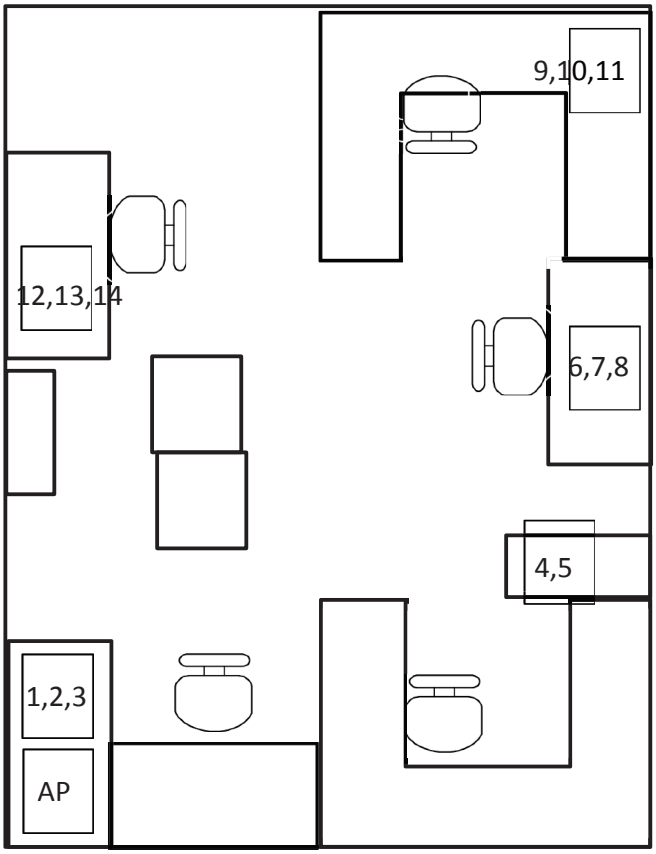

Figure 2.1: Floor Plan and Locations of The Testing Site

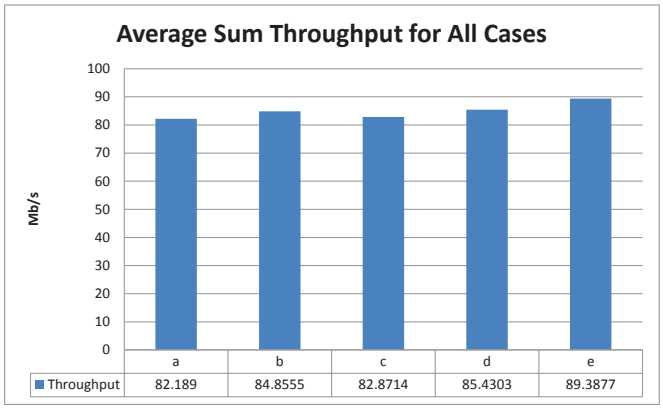

Figure 2.2: The Sum Throughput in Experiment

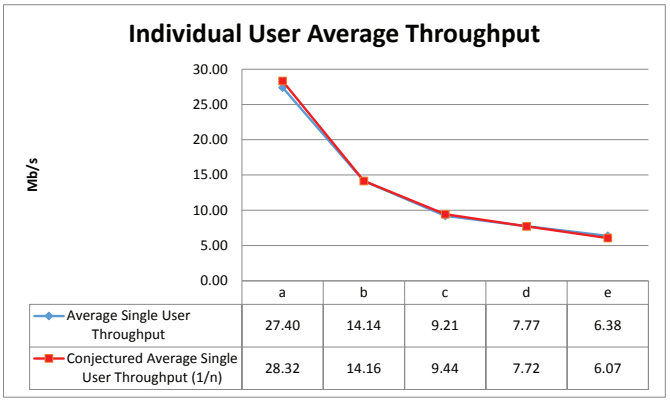

Figure 2.3: The Individual Throughput in Experiment

and decreases to close to zero very fast with the densification of the network.

One way to overcome the above issue is to add more APs. However, without elaborate planning, the effective achievable data rate of the 802.11 based system may not increase, in fact, it can even decrease due to the interference.

Similar to that in [24], we define the notion of effective achievable data rate as

$$U = G * T \tag{2.1}$$

where G is the link capacity and T is the average active time for each link in one second. In other words, it measures the maximum data rate that each link can possibly deliver in one second in the case that the wireless medium is shared by multiple links.

Consider the case that Z APs are randomly deployed in a certain area such that all of them are within the range of the others. In the 802.11 based multiple AP downlink system, they work with each other by the distributed coordination function (DCF). In the downlink case, as shown in [25], due to the DCF, each AP is either at the state of actively transmitting, back off, or blocked by other APs. In

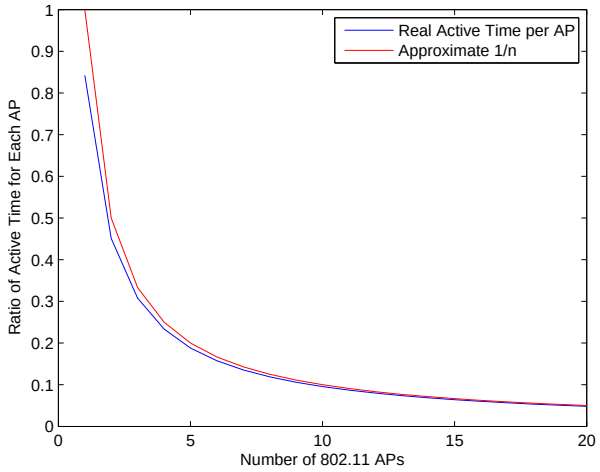

Figure 2.4: The Individual AP Active Time

other words, each AP needs to obtain the exclusive use of the wireless channel. As a result, at most one AP can be delivering downlink data to subscribed users at one particular time. The average active time of each AP can be calculated by the model in [25] by solving the fixed point equations. We show the calculated active time of APs in Fig. 2.4. As shown in the figure, as the number of APs increase, the average active time is close to $\frac{1}{Z}$, where Z is the number of APs. Therefore, if more APs are added into the system, the total active time of all the APs is almost constant, and thus the effective achievable data rate U does not increase. To make it worse, according to the experimental study in the real world traffic setting that consists of both downlink and uplink [23], without planning, the throughput actually decreases as the number of APs increases.

In this section, it is shown that scaling up the 802.11 based wireless network is not straightforward by simply adding more APs. Without proper coordination, the extra APs may even reduce the throughput of the network due to the increased in-

terference power and/or contention for the network accesss. While the coordination among 802.11 APs is difficult without sufficient interfaces, in the rest of this chapter, we propose a self-organizing TR based wireless network where the interference power is automatically mitigated without the need of coordination.

2.2 A Brief Introduction of TR Communication

In the indoor broadband wireless communication, the signal suffers from the multi-path effect caused by the reflections of the indoor environment. Instead of trying to avoid the multi-path effect, TR based communication utilizes all the multi-paths to act like a matched filter to achieve spatial and temporal focusing effects. In Fig. 2.5, we show the typical process of a TR communication. For example, transceiver B tries to transmit some information to transceiver A. Prior to the transmission, the transceiver A has to send out a delta-like pilot pulse which propagates to transceiver B through a multi-path channel, and transceiver B keeps a record of the received waveform h. Then, the transceiver B time reverses the received waveform, and use the normalized time-reversed conjugate signals as a basic waveform g, i.e.,

$$g[k] = \frac{h^*[L-1-k]}{\sqrt{\sum_{l=0}^{L-1} \|h[l]\|^2}} \tag{2.2}$$

where $L = \frac{\delta_T}{T_S}$ is the channel length, T_S is the sampling period of the transceivers such that $\frac{1}{T_S}$ equals to the bandwidth B used and δ_T is the delay spread of the channel [26]. Due to the channel reciprocity, when transceiver B transmits g, the multi-path channel forms a natural matched filter by performing $h * g$, and hence a

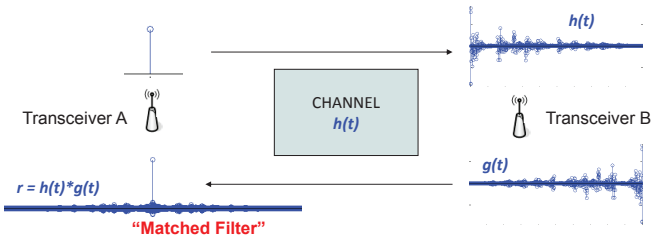

Figure 2.5: The schematic diagram of the time reversal system

peak is expected at the receiver.

2.3 System Model

We propose a system to efficiently deliver data to massive terminal devices (TDs). The proposed system consists of multiple APs that work under the TRDMA scheme. As shown in Fig. 2.6, multiple APs are distributed in an area to accommodate the various TDs. Since the coordinated transmissions among APs are always difficult, we assume that each TD is served by only one AP while the signals received from other APs are regarded as interference. Due to the focusing effects, the signal power is naturally focused at the intended TD while creating little interference to other TDs. As a result, all the APs and TDs can work in the same band that is the entire available spectrum without any partitioning, and no coordination among APs is needed to alleviate the interference.

In the following, we first introduce the channel model used for the proposed system. Then the TRDMA transmission scheme as well as the location and access models used are described.

Figure 2.6: Illustration of proposed system.

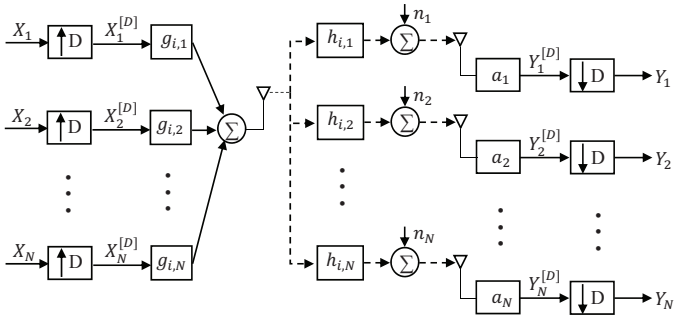

Figure 2.7: The Diagram of TRDMA downlink system.

2.3.1 Channel Model and Path Loss Models

We consider the multi-path Rayleigh fading channel at the indoor scenario. The channel impulse response (CIR) of the communication link between the i-th AP and the corresponding j-th TD is modeled as

$$h_{i,j}[k] = \sum_{l=0}^{L-1} h_{i,j}^{(l)} \cdot \delta[k-l] \tag{2.3}$$

where $h_{i,j}[k]$ is the k-th tap of the CIR with length L. For each link, we model $h_{i,j}[k]$'s as independent circular symmetric complex Gaussian random variables with zero mean and variance

$$E[|h_{i,j}[k]|^2] = e^{-\frac{kT_S}{\delta_T}}, \quad 0 \leq k \leq L-1 \tag{2.4}$$

where T_S is the sampling period of the TD such that $\frac{1}{T_S}$ equals the bandwidth B that the TD was using and δ_T is the delay spread of the channel [26].

Since the APs and TDs are deployed in a vast area, the path loss model is needed to characterize loss of the energy due to the distance. The power received by TD j transmitted by AP k can be modeled as [27]

$$P_r = \gamma_{k,j} \cdot \min(1, d_{k,j}^{-\alpha}) \cdot P_s \tag{2.5}$$

where P_r is the signal power received by TD j, P_s is the signal power transmitted by AP k, $d_{k,j}$ is the distance between the AP and the TD, and $\gamma_{k,j} \leq 1$ is the penetration loss factor representing the penetration loss of the signal through some obstructions such as the wall. For the ease of analysis, $\gamma_{k,j} = 1$ will be used.

2.3.2 The Multiple AP Downlink System

In the proposed system, each AP delivers the data to the subscribed TDs using the TRDMA scheme [16]. There are two phases in the TRDMA scheme: the channel probing phase where the AP gets the channel information $h_{i,j}$ of the TDs and the transmission phase where the AP transmits the data to all the subscribed users simultaneously. In the transmission phase, as shown in Fig. 2.7, the intended symbol sequence $X_j[k]$ for the j-th TD transmitted from the i-th AP is first up-sampled by the back-off factor D in order to alleviate the inter-symbol interference and then convolved with the signature of the channel $h_{i,j}$, which is

$$g_{i,j}[k] = h^*_{i,j}[L-1-k] / \sqrt{\sum_{l=0}^{L-1} |h_{i,j}[l]|^2}, \qquad k = 0, 1, \cdots, L-1. \tag{2.6}$$

At the TD side, the received signal is a combination of the intended signal and the interference from other users contaminated by noise. The TD will then first amplify the received signal with a_j and then down-sample it with the factor D, obtaining the received sequence Y_j. The noise is assumed to be zero-mean additive white gaussian noise with variance $E[|n_j[k]|^2] = \sigma^2, \ \forall j, k$.

2.3.3 Access and Location Model

Generally, in the multiple-AP system, there can be various access control models [28–30]. Two common ones are the open access model and the closed access model. In the open access model, each AP allows an arbitrary TD to subscribe to it. It characterizes the case that the APs are owned and operated by the same entity

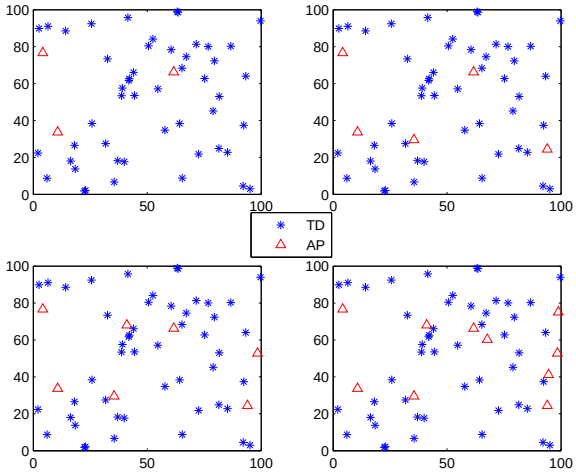

Figure 2.8: The Open Access Case. Each AP is open to all the TDs and more APs can be gradually installed to offload the traffic.

to accommodate all the TDs in a specific area, for example in an airport terminal or at a stadium. The APs can be adjusted by the operator to provide different quality of services. Fig. 2.8 characterizes a process where more and more APs are added by the operator so that they can serve to improve the system capacity.

In this case, although all the APs are owned and operated by a single entity, rather than following a regular grid, the deployment of the APs contains some randomness either due to the physical constraints of the infrastructure or the lack of thorough planning. We assume that the distribution of the APs is subject to Poisson Point Processes (PPP) with density μ [31]. Formally, the locations of the APs are given by points of a homogeneous Poisson Point Process Φ on the plane with intensity μ in that

1) the number of APs $N(\beta)$ in any finite region β is a Poisson random variable with

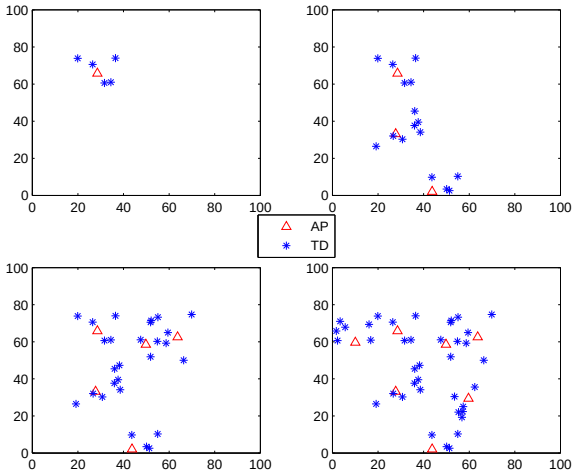

Figure 2.9: The Closed Access Case. Each AP is only open to specific TDs. When a new AP is installed, it also contributes to the traffic.

mean $\mu \times area(\beta)$

$Pr[N(\beta) = n] = e^{-\mu \times area(\beta)} \frac{[\mu \times area(\beta)]^n}{n!}$, $n \geq 0$;

2) $\forall \beta, \beta'$: $\beta \cap \beta' = \phi \Rightarrow N(\beta), N(\beta')$ are independent; and

3) $\forall \beta$, given $N(\beta) = n$, these n APs are i.i.d. uniformly distributed over β.

Note that the Poisson distribution has the memoryless property such that

$$Pr[N(\beta) > n] = Pr[N(\beta) > n + m | N(\beta) > m] = e^{-\mu \times area(\beta)} \frac{[\mu \times area(\beta)]^n}{n!}.$$

Moreover, in the real world, the APs are not exactly deployed in this random manner, especially when the APs are owned by the same operator where some centralized planning and optimization are possible. However, as shown in [32], this model can serve as a lower bound of the performance of the real world applications.

In the open access model, the locations of the TDs are also assumed to be subject to a Poisson Point Process with density λ.

On the other hand, in the closed access subscription model, the APs are always owned and operated by separate entities, for example in a community where each household has its own AP. Since the APs are always deployed in a fully distributed manner, we assume that the distribution of APs follow the Poisson Point Process defined above with density υ. However, since each AP is only open to some specific TDs, the distribution of the APs and TDs are correlated with each other. An example of the growing of the network is shown in Fig. 2.9. When a new AP is installed, it contributes to the total number of TDs as well.

We assume the number of TDs served by one single AP is a Poisson random variable $M \geq 1$ with parameter τ, i.e., each AP has at least one subscribed TD. More specifically,

$$Pr(M = k) = \begin{cases} 0 & if \quad k = 0 \\ \frac{\tau^{(k-1)} e^{-\tau}}{(k-1)!} & if \quad k \geq 1 \end{cases} \tag{2.7}$$

2.4 The Performance Analysis

In this section, we will first explain in detail how the proposed system works under the open access and closed access models. Then the SINR and achievable data rate is analyzed.

Let $\mathbf{A}$ denote the set of indices of all the APs, $\mathbf{T}$ the set of indexes of all the TDs, $\mathbf{T}_i$ the set of indexes of all the TDs subscribed to the AP indexed i, and $\mathbf{R}_j$ the set of the indices of all the interfering APs that can reach the j-th TD except

the serving one, i.e., all the interfering APs. Note that we have $\mathbf{T}_i \subseteq \mathbf{T}$, $\mathbf{R}_j \subset \mathbf{A}$. We denote the index of the AP that serves TD j by S_j.

In the open access model, each TD selects the serving AP by the strength of the focusing gain. More specifically,

$$S_j = \arg\max_k \eta_{k,j} \cdot \|h_{k,j} * g_{k,j}[L-1]\|^2 \tag{2.8}$$

where $\eta_{k,j} = \gamma_{k,j} \cdot \min(1, d_{k,j}^{-\alpha})$.

The selection of S_j is not only based on the distance, i.e., the TD j is not necessarily served by the closest AP. This scheme makes the best use of the unique spatial focusing effects of TR based communications.

In the closed access model, on the other hand, since each TD can be only served by a specific AP, S_j is pre-determined and does not change.

The open access and closed access models only affect the selection of S_j's. Once the S_j's are determined, the performance of the system only depends on the S_j's. In the following, we analyze the SINR and achievable data rate of each TD given the S_j's, which is the same for the open access and closed access models. We first analyze the signal received by each TD.

In the proposed system, each AP serves its subscribed users using the TRDMA scheme. The signal received by TD j subscribed to the AP i that equipped with Q_T transmitting antennas can be represented as

$$\begin{aligned} Y_j[k] = a_j \sum_{m\in\mathbf{T}_i} \sum_{q=1}^{Q_T} \sum_{l=0}^{(2L-2)/D} (h_{i,j}^{(q)} * g_{i,m}^{(q)})[Dl] X_m[k-l] \\ + a_j \sum_{n\in\mathbf{R}_j} \sum_{m\in\mathbf{T}_n} \sum_{q=1}^{Q_T} \sum_{l=0}^{(2L-2)/D} (h_{n,j}^{(q)} * g_{n,m}^{(q)})[Dl] X_m[k-l] + a_j n_j[k] \end{aligned} \tag{2.9}$$

where the a_j is a scalar that the TD j uses to amplify the received signal. The first term on the right hand side is the signal received from the subscribed AP, the second term is the signal received from all the interfering APs and the third term denotes the noise. In the rest of this chapter, without loss of generality, we assume that all the APs have the same number of antennas Q_T.

Eqn. (2.9) can be further written as

$$\begin{aligned} Y_j[k] = a_j \sum_{q=1}^{Q_T} X_j[k] \cdot h_{i,j}^{(q)} * g_{i,j}^{(q)}[L-1] + a_j \sum_{q=1}^{Q_T} \sum_{\substack{l=0 \\ l \neq (L-1)/D}}^{(2L-2)/D} (h_{i,j}^{(q)} * g_{i,j}^{(q)})[Dl] X_m[k-l] \\ + a_j \sum_{\substack{m \in \mathbf{T}_i \\ m \neq j}} \sum_{q=1}^{Q_T} \sum_{l=0}^{(2L-2)/D} (h_{i,j}^{(q)} * g_{i,m}^{(q)})[Dl] X_m[k-l] \\ + a_j \sum_{n \in \mathbf{R}_j} \sum_{m \in \mathbf{T}_n} \sum_{q=1}^{Q_T} \sum_{l=0}^{(2L-2)/D} (h_{n,j}^{(q)} * g_{n,m}^{(q)})[Dl] X_m[k-l] + a_j n_j[k] \end{aligned} \tag{2.10}$$

where the first term stands for the intended signal received by the TD, the second term the inter-symbol interference (ISI), the third item the inter-user interference (IUI) and the fourth term the inter-cell interference (ICI). In the following, we will analyze the the signal power and the interference power to obtain the effective SINR. Since the choice of a_j does not affect the SINR, without loss of generality, we assume $a_j = 1, \ \forall \ j$ in the following.

Similar to [16], we evaluate the effective SINR which is defined as

$$SINR_{eff} = \frac{E[P_{SIG}]}{E[P_{ISI}] + E[P_{IUI}] + E[P_{ICI}] + \sigma^2} \tag{2.11}$$

where σ^2 is the power of noise. By assuming equal power allocation in each AP among all subscribed users, the expected received signal power conditioning on the

number of subscribed users N can be represented as

$$E[P_{SIG}|\Omega] = E[\frac{PL_j}{N_{S_j}}]\frac{1+e^{-\frac{LT_S}{\delta_T}}}{1+e^{-\frac{T_S}{\delta_T}}} + E[\frac{PL_j}{N_{S_j}}]Q_T\frac{1-e^{-\frac{LT_S}{\delta_T}}}{1-e^{-\frac{T_S}{\delta_T}}} \tag{2.12}$$

where Ω is the set that contains all the location and association information. $PL_j = \min(1, d_{j,S_j}^{-\alpha})$ is the path loss for TD j where d_{j,S_j} is the distance from TD j to its serving AP S_j and N_{S_j} is the number of TDs served by the AP S_j. Similarly, the conditional expected interference power can be represented by

$$E[P_{ISI}|\Omega] = E[\frac{PL_j}{N_{S_j}}]\frac{e^{-\frac{DT_S}{\delta_T}} - e^{-\frac{(L+D-1)T_S}{\delta_T}} - e^{-\frac{(L+1)T_S}{\delta_T}} + e^{-\frac{2LT_S}{\delta_T}}}{(1+e^{-\frac{T_S}{\delta_T}})(1-e^{-\frac{DT_S}{\delta_T}})(1-e^{-\frac{LT_S}{\delta_T}})} \tag{2.13}$$

$$E[P_{IUI}|\Omega] = E[\frac{PL_j(N_{S_j}-1)}{N_{S_j}}]\cdot\frac{(1+e^{-\frac{DT_S}{\delta_T}})(1+e^{-\frac{2LT_S}{\delta_T}}) - 2e^{-\frac{(L+1)T_S}{\delta_T}}(1+e^{-\frac{(D-2)T_S}{\delta_T}})}{(1-e^{-\frac{DT_S}{\delta_T}})(1+e^{-\frac{DT_S}{\delta_T}})(1-e^{-\frac{LT_S}{\delta_T}})} \tag{2.14}$$

Next, we analyze the ICI. Since it is assumed that each AP has at least one subscribed TD, each AP is always transmitting with full power independent of the number of subscribed TDs. We first consider the ICI power from one single interfering AP close enough so that the path loss can be omitted. The ICI power can be written as

$$\begin{aligned} E[P_{ICI}^{(single)}] &= E[E_X[\left|\sum_{m\in\mathbf{T}_n}\sum_{q=1}^{Q_T}\sum_{l=0}^{(2L-2)/D}(h_{n,j}^{(q)} * g_{n,m}^{(q)})[Dl]X_m[k-l]\right|^2]] \\ &= \frac{(1+e^{-\frac{DT_S}{\delta_T}})(1+e^{-\frac{2LT_S}{\delta_T}}) - 2e^{-\frac{(L+1)T_S}{\delta_T}}(1+e^{-\frac{(D-2)T_S}{\delta_T}})}{(1-e^{-\frac{DT_S}{\delta_T}})(1+e^{-\frac{DT_S}{\delta_T}})(1-e^{-\frac{LT_S}{\delta_T}})}. \end{aligned} \tag{2.15}$$

where D is the back-off factor used by the AP. Then we have

$$E[P_{ICI}|\Omega] = E[\sum_{i\in\mathbf{T}, i\neq S_j}\eta_{i,j}]\cdot\frac{(1+e^{-\frac{DT_S}{\delta_T}})(1+e^{-\frac{2LT_S}{\delta_T}}) - 2e^{-\frac{(L+1)T_S}{\delta_T}}(1+e^{-\frac{(D-2)T_S}{\delta_T}})}{(1-e^{-\frac{DT_S}{\delta_T}})(1+e^{-\frac{DT_S}{\delta_T}})(1-e^{-\frac{LT_S}{\delta_T}})}. \tag{2.16}$$

Note that the distributions of N_{S_j} and PL_j are different for open and closed access models. While they are difficult to model through λ and μ in the open access case where the choice of S_j depends on the instantaneous channel conditions, we will evaluate the open access case through numerical results. In the following, we analyze the SINR and achievable data rate of each TD given τ and υ.

In the closed access model, each AP only allows specific TDs to subscribe. Moreover, the AP and the designated TDs are usually close. Therefore, in the closed access model, the signal path loss from the AP to the designated TDs can be neglected and the signal received by the TD is only dependent on N_{S_j} which is the number of TDs subscribed to the AP, i.e., $PL_j = 1$. By (2.7), the expected value of $\frac{1}{N_{S_j}}$ can be calculated as

$$E[\frac{1}{N_{S_j}}] = \frac{1 - e^{-\tau}}{\tau}. \tag{2.17}$$

The expected signal and interference power can be represented as

$$\begin{aligned} E[P_{SIG}] &= E[E[P_{SIG}|\Omega]] \\ &= \frac{1 - e^{-\tau}}{\tau} \cdot \left(\frac{1 + e^{-\frac{LT_S}{\delta_T}}}{1 + e^{-\frac{T_S}{\delta_T}}} + Q_T \cdot \frac{1 - e^{-\frac{LT_S}{\delta_T}}}{1 - e^{-\frac{T_S}{\delta_T}}} \right) \end{aligned} \tag{2.18}$$

$$\begin{aligned} E[P_{ISI}] &= E[E[P_{ISI}|\Omega]] \\ &= \frac{1 - e^{-\tau}}{\tau} \cdot \frac{e^{-\frac{DT_S}{\delta_T}} - e^{-\frac{(L+D-1)T_S}{\delta_T}} - e^{-\frac{(L+1)T_S}{\delta_T}} + e^{-\frac{2LT_S}{\delta_T}}}{(1 + e^{-\frac{T_S}{\delta_T}})(1 - e^{-\frac{DT_S}{\delta_T}})(1 - e^{-\frac{LT_S}{\delta_T}})} \end{aligned} \tag{2.19}$$

$$
\begin{aligned}
E[P_{IUI}] &= E[E[P_{IUI}|\Omega]] \\
&= E[\frac{M-1}{M} \cdot \frac{(1+e^{-\frac{DT_S}{\delta_T}})(1+e^{-\frac{2LT_S}{\delta_T}}) - 2e^{-\frac{(L+1)T_S}{\delta_T}}(1+e^{-\frac{(D-2)T_S}{\delta_T}})}{(1-e^{-\frac{DT_S}{\delta_T}})(1+e^{-\frac{DT_S}{\delta_T}})(1-e^{-\frac{LT_S}{\delta_T}})}] \\
&= (1-\frac{1-e^{-\tau}}{\tau}) \cdot \frac{(1+e^{-\frac{DT_S}{\delta_T}})(1+e^{-\frac{2LT_S}{\delta_T}}) - 2e^{-\frac{(L+1)T_S}{\delta_T}}(1+e^{-\frac{(D-2)T_S}{\delta_T}})}{(1-e^{-\frac{DT_S}{\delta_T}})(1+e^{-\frac{DT_S}{\delta_T}})(1-e^{-\frac{LT_S}{\delta_T}})}
\end{aligned}
\tag{2.20}
$$

Since the signal from the interfering AP suffers from the path loss, the interfering APs far away from the TD has less influence. Assuming that only the interfering APs within distance R from the TD j are considered, the expected ICI power can be represented by

$$
\begin{aligned}
E[P_{ICI}^{(R)}] &= E[\sum_{i=1}^{N_R} \min(1, d_{j,i}^{-\alpha})] \cdot E[P_{ICI}^{single}] \\
&= E[N_R] \cdot E[\min(1, d_{j,i}^{-\alpha})] \cdot E[P_{ICI}^{single}] \\
&= \upsilon(\pi + \frac{2\pi(1-R^{2-\alpha})}{\alpha-2}) \cdot E[P_{ICI}^{single}]
\end{aligned}
\tag{2.21}
$$

where N_R is the number of APs within the circle of radius R. The second equality comes from the Wald's Equation [33] and the third equality uses

$$
\begin{aligned}
E[\min(1, d_{j,i}^{-\alpha})] &= \int_0^{2\pi}\int_0^1 \frac{1}{\pi R^2} \cdot r dr d\theta + \int_0^{2\pi}\int_1^R \frac{r^{-\alpha}}{\pi R^2} \cdot r dr d\theta \\
&= \frac{1}{R^2}(1 + \frac{2-2R^{2-\alpha}}{\alpha-2}).
\end{aligned}
\tag{2.22}
$$

By taking the limit $R \to \infty$ to consider the ICI from all the interfering APs,

(2.21) becomes

$$E[P_{ICI}] = \lim_{R\to\infty} E[P_{ICI}^{(R)}]$$
$$= \upsilon(\pi + \frac{2\pi}{\alpha - 2}) \cdot \frac{(1 + e^{-\frac{DT_S}{\delta_T}})(1 + e^{-\frac{2LT_S}{\delta_T}}) - 2e^{-\frac{(L+1)T_S}{\delta_T}}(1 + e^{-\frac{(D-2)T_S}{\delta_T}})}{(1 - e^{-\frac{DT_S}{\delta_T}})(1 + e^{-\frac{DT_S}{\delta_T}})(1 - e^{-\frac{LT_S}{\delta_T}})}. \tag{2.23}$$

Substituting (2.18), (2.19), (2.20), (2.23) into (2.11), the effective SINR of individual user can be represented as

$$SINR(\tau, \upsilon) = \frac{P_{SIG}(\tau,\ \upsilon)}{P_{ISI}(\tau,\ \upsilon) + P_{IUI}(\tau,\ \upsilon) + P_{ICI}(\upsilon) + \sigma^2} \tag{2.24}$$

Accordingly, the achievable spectrum efficiency of each individual user can be expressed as

$$R(\tau,\ \upsilon) = \frac{1}{D}\log_2(1 + SINR(\tau,\ \upsilon)) \tag{2.25}$$

2.5 The Simulation Results

In this section, we show that the efficiency of the proposed TR system in addressing the massive device challenge by using simulation results.

2.5.1 Open Access Model

In this subsection, we will show the scalability of the proposed TR system in the open access model such that it can be easily extended to boost the achievable data rate in the massive device setting.

We build a simulation platform where APs and TDs are distributed in a certain area according to the Poisson Point Processes with parameters μ and λ. In this

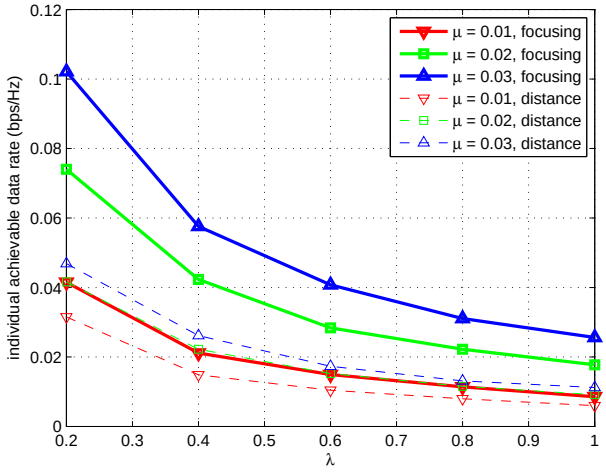

Figure 2.10: The Improvement of Single User Data Rate by Adding More APs

simulation, the APs and TDs are all single antenna devices, i.e., $Q_T = 1$. The SNR is 10 dB and $D = 10$. The path loss parameters are obtained from [34]. We calculate the signal and interference power using (2.12), (2.13), (2.14) and (2.16) for each realization and obtain the expected signal and interference power by averaging over realizations. The expected achievable data rate of a single TD is calculated by

$$R^{(OA)} = \frac{1}{D}\log_2(1 + \frac{E[P_{SIG}^{(OA)}]}{E[P_{ISI}^{(OA)}] + E[P_{IUI}^{(OA)}] + E[P_{ICI}^{(OA)}] + \sigma^2}). \tag{2.26}$$

In Fig. 2.10, we show the expected achievable rate of a TD versus λ and μ. Generally, as shown in Fig. 2.10, the achievable data rate of each single TD will decrease as the density of TDs grows due to the less power shared by each TD and stronger interference. Suppose the operator likes to maintain that the achievable data rate of each TD is above a certain threshold. The operator can easily install or turn on extra APs without additional difficulty when the achievable data rate reaches the threshold, which can automatically work with the existing ones

to boost the data rate. In other words, the extra APs bring in new resource into the system that can be shared by the TDs. On the other hand, when the density of TDs decreases, the operator can just remove or turn off unnecessary APs to save power. Moreover, we also compare the proposed scheme where the TDs select the serving AP by the focusing gain with the traditional scheme where the TDs select the serving AP by distance. It is shown that the focusing gain based association scheme enhances the benefits of the unique spatial and temporal focusing effects of TR based communications.

In the proposed TR system, the time-reversal focusing effects create natural space-time separation among users, thus reducing interference with each other, and no particular spectrum planning is needed when adding new APs into the system. Moreover, since the APs work in a fully distributed manner, there is no information shared or exchanged among APs in the transmission phase. This self-organizing property makes the network flexible such that extra APs can always be easily added to the system to boost the performance when needed, and removed when not necessary. In other words, the proposed TR-based multi-AP downlink system is highly scalable and can accommodate different user density.

2.5.2 Closed Access Model

In the previous subsection, it is shown the proposed system is scalable in the open access model where extra APs can offload the traffic. However, in the closed access model, the new AP usually does not serve the existing TDs, but is an

interference source for them. As a result, as more APs are installed by independent parties, each TD has higher risk of failure that the achievable data rate is far below expectation due to the interference from APs installed by other parties. In this subsection, we show that the proposed system is more robust to this kind of failure than the IEEE 802.11 based system in the closed access model.

We investigate the achievable data rate of each individual TD versus the density of APs. Obviously, the achievable data rate of a TD will be highest if there is no other interfering APs within range, and will decrease as more APs are placed nearby. To understand the effect of the nearby APs, we define the normalized achievable data rate, which is the ratio of the effective achievable data rate and the point to point link capacity. It characterizes the extent to which the achievable data rate degrades due to the interference from other devices sharing the medium. In this simulation, the APs and TDs are all single antenna devices, i.e., $Q_T = 1$. The SNR is 20 dB and $D = 10$. As shown in Fig. 2.11, for each fixed τ, the achievable data rate for a single TD compromises as the density of APs increases, while all of them are no better than the single AP case where there is no ICI.

Historically, the 802.11 wireless technology was designed to work in the single cell case to extend coverage [24]. In the massive device scenario, the performance of each single TD can be severely affected by the nearby closed access APs. To model this behavior, we first observe when multiple 802.11 TDs are served by one 802.11 AP, then the average active time of one TD is upper bounded by $\frac{1}{n}$ where n is the number of TDs. Moreover, as observed in subsection IV.A, when multiple APs are within the range of each other, the average time of each AP is upper bounded by

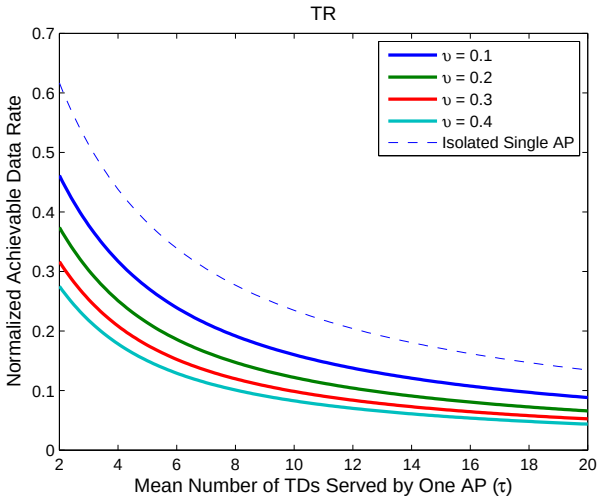

Figure 2.11: The Graceful Degradation of TR

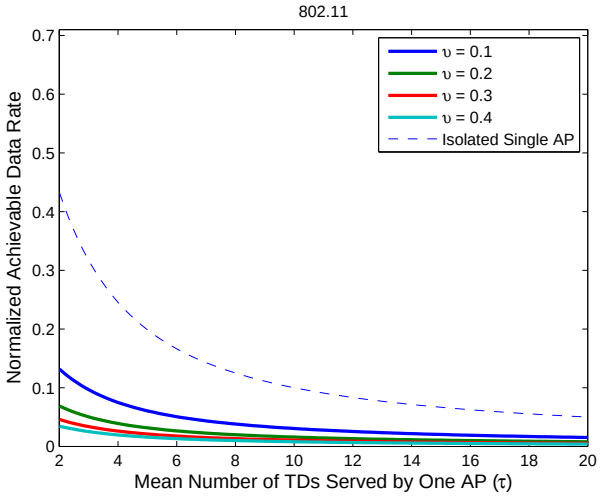

Figure 2.12: The Performance Degradation of 802.11

$\frac{1}{Z}$ where Z is the number of APs. Therefore, for an IEEE 802.11 based TD in a service group where there are totally n TDs and the AP is in range of other $Z-1$ APs, the average active time is upper bounded by $\frac{1}{nZ}$ and the effective achievable data rate U is $\frac{G}{nZ}$ where G is the point to point link capacity. The expected value of U can be expressed as

$$\begin{aligned} E[U] &= E[\frac{1}{nZ} \cdot G] \\ &= \frac{1-e^{\tau}}{\tau} \cdot \frac{1-e^{A\upsilon}}{A\upsilon} G \end{aligned} \tag{2.27}$$

where A is the interference area. In this example, A is set to be $(\pi \cdot 2.80^2)m^2$ which corresponds to the path loss model for UNII(II) channel in 5 GHz in the indoor environment [35] and SNR being 20 dB. The transmitted signal power from any AP cannot be distinguished from the noise outside this range and therefore other APs outside this range will not be affected.

As shown in Fig. 2.12, the degradation of the achievable data rate in the IEEE 802.11 based system is severe compared with the isolated single AP scenario, even when the AP density is low. This is because that each link requires exclusive use of the channel, which is inefficient if there are many devices close to each other. In contrast, the TR-based downlink system can tolerate interference so that multiple APs can share the spectrum. Due to the interference mitigation effect of TR-based communications, the influence of ICI is much reduced. As shown in Fig. 2.11, the degradation of the data rate is more graceful, and each device is more robust against the interference from nearby closed access APs.

Figure 2.13: The TDD frame structure of the proposed system

2.5.3 Packet Delay

In addition to the achievable data rate, another important issue is the latency, i.e., the delay for delivering a packet. In this subsection, we will show another advantage of the proposed TR system in delivering the packet with minimal delay.

Along the same approach of [36], we build a two-layer model to evaluate the packet delay in the proposed system. The TRDMA is applied in the physical layer model to simulate the bit error rate (BER), which is transferred to the MAC layer model to further measure the packet delay. The delay of a packet is defined as the duration of time from the moment that it is at the head of the MAC queue until the time that the ACK packet is received. As shown in Fig. 2.13, the TR based communication works in time division duplexing (TDD). One PHY frame consists of a downlink frame and an uplink frame. In the downlink frame, the AP first transmits the downlink packet to the TD. Upon completion of the downlink frame, the TD checks whether the reception of the current packet is complete, and sends an ACK to the AP if the received packet is complete and valid. If the ACK is successfully received by the AP, the AP starts to transmit the next packet in the next downlink frame. Otherwise, the AP keeps transmitting the same packet to the TD until ACK is received. Therefore, in this system, the delay for the packet is the

time needed for transmission as well as repeated re-transmissions in case of error. The expected delay of a packet can be represented by

$$delay = \frac{T_{pac}}{1 - PER} \tag{2.28}$$

where $T_{pac} = N_f \cdot T_f$ is the time needed for one complete transmission of a packet. N_f is the number of PHY frames needed to transmit a packet, and T_f is the time of one PHY frame. $PER = 1 - (1 - BER_{dl})^{S_{pac}} \cdot (1 - BER_{ul})^{S_{ack}}$ is the packet error rate where S_{pac} is the downlink packet size in bits, S_{ack} is the ACK signal size in bits. BER_{dl} and BER_{ul} are the BERs in downlink an uplink, respectively. The T_{pac} can be equivalently written as follows

$$T_{pac} = \lceil \frac{S_{pac} \cdot D \cdot T_S}{F_{dl}} \rceil \cdot (F_{ul} + F_{dl}) \tag{2.29}$$

where F_{ul} is the length of an uplink frame in time, and F_{dl} is the length of a downlink frame in time, D is the back-off factor, T_S is the chip time of the system. In this example, we use $F_{dl} = 12ms$ and $F_{ul} = 6ms$. D and T_S are tuned so that the channel bit rate fits that in Table 2.2. Note that the parameters used in this experiment shown in 2.2 are the same as those in Table I of [37] so that the results are comparable.

In Fig. 2.14, we show the mean packet delay of the proposed system obtained by (2.28) and the mean packet delay of IEEE 802.11 base systems obtained from [37]. It is shown that the delay of a packet in the proposed system is almost constant with the increasing number of APs. This feature is highly desirable in the wireless communications since that the QoS of each individual TD can be preserved when the system scales up. It is due to the fact that all the APs and TDs share the wireless

Table 2.2: The Packet and Link Parameters

Parameter	**Value**
Packet payload	8184 bits
MAC header	224 bits
PHY header	192 bits
ACK packet	112 bits + PHY header
Channel bit rate	1 Mbps

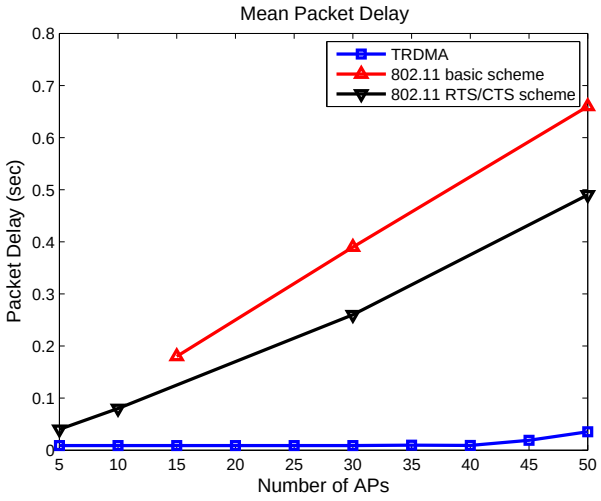

Figure 2.14: The Mean Delay of TRDMA and IEEE 802.11 multi-AP Downlink System

medium rather than requiring exclusive use, and consequently the transmission of a packet does not have to wait. Moreover, additional APs will only contribute to the ICI of the intended receiver which is mitigated by the spatial and temporal focusing effect of the TR scheme, and thus the influence of additional APs is minimal. On the other hand, in the IEEE 802.11 based system, due to the DCF that coordinates multiple devices, each device needs to go through the back off stages before a packet is allowed to be transmitted, where the number of back off stages grows with the number of other devices around. As a result, this mechanism is not efficient and the delay of a packet grows approximately linearly with the system size. It is obvious that the packet delay in the proposed system is far below that in the IEEE 802.11 based system.

2.6 Experimental Measurements

In this section, we demonstrate some experimental measurements taken in practical multi-path channels. We build a TR radio prototype to measure the multi-path channels. A snapshot of the radio stations of our prototype is illustrated in Fig. 2.15, where a single antenna is attached to a small cart with RF board and computer installed on the cart. The tested signal bandwidth spans from 5.3375 GHz to 5.4625 GHz, centered at 5.4 GHz. An office room in the J. H. Kim Engineering Building at University of Maryland is considered. As shown in Fig. 2.16, the APs are placed at 6 location across the room, while the TDs are placed in multiple locations in the small room marked with "A". The layout of room "A" and an example of the

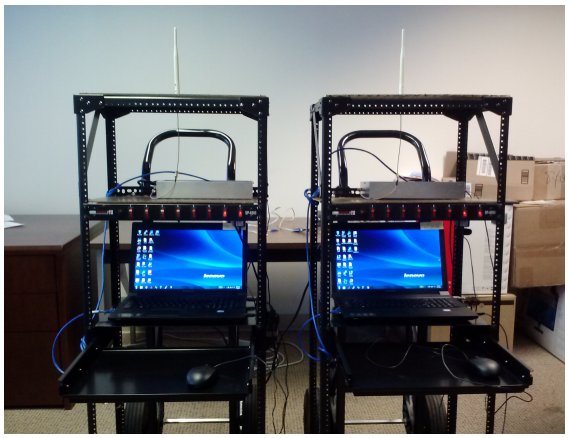

Figure 2.15: The TR Radio Prototype

placement of the TDs is shown in Fig. 2.17. In this experiment, we have 800 possible TD locations where two neighboring locations are 10 cm apart, and 6 possible AP locations, from which 4800 multi-path channel measurements are obtained. In [38], it is shown that channel impulse responses obtained from locations beyond 5 cm apart are independent, and thus the 4800 multi-path channel measurements are independent. In the following subsections, the performance of the proposed system is evaluated using the measured channels.

2.6.1 Open Access Model

We show the scalability of the proposed system with the measured channels. In this experiment, the SNR is 10 dB and $D = 10$. We calculate the average signal power and interference power by averaging over all the measured channels. More specifically,

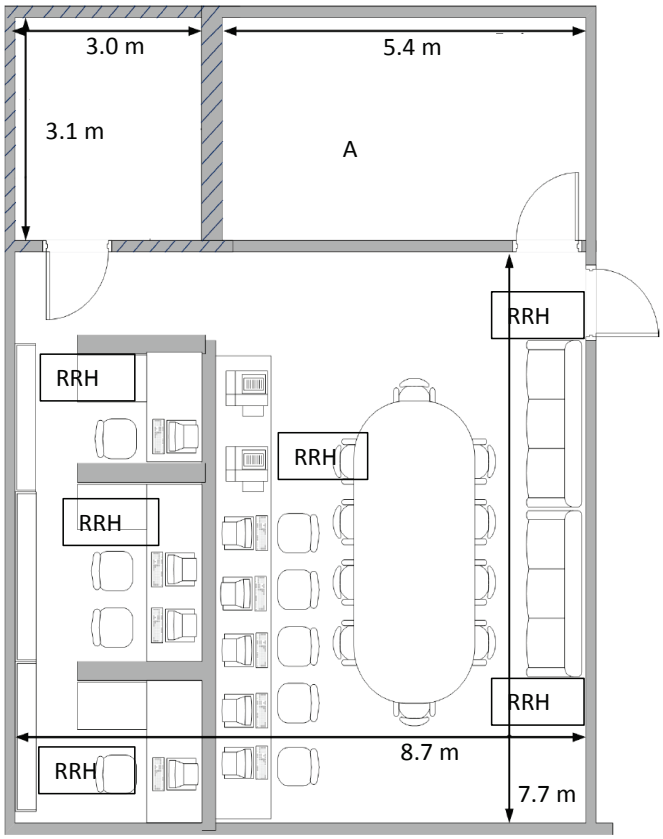

Figure 2.16: The Floor Plan of The Testing Room

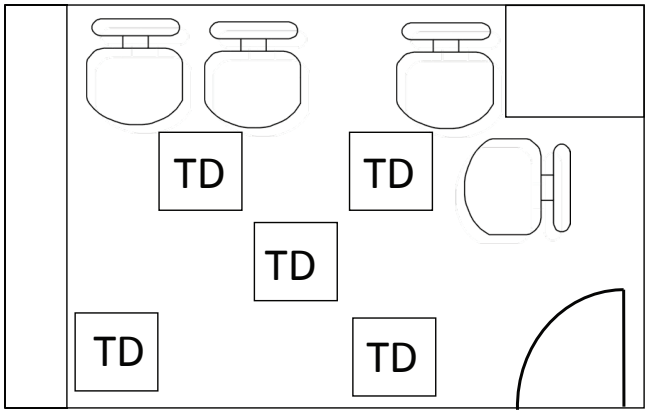

Figure 2.17: Floor Plan of Room A

$$P_{SIG}^{exp} = \sum_{n=1}^{N_{AP}} \sum_{m=1}^{N_{TD}} |h_{n,m} * g_{n,m}[L-1]|^2/(N_{AP} * N_{TD})$$

$$P_{ISI}^{exp} = \sum_{n=1}^{N_{AP}} \sum_{m=1}^{N_{TD}} \sum_{\substack{l=0 \\ l \neq (L-1)/D}}^{(2L-2)/D} |(h_{n,m} * g_{n,m})[Dl]|^2/(N_{AP} * N_{TD})$$

$$P_{IUI}^{exp} = \sum_{n=1}^{N_{AP}} \sum_{m=1}^{N_{TD}} \sum_{\substack{k=1 \\ k \neq m}}^{N_{TD}} \sum_{l=0}^{(2L-2)/D} |(h_{n,m} * g_{n,k})[Dl]|^2/(N_{AP} * N_{TD} * (N_{TD}-1))$$

$$P_{ICI}^{exp} = \sum_{n=1}^{N_{AP}} \sum_{m=1}^{N_{TD}} \sum_{\substack{k=1 \\ k \neq n}}^{N_{AP}} \sum_{l=0}^{(2L-2)/D} |(h_{n,m} * g_{k,m})[Dl]|^2/(N_{AP} * N_{TD} * (N_{AP}-1))$$

where N_{AP} is the total number of APs and N_{TD} is the total number of locations of TDs we measure for each AP. The measured data enable us to understand the statistical distribution of the multi-paths of the real world channels without considering the path loss. To evaluate the scalability of the proposed system in the open access scenario, we employ the platform used in section 2.5.1 where the locations of the APs and TDs are randomly generated and the path loss is considered. The approximate expected signal and interference power can be calculated by averaging over these realizations as

$$\tilde{E}[P_{SIG}|\Omega] = E[\frac{PL_j}{N_{S_j}}] * P_{SIG}^{exp} \tag{2.30}$$

$$\tilde{E}[P_{ISI}|\Omega] = E[\frac{PL_j}{N_{S_j}}] * P_{ISI}^{exp} \tag{2.31}$$

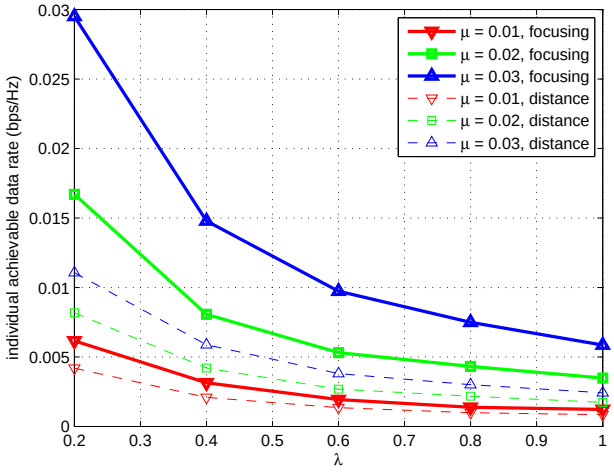

Figure 2.18: The Improvement of Single User Data Rate by Adding More APs

$$\tilde{E}[P_{IUI}|\Omega] = E[\frac{PL_j(N_{S_j}-1)}{N_{S_j}}] * P_{IUI}^{exp} \tag{2.32}$$

$$\tilde{E}[P_{ICI}^{(single)}] = P_{ICI}^{exp} \tag{2.33}$$

The achievable data rate of each TD is calculated using (2.26). In Fig. 2.18, the trends in Fig. 2.10 are observed. The total achievable sum rate can be boosted by simply adding more APs into the system without any coordination with other APs while the self-organizing feature automatically makes the APs work together. The difference in the achievable data rates is due to the reason that in the simulation we use 500 MHz bandwidth while in the experiment it is 125 MHz. Since the focusing effect is more significant with larger bandwidth, the achievable data rate is improved if larger bandwidth is available.

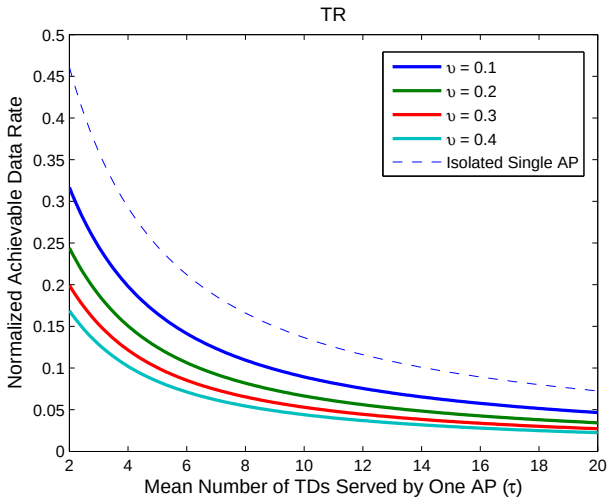

Figure 2.19: The Graceful Degradation of TR using Collected Channel

2.6.2 Closed Access Model

We validate the feature of failure-robustness of the proposed system in the dense network setting using the real channel data. In this experiment, the SNR is 20 dB and $D = 10$. By plugging Eqn. (2.30), (2.31), (2.32) and (2.33) into Eqn. (2.18), (2.19), (2.20) and (2.21), the same trends in Fig. 2.11 can still be observed in Fig. 2.19. It illustrated that in the TR-based multi-AP downlink system, the performance loss caused by neighboring closed access APs is much less severe than that in the 802.11 based system because of the focusing effect of TR-based communications.

2.6.3 Packet Delay

We also use the real world experiment to validate the low-delay feature of TR based communications. In the experiment, multiple TR-based APs are placed across the room in the locations denoted in Fig. 2.16 and they work independently

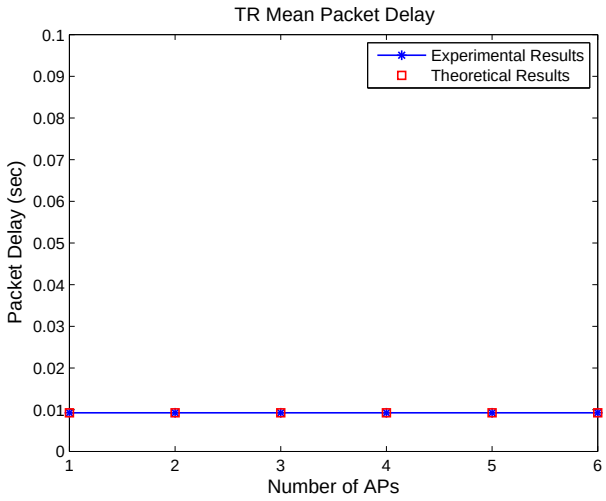

Figure 2.20: The Mean Delay of TRDMA System with 125 MHz Bandwidth using Rayleigh Channel Model and Real Channel

to deliver the downlink data to the subscribed TDs that placed inside the grid. As a result, each TD suffers from the ICI from other APs. However, as it is shown in Fig. 2.20, the packet delay is minimal, and does not grow with the increasing number of APs. Moreover, the results using real channel matches well with the results using Rayleigh channel model specified in section 2.3.1 under 125 MHz bandwidth.

2.7 Conclusions

In this chapter, after illustrating the scalability issues in traditional wireless network, we proposed a TR-based self-organizing wireless network. Due to the natural focusing effects of TR communications, the interference is automatically mitigated without any coordination among APs in the transmission phase, and the proposed system has the self-organizing feature. As a result, it is highly scalable without the need in coordinating multiple APs. The achievable data rate of the

proposed system was investigated under both open access model where each AP is open to any terminal device (TD), and the closed access model where each AP is only open to specific TDs. We show through numerical results that the proposed system can be easily extended to serve more devices and/or higher data rate in the open access model, and is failure-robust in the closed access model where the data rate degradation caused by nearby closed access APs is more graceful than the IEEE 802.11 based system. Based on the nice properties shown by the analysis and numerical results, the proposed TR-based self-organizing network is a promising scalable network that can be utilized in the future of wireless communication.

Chapter 3: Time-Reversal Tunneling Effects for Cloud Radio Access Network

To accommodate massive devices in the wireless network, the spectrum is one of the precious resources. Boosting the spectrum efficiency is one of the key considerations in the future wireless networks. To achieve higher spectral efficiency, coordination among multiple access points (APs) is essential so that the multiplexing gain can be leveraged. However, efficient collaborative radio techniques cannot work efficiently due to the high latency and low bandwidth interface between the APs in traditional wireless networks.

To address the aforementioned challenge, cloud based radio access network (C-RAN) has been proposed as a viable solution recently [2–5]. It is a novel type of RAN architecture, where a pool of base band units (BBUs) are connected to the distributed remote radio heads (RRHs) via high bandwidth and low latency links. The BBUs are responsible for all the baseband processing through high performance computing. In this centralized structure, many coordinated communication schemes become possible or more efficient. For example, the coordinated multiple-point process (CoMP) in the LTE-A standard [6] can be implemented in the C-RAN to improve network capacity and energy efficiency [7]. In addition, by moving the

baseband processing to the cloud, the RRHs need only support the basic transmission/reception functionalities, which further reduces their energy consumption and deployment cost.

Nevertheless, the limited front-haul link capacity [8] between the BBU and the RRH may prevent the C-RAN from fully utilizing the benefits made possible by concentrating the processing intelligence. In most of the current C-RAN structures, the data transmitted in the front-haul is proportional to the aggregate traffic of all the terminal devices (TDs) [9,10]. As a result, the front-haul link capacity becomes a bottleneck when there are massive TDs in the network. To tackle this challenge, several solutions have been proposed. One of them is to use compression where the baseband signal is compressed before the front-haul transmission and then decompressed after the front-haul transmission [11–13]. Although signal compression can alleviate the traffic in the front-haul under certain cases, it introduces extra computation complexity at the RRH side, which makes this approach less cost effective. Moreover, although the compression reduces the data rate consumption of each individual TD, since the total data rate consumption is the aggregate of all the TDs, there is still a deficit of the front-haul link capacity in a dense network. An alternative solution is the sparse beamforming [9,10,14] where each TD is associated with a cluster of APs. However, the data rate in the front-haul link is related to the cluster size, and a larger cluster requires a higher front-haul link capacity [9]. As a result, the limited front-haul link capacity makes it impossible to fully take advantage of the available spatial diversity, which is one of the main benefits of the C-RAN structure.

In Chapter 2, we realize the advantage of time-reversal (TR) based communications in constructing the scalable wireless network in that it provides another division of separation among devices: by their location-specific signatures. Rather than artificially separated by time, frequency or code, this separation is naturally embedded in the wireless communication procedures. In the C-RAN, since all the TDs are naturally separated by their location-specific signatures, the baseband signals for all the TDs can be efficiently combined and transmitted if TR communication is used as the air interface. We aim to leverage this unique feature of the TR based communications to create in essence a tunneling effect between the BBU and RRH to alleviate the traffic load in the front-haul link of C-RAN. Specifically, in this chapter, we propose a C-RAN framework using TR communication as the air interface. The architectures for both downlink and uplink data transmissions are designed. We analyze the performance of both the downlink and uplink transmissions in terms of the spectral efficiency and the data rate consumption in the front-haul link. To illustrate the effectiveness of the proposed system, we conduct experiments to measure the multi-path channel information in the real-world environment, based on which we show that the TR based C-RAN creates unique "tunneling effects" such that more information can be transmitted in the front-haul link with the same amount of bits/energy when there are more TDs in the system. This feature is highly desirable in the C-RAN system since it significantly alleviates the traffic load in the front-haul link caused by the network densification, which makes the proposed TR based C-RAN a perfect candidate to work in the multipath-rich environments such as indoor and urban areas to provide wireless connections

to massive TDs using relatively broad bandwidth.

This chapter is organized as follows: in section 3.1, the system model and the working phases are introduced. We analyze the performance of the downlink and uplink schemes in section 3.2 and 3.3, respectively. In section 3.4, the real-world channel measurement setting is introduced, followed by numerical results demonstrating the effectiveness of the downlink and uplink schemes. Section 3.5 concludes the section.

3.1 System Model

In this chapter, we consider a C-RAN in the indoor environments to accommodate the massive terminal devices (TDs) in both uplink and downlink data transmissions. The proposed system consists of multiple RRHs that connect to the cloud via front-haul links. As shown in Fig. 3.1, multiple RRHs are distributed in an area and transmit/receive data to/from various TDs in this area. Each of the RRHs uses TR-based communication to communicate with the TDs. All the RRHs work in the same spectrum.

In the following, we first briefly introduce the channel model adopted in this chapter. After that, we will describe the three working phases of the system in detail: the channel probing phase, the downlink data transmission phase and the uplink data transmission phase.

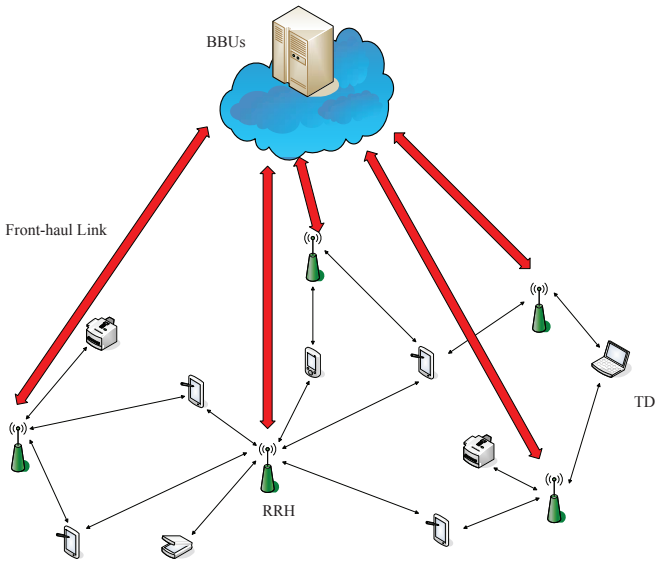

Figure 3.1: The System Model

3.1.1 Channel Model

Without loss of generality, we assume that each RRH is equipped with M_T antennas and each TD is equipped with 1 antenna. We assume a multi-path Rayleigh fading channel and the channel impulse response (CIR) of the communication link between the m-th antenna of the i-th RRH and the j-th TD is modeled as

$$h_{i,j}^{(m)}[k] = \sum_{l=0}^{L-1} h_{i,j}^{(m),(l)} \cdot \delta[k-l], \tag{3.1}$$

where $h_{i,j}^{(m),(l)}$ is the complex amplitude of the l-th tap of the CIR with length L, $h_{i,j}^{(m)}[k]$ is the k-th tap of the CIR. In practice, the $h_{i,j}^{(m)}$ is an equivalent channel which is a combination of the multi-path environment, the raised-cosine filter and the antenna. Since the raised-cosine filter and the antenna remain the same for the same radio, there is no need to counter the effects of them for TR to work. In the rest of this chapter, we treat $h_{i,j}^{(m)}$ as the channel for the proposed system.

3.1.2 The TR-based C-RAN Channel Probing Phase

In the C-RAN, all the RRHs work together to serve the TDs in downlink and uplink. To achieve this, the BBUs first need to gather all the necessary information of all the TDs. In the TR-based communication, the TDs are separated naturally by their CIR's as the location-specific signature. Therefore, the BBUs need to collect the CIR information of all the TDs before all the TDs can be served. We propose the channel probing phase in the C-RAN where the BBUs get the channel information $h_{i,j}^{(m)}$'s of from all the RRHs to the TDs. In the proposed system, the system periodically switches between the channel probing, downlink transmission and uplink transmission phases. The downlink and uplink transmissions work by time division duplexing (TDD) such that the channel information can be shared by the downlink and uplink. In the following, we will first introduce the channel probing phase which is common and necessary for both downlink and uplink transmissions, after which we describe in details the downlink and uplink transmission phases respectively.

Let $\mathbf{R}$ denote the set of indices of all the RRHs, $\mathbf{T}$ the set of indices of all the TDs, $\mathbf{T}_i$ the set of indices of all the TDs subscribed to the RRH i, and $\mathbf{R}_j$ the set of the indices of all the RRHs that the j-th TD is subscribed to. Note that we have $\mathbf{T}_i \subseteq \mathbf{T}$, $\mathbf{R}_j \subseteq \mathbf{R}$.

In the channel probing phase, the N TDs first take turns to transmit a channel probing signal to all the RRHs, and the RRHs transmit the received channel probing signal through the front-haul links to the BBUs where the channel information is

extracted. The channel probing signal can be an impulse signal or a pre-defined pseudo random code known by the BBUs beforehand. Since all the RRHs work in the same band, the channel probing signal transmitted by user j can be received by all the corresponding RRHs simultaneously, and the BBUs can extract the channel information between each TD and all its corresponding RRHs using various methods. For instance, the pre-defined pseudo random sequence can be the Golay sequence [39] and the channel information $h_{i,k}^{(m)}$ can be obtained by calculating the cross correlation of the transmitted Golay sequence and the sequence received by the m-th antenna of RRH i. At the end of the channel probing phase, the BBUs have the channel knowledge between all the TDs and their corresponding RRHs. Since the downlink and uplink transmissions use the TDD, the channel information works for both uplink and downlink. Moreover, since all the baseband processing is conducted in the BBUs, the TDs do not need to have the channel information in either downlink or uplink. Therefore, no feedback is needed to deliver the channel information back to the TDs.

To understand the overhead caused by the channel probing phase in the proposed system, we analyze it quantitatively. In [40], it was shown through experiments that the channel information in the indoor environment does not change in hours for a TD that does not move. On the other hand, in our experiment, we discover that the channel information changes much as one moves more than 3 cm. Therefore, frequent channel information update is needed for those TDs that are moving. For example, we consider a typical hand-held device. As the typical walking speed is 1.4 m per second, the TD needs to do channel probing every 18 ms.

In the experiment described in section 3.4, we use Golay sequence of total length 2048 as the channel probing sequence, and the sampling rate is 125 MHz. The time needed for a single channel probing is 16 μs. Compared with the channel updating period which is 18 ms, the channel probing overhead is less than 0.1% of the total time for a typical moving TD, which is comparable to the channel estimation overhead in the LTE systems [41]. While the C-RAN system has to handle the channel probing for every single TD, the system-wide overhead will be the aggregation of the individual overheads.

An implicit feature of the proposed channel probing phase is that each TD is only subscribed to the RRHs close enough to it. The RRHs far away from the TD j can not get the channel probing signal and will not add it to the subscription list. The searching range of the TD j can be adjusted by tuning the power of the channel probing signal. Increasing the power will extend the searching range so that the TD can possibly subscribe to more RRHs. On the RRH side, this feature enables automatic power management. If an RRH is far away from all the active TDs, using this RRH to serve the TDs might not be energy efficient. In the proposed method, this RRH does not get any channel probing signal and does not use any power to transmit data to the TDs, while the TDs are better served by other RRHs closer to them.

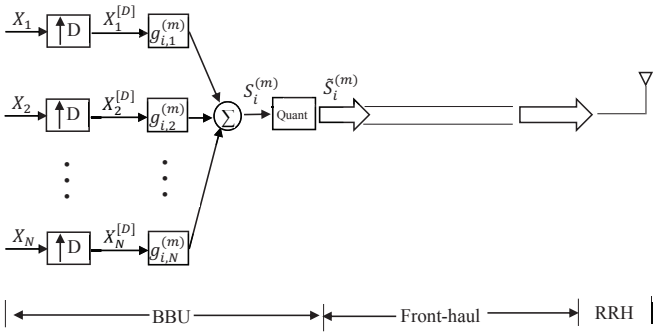

Figure 3.2: BBU to RRH through Front-haul

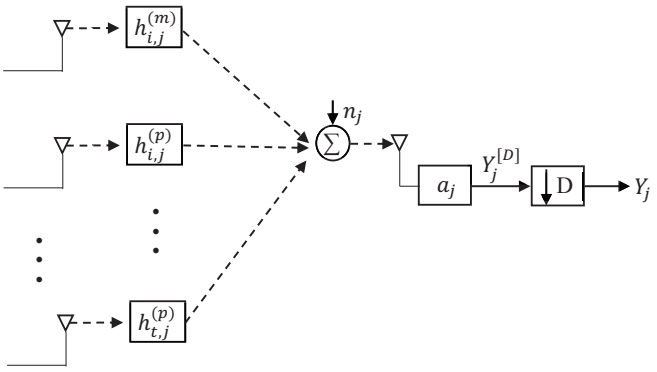

Figure 3.3: RRHs to Subscribed TD j

3.1.3 The Downlink Transmission Architecture

After the channel probing phase, the BBUs start to utilize the collected channel information to serve the downlink and uplink data transmissions. The system uses TDD to support downlink and uplink transmissions. In this subsection, we describe the downlink transmission phase.

In the downlink transmission, as shown in Fig. 3.2 and Fig. 3.3, there are two steps: in step (1), the transmitted signals are calculated at the BBUs and quantized before they are transmitted through the front-haul to the RRH; in step (2), the RRH converts the baseband signals to the RF signals and transmits them to the TDs through the multi-path channel.

As shown in Fig. 3.2, the intended symbol sequence $X_j[k]$ for the j-th TD transmitted from the m-th antenna of the i-th RRH is first up-sampled by the back-off factor D in order to alleviate the inter-symbol interference (ISI) and then convolved with the signature $g_{i,j}^{(m)}[k]$ of the channel $h_{i,j}^{(m)}[k]$, which is

$$g_{i,j}^{(m)}[k] = \frac{h_{i,j}^{(m)*}[L-1-k]}{\sqrt{\sum_{t\in\mathbf{T}_i}\sum_{m=1}^{M_T}\sum_{l=0}^{L-1}|h_{i,j}^{(m)}[l]|^2}}, \tag{3.2}$$

$$k = 0, 1, \cdots, L-1.$$

where $h_{i,j}^{(m)*}[L-1-k]$ denotes the conjugate of $h_{i,j}^{(m)}[L-1-k]$.

After that, the intended signals for all the subscribed TDs at the m-th antenna of RRH i are combined as

$$S_i^{(m)}[k] = \sum_{j\in\mathbf{T}_i}\left(X_j^{[D]} * g_{i,j}^{(m)}\right)[k]. \tag{3.3}$$

where $\left(X_j^{[D]} * g_{i,j}^{(m)}\right)[k]$ denotes the convolution of $X_j^{[D]}[k]$ and $g_{i,j}^{(m)}[k]$.

The average power of the baseband signal $S_i^{(m)}[k]$ can be calculated as

$$E[\|S_i^{(m)}[k]\|^2] = \frac{\theta}{D} \tag{3.4}$$

where $\theta = E[\|X_j[k]\|^2]$.

Then the $S_i^{(m)}$ is quantized and the BBUs transmit the quantized $\tilde{S}_i^{(m)}[k]$ through the front-haul with a limited capacity. The quantization of $S_i^{(m)}$ can be modeled as

$$\tilde{S}_i^{(m)}[k] = S_i^{(m)}[k] + q_i^{(m)}[k], \tag{3.5}$$

where $q_i^{(m)}[k]$ is the quantization noise at the m-th antenna of RRH i. By (3.3), $S_i^{(m)}[k]$ is a summation of multiple independent variables and can be approximated as a complex Gaussian random variable by the law of large numbers, and $q_i^{(m)}[k]$ can be approximated as a complex random variable whose real and imaginary parts are uniformly distributed in the range $(-\frac{Q_i^{(m)}}{2}, \frac{Q_i^{(m)}}{2})$ where $Q_i^{(m)} = \frac{2K_i^{(m)}}{2^{B_i^{(m)}}}$ is the quantization level [42] of the baseband signal at the m-th antenna of i-th AP, $B_i^{(m)}$ is the number of bits used to represent the real/imaginary part of $S_i^{(m)}[k]$, and $[-K_i^{(m)}, K_i^{(m)}]$ is the dynamic range of the real/imaginary part of $S_i^{(m)}[k]$.

In step (2), each RRH i simultaneously transmits the baseband signal $\tilde{S}_i^{(m)}[k]$ via the m-th antenna over the air to all the subscribed TDs for $m = 1, 2, \cdots, M_T$, and each subscribed TD will receive the signal from all the corresponding RRHs simultaneously. The received signal is a combination of the intended signal and the interference contaminated by noise. The TD j then first amplifies the received signal with a_j and then down-samples it with the factor D, obtaining the received

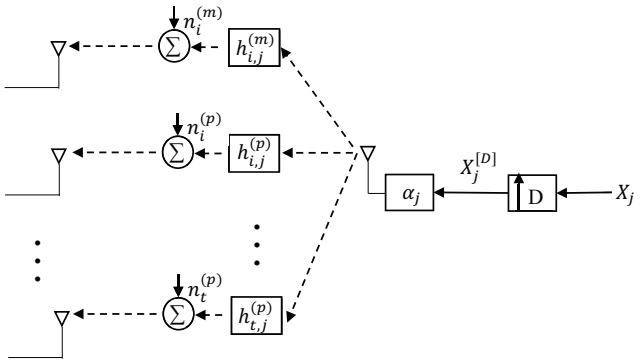

Figure 3.4: TD j to All Corresponding RRHs

sequence Y_j. The noise is assumed to be zero-mean additive white gaussian noise with variance $E[|n_j[k]|^2] = \sigma^2, \ \forall j, k$. In the next section, we will investigate the received signal Y_j to analyze the performance of the proposed system in the downlink phase.

3.1.4 The Uplink Transmission Architecture

In the uplink transmission, as shown in Fig. 3.4 and Fig. 3.5, there are two similar steps in the opposite direction: in step (1), the TDs simultaneously transmit the data through the multi-path channels to the corresponding RRHs; in step (2), the RRHs convert the RF signal into baseband signal, and quantize them before they are transmitted via the front-haul to the BBUs. The BBUs jointly process the received baseband signal to extract the uplink data.

In step 1, all the TDs simultaneously transmit the symbol sequences over the air to the corresponding RRHs. The intended symbol sequence $X_j[k]$ from the j-th TD is first up-sampled by the back-off factor D in order to alleviate the ISI and

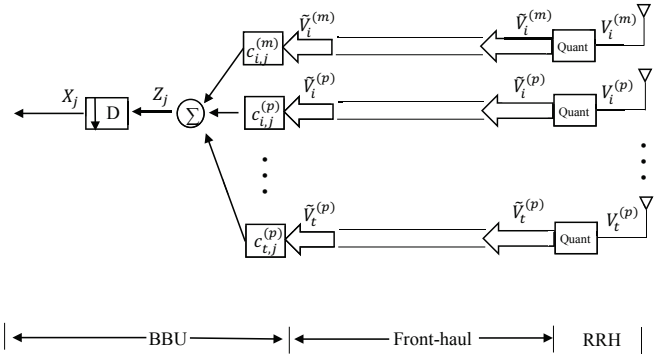

Figure 3.5: RRHs to BBUs through front-haul link

then scaled by the factor α_j before transmitted through the multi-path channel to all the corresponding RRHs. The purpose of the scaling factor α_j is to realize the power control. It is assumed that the values of α_j's are calculated by the BBUs and signaled to the TDs through the feedback/control channel. The signal received at the m-th antenna of RRH i is a combination of the signals from all the TDs that can reach RRH i and contaminated by the white Gaussian noise upon receiving,

$$V_i^{(m)}[k] = \sum_{j \in \mathbf{T}_i} \alpha_j \left(X_j^{[D]} * h_{i,j}^{(m)} \right)[k] + n_i^{(m)}[k] \tag{3.6}$$

where $n_i^{(m)}[k]$ is the AWGN with variance $E[|n_i^{(m)}[k]|^2] = \sigma^2, \ \forall i, k$.

The average power of the baseband signal $V_i^{(m)}[k]$ can be calculated as

$$E[\|V_i^{(m)}[k]\|^2] = \frac{\theta \cdot \sum_{j \in \mathbf{T}_i} \alpha_j^2 \sum_{l=0}^{L-1} \|h_{i,j}^{(m)}[l]\|^2}{D} + \sigma^2 \tag{3.7}$$

The signal received at the RRH is then quantized and transmitted to the BBU pool through the front-haul, which can be represented as

$$\tilde{V}_i^{(m)}[k] = V_i^{(m)}[k] + q_i^{(m)}[k] \tag{3.8}$$

where $q_i^{(m)}[k]$ is the quantization noise. Similar to the downlink case, $q_i^{(m)}[k]$ can

be approximated as a complex random variable whose real and imaginary parts are uniformly distributed in the range $(-\frac{Q_i^{(m)}}{2}, \frac{Q_i^{(m)}}{2})$. Note that although we use the same notation for the downlink and uplink quantization noise, they can be different due to distinction in the signal dynamic range and number of bits used.

Upon receiving the transmitted baseband signals from all the RRHs, the BBUs work together to extract the data of each TD. As shown in Fig. 3.5, the data of TD j is extracted by combining the baseband signals from all the antennas of all the corresponding RRHs. The signal from m-th antenna of the i-th RRH is first convolved with $c_{i,j}^{(m)}$ where

$$c_{i,j}^{(m)}[k] = \frac{h_{i,j}^{(m)*}[L-1-k]}{\sqrt{\sum_{l=0}^{L-1} \|h_{i,j}^{(m)*}[l]\|^2}}, \quad k = 0, 1, \cdots, L-1. \tag{3.9}$$

After that, the processed signal from all the antennas of all the corresponding RRHs are combined as

$$Z_j[k] = \sum_{i \in R_j} \sum_{m=1}^{M_T} c_{i,j}^{(m)} * \tilde{V}_i^{(m)}[k]. \tag{3.10}$$

In section 3.3, we will look into the signal $Z_j[k]$ to investigate the uplink performance of the proposed system.

3.2 Downlink Performance Analysis

In this section, we analyze the performance of the proposed system from two perspectives, the spectral efficiency and the data rate in the front-haul. The spectral efficiency indicates how efficiently the proposed system uses the available spectrum, and the data rate in the front-haul evaluates how much capacity is necessary to deploy the proposed system.

3.2.1 Spectral Efficiency

Since all the RRHs and TDs work in the same spectrum, the signal received by each TD is a mixture of the intended signal, interference and noise. The signal received by TD j can be represented as

$$\begin{aligned} Y_j[k] &= a_j \sum_{i\in\mathbf{R}_j} \sum_{m=1}^{M_T} \tilde{S}_i^{(m)} * h_{i,j}^{(m)}[k] + a_j n_j[k] \\ &= a_j \sum_{i\in\mathbf{R}_j} \sum_{m=1}^{M_T} \sum_{t\in\mathbf{T}_i} X_t^{[D]} * g_{i,t}^{(m)} * h_{i,j}^{(m)}[k] \\ &\quad + a_j \sum_{i\in\mathbf{R}_j} \sum_{m=1}^{M_T} q_i^{(m)} * h_{i,j}^{(m)}[k] + a_j n_j[k], \end{aligned} \tag{3.11}$$

where, in the last equality, the first term is the intended signal combined with the interference, the second term is the received quantization noise, and the third term is the white Gaussian noise. In the following, we will analyze the first and second term subsequently.

The first term can be further written as

$$\begin{aligned} & a_j \sum_{i\in\mathbf{R}_j} \sum_{m=1}^{M_T} \sum_{t\in\mathbf{T}_i} X_t^{[D]} * g_{i,t}^{(m)} * h_{i,j}^{(m)}[k] \\ &= a_j \sum_{i\in\mathbf{R}_j} \sum_{m=1}^{M_T} X_j^{[D]} * g_{i,j}^{(m)} * h_{i,j}^{(m)}[k] \\ &\quad + \sum_{i\in\mathbf{R}_j} \sum_{m=1}^{M_T} \sum_{\substack{l=0 \\ l\neq\frac{L-1}{D}}}^{\frac{2L-2}{D}} X_j[k + \frac{L-1}{D} - l] \cdot g_{i,j}^{(m)} * h_{i,j}^{(m)}[Dl] \\ &\quad + \sum_{i\in\mathbf{R}_j} \sum_{m=1}^{M_T} \sum_{\substack{t\in\mathbf{T}_i \\ t\neq j}} \sum_{l=0}^{\frac{2L-2}{D}} X_t[k + \frac{L-1}{D} - l] \cdot g_{i,t}^{(m)} * h_{i,j}^{(m)}[Dl]. \end{aligned} \tag{3.12}$$

The first term is the intended signal for TD j, the second term is the ISI, and the third term is the inter-user interference (IUI). Note that by the channel reciprocity

in the channel probing phase, for any RRH u with $u \notin \mathbf{R}_j$, TD j and RRH u can not reach each other and therefore TD j does not suffer from the interference from RRH u.

Since the one-tap gain a_j does not affect the SINR, we assume it as $a_j = 1$ in the subsequent analysis, without loss of generality.

The signal power in the downlink can be written as

$$\begin{aligned} P_{sig}^{(dl)} &= E_X[\| \sum_{i \in \mathbf{R}_j} \sum_{m=1}^{M_T} X_j[k] \cdot g_{i,j}^{(m)} * h_{i,j}^{(m)}[L-1] \|^2] \\ &= \theta \| \sum_{i \in \mathbf{R}_j} \sum_{m=1}^{M_T} g_{i,j}^{(m)} * h_{i,j}^{(m)}[L-1] \|^2. \end{aligned} \tag{3.13}$$

Accordingly, the ISI and IUI power can be written as

$$\begin{aligned} P_{isi}^{(dl)} &= E_X[\| \sum_{i \in \mathbf{R}_j} \sum_{m=1}^{M_T} \sum_{\substack{l=0 \\ l \neq \frac{L-1}{D}}}^{\frac{2L-2}{D}} X_j[k + \frac{L-1}{D} - l] \\ &\quad \cdot g_{i,j}^{(m)} * h_{i,j}^{(m)}[Dl] \|^2] \\ &= \theta \sum_{\substack{l=0 \\ l \neq \frac{L-1}{D}}}^{\frac{2L-2}{D}} \| \sum_{i \in \mathbf{R}_j} \sum_{m=1}^{M_T} g_{i,j}^{(m)} * h_{i,j}^{(m)}[Dl] \|^2, \end{aligned} \tag{3.14}$$

and

$$\begin{aligned} P_{iui}^{(dl)} &= E_X[\| \sum_{i \in \mathbf{R}_j} \sum_{m=1}^{M_T} \sum_{\substack{t \in \mathbf{T}_i \\ t \neq j}} \sum_{l=0}^{\frac{2L-2}{D}} X_t[k + \frac{L-1}{D} - l] \\ &\quad \cdot g_{i,t}^{(m)} * h_{i,j}^{(m)}[Dl] \|^2] \\ &= \theta \sum_{l=0}^{\frac{2L-2}{D}} \| \sum_{i \in \mathbf{R}_j} \sum_{m=1}^{M_T} \sum_{\substack{t \in \mathbf{T}_i \\ t \neq j}} g_{i,t}^{(m)} * h_{i,j}^{(m)}[Dl] \|^2. \end{aligned} \tag{3.15}$$

Next, we analyze the quantization noise in the received signal. From (3.11),

we can have the quantization noise power as

$$\begin{aligned}\sigma^2_{q,(dl)} &= E[\| \sum_{i\in\mathbf{R}_j} \sum_{m=1}^{M_T} q_i^{(m)} * h_{i,j}^{(m)}[k]\|^2] \\ &= E[\sum_{i\in\mathbf{R}_j} \sum_{m=1}^{M_T} \| \sum_{l=0}^{L-1} h_{i,j}^{(m)}[l] \cdot q_i^{(m)}[k-l]\|^2] \\ &= \sum_{i\in\mathbf{R}_j} \sum_{m=1}^{M_T} \sum_{l=0}^{L-1} \|h_{i,j}^{(m)}[l]\|^2 \cdot E[\|q_i^{(m)}[k]\|^2], \end{aligned} \tag{3.16}$$

since we assume that $q_i^{(m)}$ is independent of $h_{i,j}^{(m)}$. By [42], we have

$$E[\|q_i^{(m)}[k]\|^2] = \frac{(Q_i^{(m)})^2}{12} + \frac{(Q_i^{(m)})^2}{12} = \frac{(Q_i^{(m)})^2}{6} \tag{3.17}$$

which is the summation of the quantization noise power in the real and imaginary parts.

The spectral efficiency of the TD j can be defined as

$$r_j^{(dl)} = \log_2(1 + \frac{P_{sig}^{(dl)}}{P_{isi}^{(dl)} + P_{iui}^{(dl)} + \sigma^2_{q,(dl)} + \sigma^2})/D \tag{3.18}$$

3.2.2 Front-haul Rate

In this subsection, we analyze the front-haul rate in the proposed system in the downlink mode. As shown in Fig. 3.2, in the downlink mode, the quantized signal $\tilde{S}_i^{(m)}[k]$ is transmitted from the BBUs to the RRH through the front-haul. The data rate in the front-haul connecting the BBUs and the i-th RRH can be expressed as

$$R_{fh,i} = 2 \cdot W \cdot \sum_{m=1}^{M_T} B_i^{(m)} \tag{3.19}$$

where W is the bandwidth of the system. It can be seen that $R_{fh,i}$ is solely dependent on the number of bits used for each symbol given the bandwidth of the system and

the number of transmitting antennas. If $B_i^{(m)}$ is large, the power of the quantization noise goes down while the data rate in the front-haul increases, and vice versa if $B_i^{(m)}$ is small.

By (3.17), if the dynamic range $K_i^{(m)}$ of the signal grows, it needs to increase $B_i^{(m)}$ to keep the same quantization noise level. In section 3.4, we will show through numerical results that $K_i^{(m)}$ does not change much as the number of TDs in the system grows, and therefore the proposed system has a "tunneling" effect such that the front-haul rate keeps almost constant while serving more TDs.

3.3 Uplink Performance Analysis

In this section, we analyze the uplink performance of the proposed system in two perspectives: the spectral efficiency and the data rate in the front-haul.

3.3.1 Spectral Efficiency

The combined signal can be written as

$$\begin{aligned} Z_j[k] &= \sum_{i\in\mathbf{R}_j}\sum_{m=1}^{M_T} \tilde{V}_i^{(m)} * c_{i,j}^{(m)}[k] \\ &= \sum_{i\in\mathbf{R}_j}\sum_{m=1}^{M_T}\sum_{t\in\mathbf{T}_i} \alpha_t X_t^{[D]} * h_{i,t}^{(m)} * c_{i,j}^{(m)}[k] \\ &\quad + \sum_{i\in\mathbf{R}_j}\sum_{m=1}^{M_T} q_i^{(m)} * c_{i,j}^{(m)}[k] + \sum_{i\in\mathbf{R}_j}\sum_{m=1}^{M_T} n_i^{(m)} * c_{i,j}^{(m)}[k] \end{aligned} \tag{3.20}$$

where the first term is the mixture of the intended signal and interference for TD j, the second term is caused by the quantization noise and the third term is caused by the white Gaussian noise. In the following, we will analyze them subsequently.

The first term can be further written as

$$\begin{aligned}
&\sum_{i\in\mathbf{R}_j}\sum_{m=1}^{M_T}\sum_{t\in\mathbf{T}_i}\alpha_t X_t^{[D]} * h_{i,t}^{(m)} * c_{i,j}^{(m)}[k] \\
&= \sum_{i\in\mathbf{R}_j}\sum_{m=1}^{M_T}\alpha_j X_j^{[D]} * h_{i,j}^{(m)} * c_{i,j}^{(m)}[k] \\
&+ \sum_{i\in\mathbf{R}_j}\sum_{m=1}^{M_T}\sum_{\substack{l=0 \\ l\neq\frac{L-1}{D}}}^{\frac{2L-2}{D}}\alpha_j X_j[k+\frac{L-1}{D}-l]\cdot h_{i,j}^{(m)} * c_{i,j}^{(m)}[Dl] \\
&+ \sum_{i\in\mathbf{R}_j}\sum_{m=1}^{M_T}\sum_{\substack{t\in\mathbf{T}_i \\ t\neq j}}\sum_{l=0}^{\frac{2L-2}{D}}\alpha_t X_t[k+\frac{L-1}{D}-l]\cdot h_{i,t}^{(m)} * c_{i,j}^{(m)}[Dl]. \qquad (3.21)
\end{aligned}$$

The first term in (3.21) is the intended signal from TD j, the second term is the ISI, and the third term is the IUI.

The signal power in the uplink can be written as

$$\begin{aligned}
P_{sig}^{(ul)} &= E_X[\|\sum_{i\in\mathbf{R}_j}\sum_{m=1}^{M_T}\alpha_j X_j[k]\cdot h_{i,j}^{(m)} * c_{i,j}^{(m)}[L-1]\|^2] \\
&= |\alpha_j|^2\theta\|\sum_{i\in\mathbf{R}_j}\sum_{m=1}^{M_T} h_{i,j}^{(m)} * c_{i,j}^{(m)}[L-1]\|^2, \qquad (3.22)
\end{aligned}$$

where $\theta = E[\|X_j[k]\|^2]$. Accordingly, the ISI and IUI power can be written as

$$\begin{aligned}
P_{isi}^{(ul)} =& E_X[\|\sum_{i\in\mathbf{R}_j}\sum_{m=1}^{M_T}\sum_{\substack{l=0 \\ l\neq\frac{L-1}{D}}}^{\frac{2L-2}{D}}\alpha_j X_j[k+\frac{L-1}{D}-l] \\
&\cdot h_{i,j}^{(m)} * c_{i,j}^{(m)}[Dl]\|^2] \\
&= |\alpha_j|^2\theta\sum_{\substack{l=0 \\ l\neq\frac{L-1}{D}}}^{\frac{2L-2}{D}}\|\sum_{i\in\mathbf{R}_j}\sum_{m=1}^{M_T} h_{i,j}^{(m)} * c_{i,j}^{(m)}[Dl]\|^2, \qquad (3.23)
\end{aligned}$$

and

$$P_{iui}^{(ul)} =$$

$$E_X[\| \sum_{i\in\mathbf{R}_j} \sum_{m=1}^{M_T} \sum_{\substack{t\in\mathbf{T}_i \\ t\neq j}} \sum_{l=0}^{\frac{2L-2}{D}} \alpha_t X_t[k + \frac{L-1}{D} - l]$$

$$\cdot h_{i,t}^{(m)} * c_{i,j}^{(m)}[Dl]\|^2]$$

$$= \theta \sum_{l=0}^{\frac{2L-2}{D}} \| \sum_{i\in\mathbf{R}_j} \sum_{m=1}^{M_T} \sum_{\substack{t\in\mathbf{T}_i \\ t\neq j}} \alpha_t \cdot h_{i,t}^{(m)} * c_{i,j}^{(m)}[Dl]\|^2. \tag{3.24}$$

We assume the α_j is chosen as

$$\alpha_j = \frac{\eta}{\sum_{i\in\mathbf{R}_j} \sum_{m=1}^{M_T} h_{i,j}^{(m)} * c_{i,j}^{(m)}[L-1]} \tag{3.25}$$

where η is a scalar common for all the TDs. In this way, $\alpha_j \cdot \sum_{i\in\mathbf{R}_j} \sum_{m=1}^{M_T} h_{i,j}^{(m)} * c_{i,j}^{(m)}[L-1]$ is common for all the TDs, which ensures that the signal power for all the TDs are the same according to (3.22). The parameter η can be adjusted according to the maximum transmitting power allowed at each TD.

Next, we analyze the quantization noise in the received signal. From (3.20), we can have the quantization noise power as

$$\begin{aligned}
\sigma_{q,(ul)}^2 &= E[\| \sum_{i\in\mathbf{R}_j} \sum_{m=1}^{M_T} q_i^{(m)} * c_{i,j}^{(m)}[k]\|^2] \\
&= E[\sum_{i\in\mathbf{R}_j} \sum_{m=1}^{M_T} \| \sum_{l=0}^{L-1} c_{i,j}^{(m)}[l] \cdot q_i^{(m)}[k-l]\|^2] \\
&= \sum_{i\in\mathbf{R}_j} \sum_{m=1}^{M_T} \sum_{l=0}^{L-1} \|c_{i,j}^{(m)}[l]\|^2 \cdot E[\|q_i^{(m)}[k]\|^2],
\end{aligned} \tag{3.26}$$

since we can assume that $q_i^{(m)}$ is independent of $c_{i,j}^{(m)}$. Similar to the downlink scenario, we have

$$E[\|q_i^{(m)}[k]\|^2] = \frac{(Q_i^{(m)})^2}{12} + \frac{(Q_i^{(m)})^2}{12} = \frac{(Q_i^{(m)})^2}{6}. \tag{3.27}$$

The last term in (3.20) is the AWGN collected from all the corresponding antennas of TD j. Its power can be calculated by

$$\sigma^2_{n,(ul)} = E[\| \sum_{i \in \mathbf{R}_j} \sum_{m=1}^{M_T} n_i^{(m)} * c_{i,j}^{(m)}[k] \|^2] = |\mathbf{R}_j| * M_T * \sigma^2 \tag{3.28}$$

where $|\mathbf{R}_j|$ stands for the cardinality of the set $\mathbf{R}_j$. We can see that the AWGN functions differently in the downlink and uplink. In the downlink, since the AWGN affects the TD when the TD receives the signal, it does not depend on the number of corresponding antennas. On the other hand, in the uplink, since the AWGN is gathered when each of the corresponding antennas receives the signal, the noise power scales up with the number of corresponding antennas.

The spectral efficiency of the TD j in the uplink can be defined as

$$r_j^{(ul)} = \log_2(1 + \frac{P_{sig}^{(ul)}}{P_{isi}^{(ul)} + P_{iui}^{(ul)} + \sigma^2_{q,(ul)} + \sigma^2_{n,(ul)}})/D \tag{3.29}$$

3.3.2 Front-haul Rate

In this subsection, we analyze the front-haul rate in the proposed system in the uplink mode. As shown in Fig. 3.4, in the uplink mode, the quantized signal $\tilde{V}_i[k]$ is transmitted from the RRH to the BBU through the front-haul. Similar to the downlink case, the data rate in the front-haul can be expressed as

$$R_{fh,i} = 2 \cdot W \cdot \sum_{m=1}^{M_T} B_i^{(m)}. \tag{3.30}$$

Similar to the downlink mode, $R_{fh,i}$ is solely dependent on the number of bits used for each symbol given the bandwidth of the system and the number of transmitting

antennas. If $B_i^{(m)}$ is large, the power of the quantization noise goes down while the data rate in the front-haul increases, and vice versa if $B_i^{(m)}$ is small.

By (3.27), if the dynamic range $K_i^{(m)}$ of the signal grows, it needs to increase $B_i^{(m)}$ to keep the same quantization noise level. In the uplink, the total baseband signal power is dependent on the number of TDs, which is different from the downlink scenario. Therefore, when the number of TDs increases in the system, the dynamic range $K_i^{(m)}$ grows, where more bits are needed to keep the same quantization noise level.

In the next section, we will show through numerical results how $K_i^{(m)}$ and $B_i^{(m)}$ change with the number of TDs in the system.

3.4 Performance Evaluation

In this section, we evaluate the performance of the proposed system using measured channels. We first introduce the experimental setting where we measure the multi-path channels. Then we show some numerical results obtained by using the measured channels.

3.4.1 Channel Measurement

The experimental setting is the same as that described in section 2.6 of this dissertation where 4800 independent channel measurements from the indoor environment are obtained. The following numerical results are based on these channel measurements.

3.4.2 Downlink Front-haul Rate and Spectral Efficiency

In this subsection, we show the unique features of the proposed system in the downlink through numerical results. We first show that the front-haul rate keeps almost constant independent of the number of TDs in the system, after which we show the achievable spectral efficiency of the system under various settings in deployment and load. We also compare the result with the C-RAN based on LTE to show the advantage of the proposed system in being able to utilize the wireless channel more efficiently.

In Fig. 3.6 and 3.7, we generate the baseband signal $S_i^{(m)}[k]$ according to (3.3) using the measured channels and show the complementary cumulative distribution function (CCDF) [43] of the peak to average power ratio (PAPR) of the signal $S_i^{(m)}[k]$ in-band (I) and quadrature (Q) parts under various conditions. The $X_j[k]$'s are QPSK modulated. Let $N_i = \|\mathbf{T}_i\|$ denote the number of TDs subscribed to RRH i, and it is shown that the PAPR of the $S_i^{(m)}[k]$ does not change much with N_i. For example, if we look at the dotted horizontal line at $CCDF = 0.05$, it always crosses the curves at around 6 db. The detailed statistics are shown in Table 3.1. It means 95% of the baseband symbols $S_i^{(m)}[k]$ have the power no more than 4 times the average power. By (3.4), the average power of $S_i^{(m)}[k]$ is only dependent on θ and D. Therefore, the dynamic range $[-K_i^{(m)}, K_i^{(m)}]$ of $S_i^{(m)}[k]$ changes very little for different N_i's, where some $B_i^{(m)}$ can be used to always maintain the same level of quantization noise power. As a result, the data rate in each front-haul link is constant.

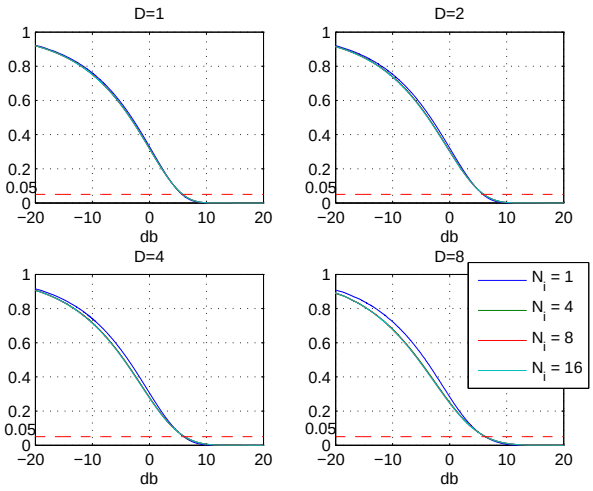

Figure 3.6: The CCDF of Downlink QPSK Baseband Signal PAPR (I)

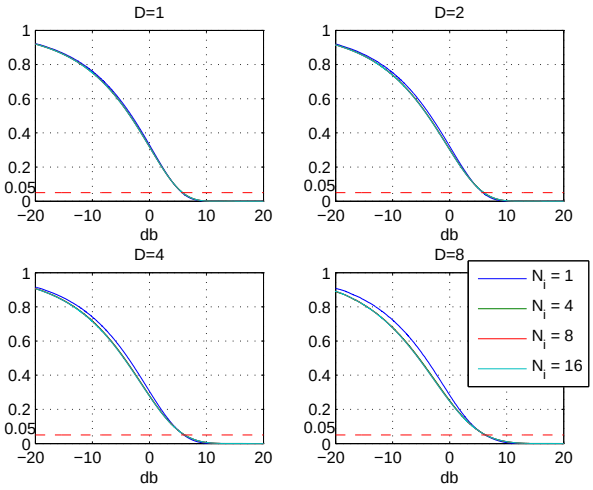

Figure 3.7: The CCDF of Downlink QPSK Baseband Signal PAPR (Q)

Next, we evaluate the spectral efficiency of the system with different number of RRHs and TDs. For each single channel realization, the $P_{sig}^{(dl)}$, $P_{isi}^{(dl)}$, $P_{iui}^{(dl)}$, and $\sigma_{q,(dl)}^2$ can be calculated by (3.13), (3.14), (3.15) and (3.16). By plugging them into (3.18), the spectral efficiency of each individual TD can be calculated. By averaging over all the channel realizations, we show the average and sum spectral efficiency in Fig. 3.8 through 3.11.

As shown in the figures, for each given number of RRHs in this system, the individual spectral efficiency decreases with more TDs in the system, while the sum spectral efficiency increases with more TDs in the system. Note that by previous analysis, the data rate in the front-haul keeps constant. It means that more information can be transmitted in the front-haul link with the same amount of bits and energy consumed. The reason is that by using TR-based air interface, multiple TDs

Table 3.1: the 5% PAPR for Different N_i's in Downlink (db)

	$N_i = 1$	$N_i = 4$	$N_i = 8$	$N_i = 16$
D = 1, (I)	5.74	5.86	6.06	6.26
D = 1, (Q)	5.74	5.88	6.06	6.26
D = 2, (I)	5.86	6.02	6.22	6.36
D = 2, (Q)	5.86	6.04	6.22	6.36
D = 4, (I)	5.88	6.04	6.24	6.36
D = 4, (Q)	5.86	6.04	6.22	6.36
D = 8, (I)	5.88	6.04	6.24	6.36
D = 8, (Q)	5.88	6.04	6.22	6.36

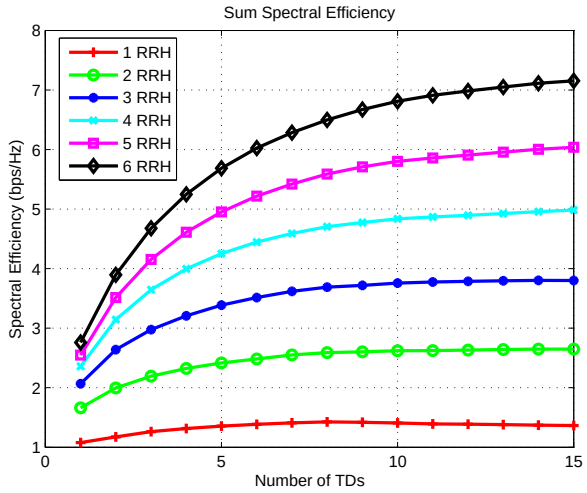

Figure 3.8: The Sum Spectral Efficiency (D=1)

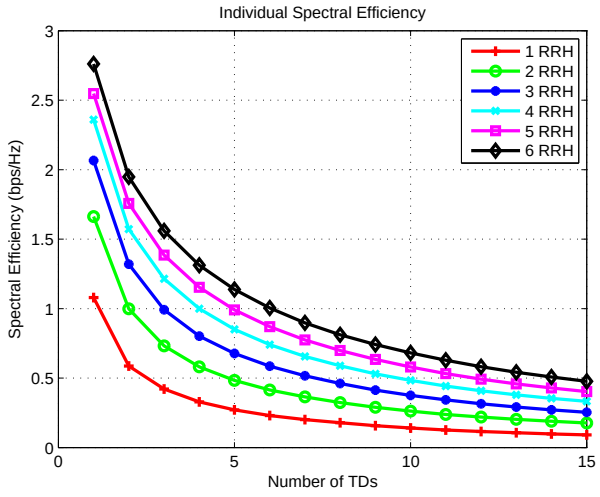

Figure 3.9: The Individual Spectral Efficiency (D=1)

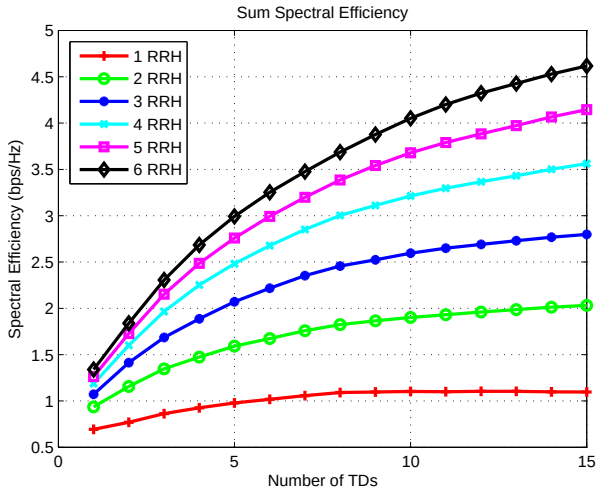

Figure 3.10: The Sum Spectral Efficiency (D=4)

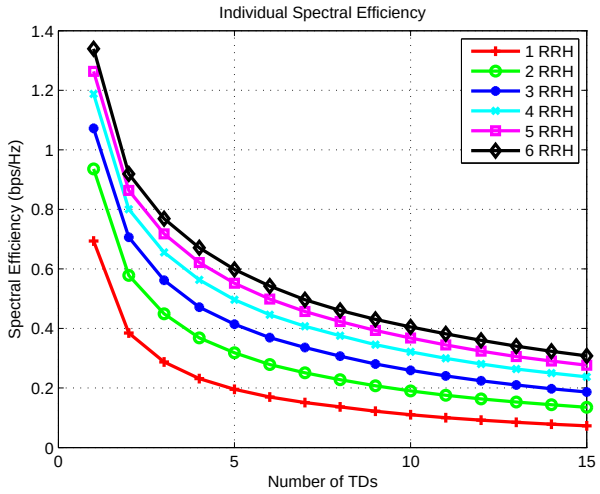

Figure 3.11: The Individual Spectral Efficiency (D=4)

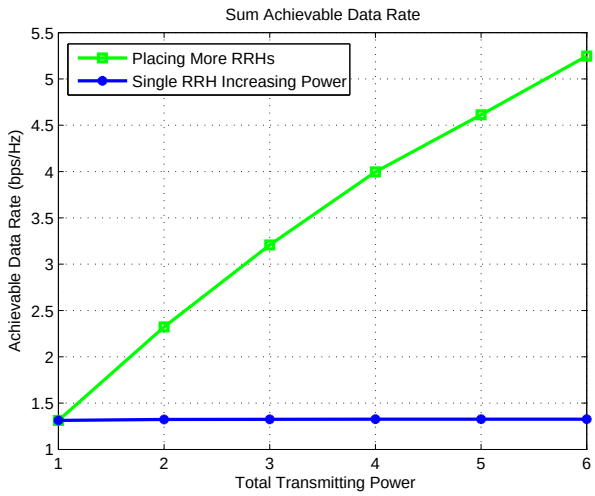

Figure 3.12: The Comparison between Adding More RRHs and Single RRH Increasing Power

are naturally separated by the location-specific signatures. Therefore, even though the baseband signals for multiple TDs are mixed together in the front-haul link, they can still be separated when transmitted through the air interface. In other words, with the TR-based air interface, we are able to create a "tunnel" in the front-haul link such that the baseband signals can be efficiently combined to alleviate the traffic in front-haul.

Moreover, it can be observed that both the individual and sum spectral efficiency are improved if more RRHs are added into this system. The new RRHs contribute both extra power and degree of freedom to the system. The extra power alleviates the influence of the quantization and environmental noise, while the extra degree of freedom helps enhancing the focusing effect [15] and thus mitigating the interference. Usually, in a dense wireless network, the interference is the dominating factor that limits the performance of the system. To illustrate this phenomenon,

we compare the effect of adding in more RRHs with that of increasing the power of a single RRH. As it can be seen from Fig. 3.12, the blue curve shows that by just increasing the power of one single RRH, the spectral efficiency keeps almost constant, while the green curve shows that by adding in more RRHs, the spectral efficiency is improved significantly.

3.4.3 Uplink Front-haul Rate and Spectral Efficiency

In this subsection, we show through numerical results to illustrate the effectiveness of the proposed system in the uplink.

In Fig. 3.13 and 3.14, we generate the baseband signal $V_i^{(m)}[k]$ according to (3.6) using the measured channels and show the CCDF of the PAPR of both I and Q parts of the signal $V_i^{(m)}[k]$ under various conditions. The $X_j[k]$'s are QPSK modulated. It is shown that the PAPR of $V_i^{(m)}[k]$ does not change much with the number of TDs subscribed to the RRH i. Similarly, the $CCDF = 0.05$ line always crosses the CCDF curves at around 6 db. The detailed statistics are shown in Table 3.2. It means 95% of the baseband symbols $V_i^{(m)}[k]$ have the power no more than 4 times the average power. By plugging (3.25) into (3.7), the average power of $V_i^{(m)}[k]$ can be calculated as

$$E[\|V_i^{(m)}[k]\|^2] = \\ \frac{\eta^2\theta}{D} \cdot \sum_{j\in\mathbf{T}_i} \cdot \frac{\sum_{l=0}^{L-1} \|h_{i,j}^{(m)}\|^2}{(\sum_{t\in\mathbf{R}_j} \sum_{m=1}^{M_T} h_{t,j}^{(m)} * c_{t,j}^{(m)}[L-1])^2} + \sigma^2, \tag{3.31}$$

which grows approximately linearly with N_i. Therefore, the dynamic range $[-K_i^{(m)}, K_i^{(m)}]$ of $V_i^{(m)}[k]$ increases linearly with $\sqrt{N_i}$. In order to maintain the same level of quan-

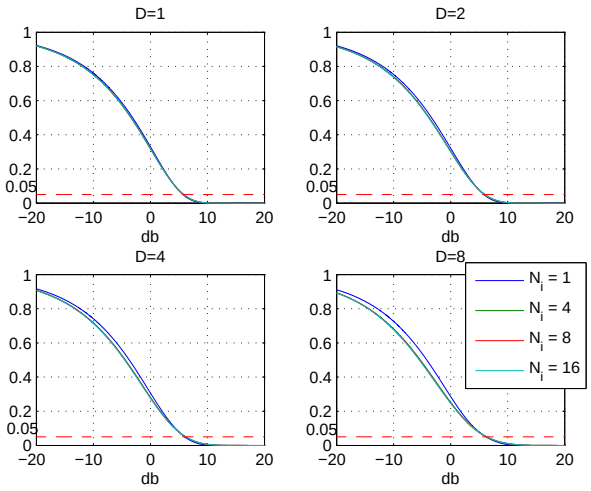

Figure 3.13: The CCDF of Uplink QPSK Baseband Signal PAPR (I)

tization noise power, more bits are needed to represent $V_i^{(m)}[k]$. However, since $Q_i^{(m)} = \frac{2K_i^{(m)}}{2^{B_i^{(m)}}}$, in order to maintain the same level of quantization noise power, $B_i^{(m)}$ grows to the order of $\log_2(K_i^{(m)})$ and thus $\log_2(\sqrt{N_i})$. For example, $E[\|q_i^{(m)}[k]\|^2]$ is the same for $B_i^{(m)} = 12, N_i = 1$ and $B_i^{(m)} = 14, N_i = 16$. In other words, when there are more TDs in the system, it is necessary to use slightly more bits in the front-haul link, which is much less significant compared to the increase of the number of TDs.

Similar to the downlink scenario, we evaluate the spectral efficiency of uplink by averaging over all the channel realizations. We slightly increase $B_i^{(m)}$ when it is necessary to keep the same level of quantization noise power. We show the average and sum spectral efficiencies under various conditions in Fig. 3.15 through Fig. 3.18 and observe similar trends as in downlink.

Similar to the downlink scenario, the "tunneling" effect is also observed in the uplink case. When there are more TDs in the system, with using almost the same amount of bits in the front-haul link, more information can be extracted at the BBU

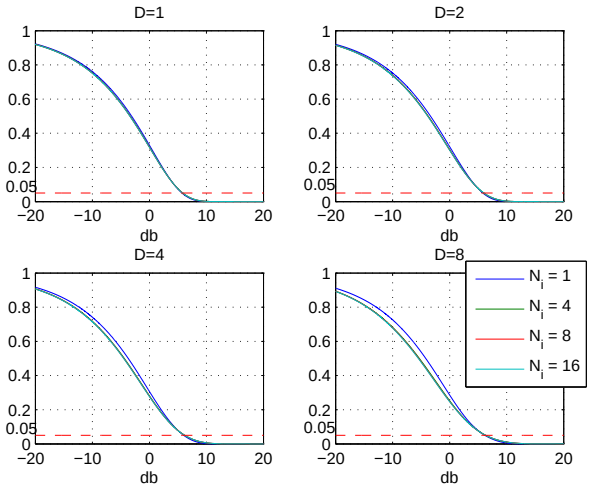

Figure 3.14: The CCDF of Uplink QPSK Baseband Signal PAPR (Q)

Table 3.2: the 5% PAPR for Different N_i's in Uplink (db)

	$N_i = 1$	$N_i = 4$	$N_i = 8$	$N_i = 16$
D = 1, (I)	5.74	5.86	6.06	6.22
D = 1, (Q)	5.74	5.88	6.06	6.22
D = 4, (I)	5.86	6.02	6.22	6.34
D = 4, (Q)	5.86	6.02	6.22	6.36
D = 8, (I)	5.88	6.04	6.22	6.36
D = 8, (Q)	5.86	6.04	6.22	6.36
D = 16, (I)	5.88	6.04	6.24	6.36
D = 16, (Q)	5.88	6.04	6.22	6.36

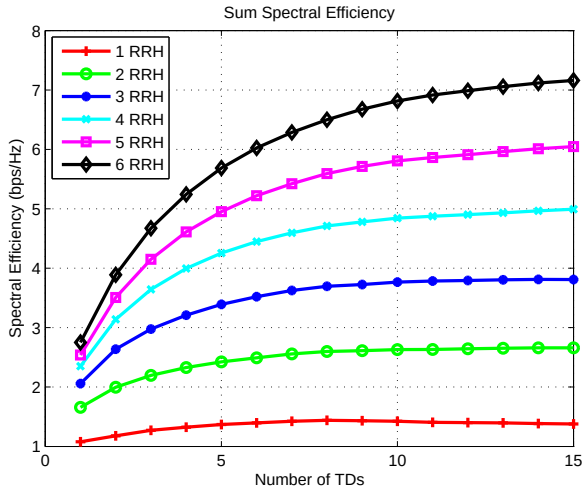

Figure 3.15: The Sum Spectral Efficiency (D=1)

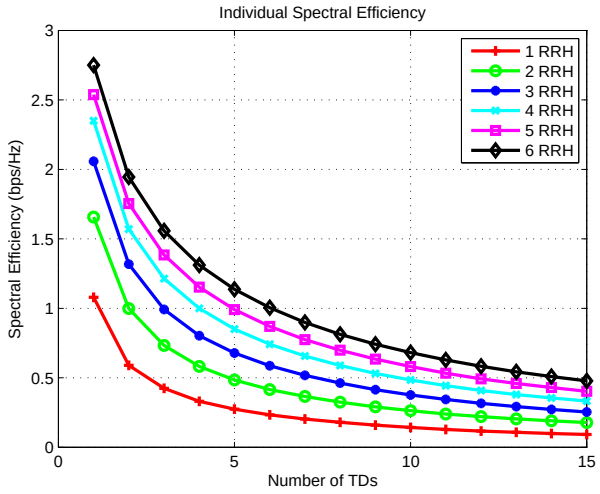

Figure 3.16: The Individual Spectral Efficiency (D=1)

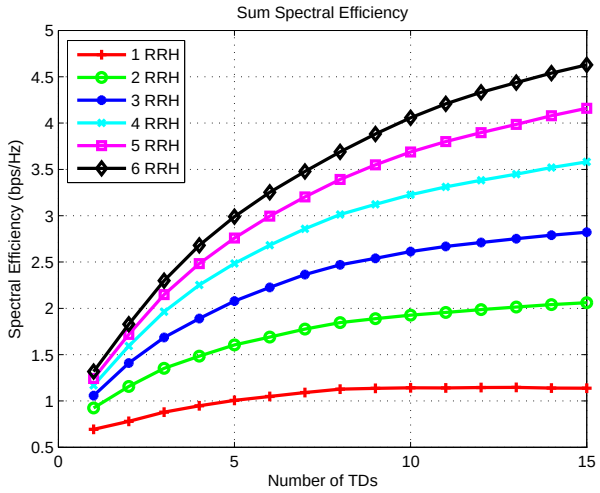

Figure 3.17: The Sum Spectral Efficiency (D=4)

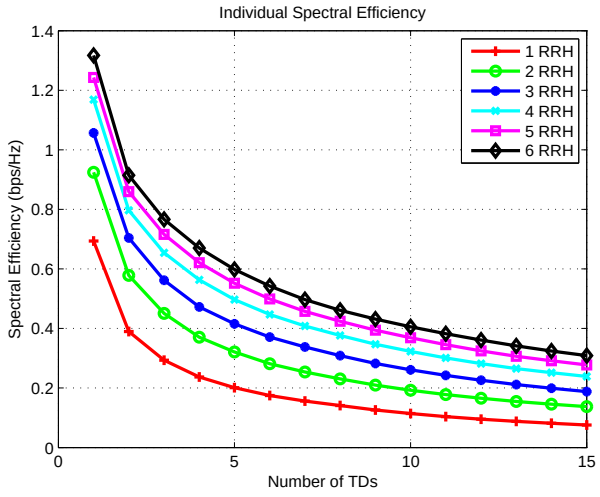

Figure 3.18: The Individual Spectral Efficiency (D=4)

side.

3.4.4 Comparison with LTE based C-RAN

To illustrate the advantage of the TR "tunneling" effect in the C-RAN, in this subsection, we compare the proposed system with LTE based C-RAN in multiple scenarios.

Suppose we have a certain number of RRHs distributed in an area where there are N TDs and each of them has Ω bits of data to be transmitted. We first consider the donwlink. In the LTE based C-RAN, all the RRHs work in separate bands, and each of the RRHs is responsible for serving part of the TDs. Since each RRH serves multiple TDs by dividing the time and/or frequency resource, the baseband signals for multiple TDs cannot be mixed together. As a result, the total amount of baseband signal is proportional to $N \times \Omega$, which can be approximated by $\phi_N^{(dl)} = N \times \Omega \times \lambda^{(dl)}$ where $\lambda^{(dl)}$ is some constant accounting for the modulation and channel coding. On the other hand, in the TR based C-RAN, as analyzed in section 3.4.2, the data for multiple TDs can be efficiently combined without increasing the traffic in the front-haul. As a result, the total amount of baseband signal transmitted in the front-haul link is constant independent of N, which can be approximated by $\varphi_N^{(dl)} = \Omega \times \mu^{(dl)}$ where $\mu^{(dl)}$ is some constant accounting for the modulation and channel coding. We define $\tau_N^{(dl)} = \frac{\phi_N^{(dl)}}{\phi_1^{(dl)}}$ and $\upsilon_N^{(dl)} = \frac{\varphi_N^{(dl)}}{\varphi_1^{(dl)}}$ to characterize the growth of data transmitted in the front-haul caused by increasing the number of TDs.

In the uplink, the LTE works by single-carrier frequency division multiple

access (SC-FDMA) [44], where multiple TDs are separated by the division of the frequency resource. As a result, the aggregate data transmitted in the front-haul is also proportional to $N \times \Omega$, and $\tau_N^{(ul)}$ is the same as the $\tau_N^{(dl)}$. On the other hand, in the TR based C-RAN, as analyzed in section 3.4.3, the data transmitted in the front-haul only increases slightly. We define $\varphi_N^{(ul)} = \Omega \times B_N^{(ul)} \times \mu^{(ul)}$ where $B_N^{(ul)}$ is the average number of bits to represent a baseband signal symbol when there are N TDs, and similarly $\upsilon_N^{(ul)} = \frac{\varphi_N^{(ul)}}{\varphi_1^{(ul)}}$. In this example, we have $B_1^{(ul)} = 12$ and $B_N^{(ul)}$ is increased when necessary according to the analysis in section 3.3.2.

In Fig. 3.19, we show the $\tau_N^{(dl)}$, $\tau_N^{(ul)}$, $\upsilon_N^{(dl)}$ and $\upsilon_N^{(ul)}$ with different N's. It is illustrated that in both downlink and uplink, the total amount of data transmitted in the front-haul of LTE based C-RAN increases linearly with the number of TDs. In contrast, the total amount of data transmitted in the front-haul of TR based C-RAN keeps constant in the downlink regardless of the number of TDs, while only slightly increases in the uplink. It is due to the unique "tunneling" effect such that more information can be transmitted with nearly the same amount of bits consumed in the front-haul.

We also compare the spectral efficiency of the proposed system with that of LTE based C-RAN. Suppose there are N TDs distributed in an area to be served. We gradually add in extra RRHs to the C-RAN. In the TR based C-RAN, the extra RRHs mainly help enhance the focusing effect and thus improve the spectral efficiency. More specifically, we define $r_{M,N}^{(avg)}$ as the average spectral efficiency of an individual TD when there are M RRHs and N TDs in the system. To evaluate the

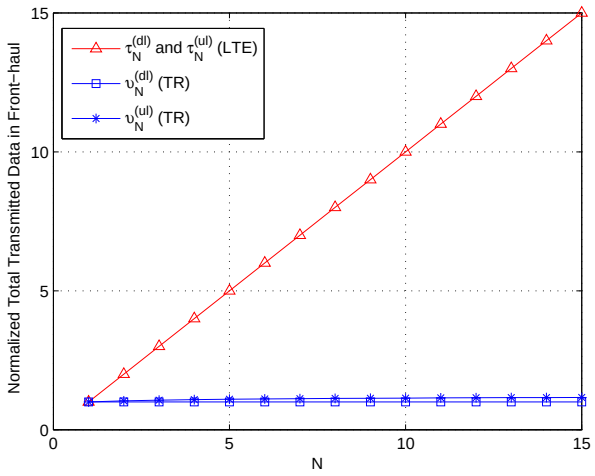

Figure 3.19: The Comparison of Normalized Total Transmitted Data in Front-haul between TR based C-RAN and LTE based C-RAN

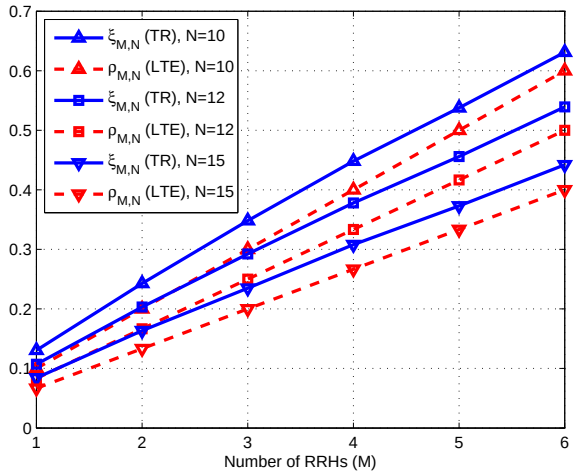

Figure 3.20: The Comparison of Normalized Effective Individual Spectral Efficiency between TR based C-RAN and LTE based C-RAN

effect of adding in extra RRHs and TDs, we define

$$\xi_{M,N} = \frac{r_{M,N}^{(avg)}}{r_{1,1}^{(avg)}}, \tag{3.32}$$

which normalizes the average spectral efficiency to that when the wireless channel is exclusively used by a single pair of RRH and TD.

On the other hand, in the LTE based C-RAN, we assume that each TD is associated with only one RRH and multiple RRHs work in separate bands. The extra RRHs will offload part of the TDs from the existing RRHs, and thus each TD has an improved chance of being scheduled. Similar to the TR-based C-RAN, we define the effective average spectral efficiency $\delta_{M,N}^{(avg)} = C_{M,N}^{(avg)} \cdot \beta_{M,N}^{(avg)}$ where $\beta_{M,N}^{(avg)}$ is the average portion of time and frequency resource that a single TD shares when there are M RRHs and N TDs, and $C_{M,N}^{(avg)}$ is the average spectral efficiency of a TD conditioning on it is scheduled and allocated the entire time and frequency resource of a RRH. Since the RRHs work in separate bands, $C_{M,N}^{(avg)}$ does not change with M or N, and $\beta_{M,N}^{(avg)} = \min(\frac{M}{N}, 1)$. Similarly, we define

$$\rho_{M,N} = \frac{\delta_{M,N}^{(avg)}}{\delta_{1,1}^{(avg)}} \tag{3.33}$$

in order to evaluate the effect of adding in extra RRHs and TDs.

We plot $\xi_{M,N}$ and $\rho_{M,N}$ for multiple combinations of M and N in Fig. 3.20. It is observed that $\xi_{M,N}$ is above $\rho_{M,N}$ for each combination. Note that the achievable data rate of a TD is the product of the spectral efficiency and the bandwidth. We define the achievable downlink data rate of a single TD in the TR based C-RAN as $R_{M,N}^{TR} = r_{M,N}^{(avg)} \times W^{TR}$ where W^{TR} is the bandwidth that a TR based TD utilizes, and the achievable downlink data rate of a single TD in the LTE based C-RAN as

$R_{M,N}^{LTE} = \delta_{M,N}^{(avg)} \times W^{LTE}$ where W^{LTE} is the bandwidth that a LTE based TD utilizes. In the TR based system, since larger bandwidth can be easily utilized with much reduced cost [45], the $R_{1,1}^{TR}$ can be greater than $R_{1,1}^{LTE}$ by utilizing larger bandwidth. For example, in this experiment, $W^{TR} = 125MHz$ and $W^{LTE} = 20MHz$. By $\xi_{M,N}$ and $\rho_{M,N}$ in Fig. 3.20 where $r_{M,N}^{(avg)}$ and $\delta_{M,N}^{(avg)}$ are normalized to $r_{1,1}^{(avg)}$ and $\delta_{1,1}^{(avg)}$, $R_{M,N}^{TR}$ will be greater than $R_{M,N}^{LTE}$ for any M and N. It means that the TR-based C-RAN is able to more efficiently utilize the wireless channel in the multiple-RRH and multiple-TD setting.

3.5 Conclusion

In this chapter, we proposed a time-reversal (TR) based cloud radio access network (C-RAN) architecture. Both the downlink and uplink working schemes were designed and analyzed. Through analysis, we discovered the TR "tunneling effects" in the proposed C-RAN architecture, i.e., the baseband signals for multiple terminal devices (TDs) can be efficiently combined and transmitted in the front-haul link to alleviate the traffic load. We built a TR radio prototype to measure the wireless channel in the real-world environment, with which we illustrated the "tunneling" effect in both downlink and uplink of the proposed C-RAN architecture. It is observed that for both downlink and uplink, the sum spectral efficiency of multiple TDs increases with the number of TDs in the system while the front-haul data rate keeps almost constant. Based on the nice properties shown in this chapter, the proposed TR-based C-RAN architecture serves as a promising solution to tackle

the challenge to the C-RAN front-haul link capacity caused by network densification.

Chapter 4: Waveforming for Time-Reversal Cloud Radio Access Network

In last chapter, the time-reversal (TR) communication has been proposed as the air interface in cloud radio access network (C-RAN) to alleviate the traffic in the front-haul links, where it creates unique "tunneling effects" such that more information can be transmitted with the same amount of traffic load when there are more terminal devices (TDs) to be served [46].

The TR communication has been shown to be able to boost the signal to noise ratio (SNR) by collecting most energy of the multipaths [19]. However, when the symbol duration is shorter than the delay spread of the multipath channel in high rate transmissions, the inter-symbol interference (ISI) may limit the performance of the system. Moreover, with network densification, e.g., in a C-RAN that needs to support a massive number of TDs, the severe inter-user interference (IUI) becomes the limiting factor that impairs both the spectral and energy efficiency. Therefore, it is very important to design effective interference management schemes to improve the spectral and power efficiency in TR communication systems. Algorithms for waveform design to maximize the sum achievable data rate in the downlink transmission was proposed in [19]. In [47], the authors designed an interference alignment

scheme aiming at managing the ISI in the single user case. In [17], a successive interference cancellation scheme was proposed to improve the performance in the uplink transmission. Nevertheless, these works only considered the case with single access point (AP) and one or more TDs, which might not be applicable to systems with multiple APs, e.g., a C-RAN architecture where multiple remote radio heads (RRHs) are expected to work together to deliver information.

In C-RAN, a lot works have been done to utilize the computing power at the baseband units (BBUs) to optimize both the downlink and uplink transmissions. In [48], a joint precoding and compression scheme was proposed to alleviate the effect of interference and quantization noise so as to maximize the weighted sum rate in the downlink transmission. In order to comply with the limited front-haul link capacity of each RRH, a sparse beamforming and clustering technique was proposed in [49]. In [50], the authors proposed a joint beamforming and compression scheme for the uplink transmission in C-RAN. Researchers also investigated the power consumption issues of C-RAN in [51] and [52]. However, to the best of our knowledge, no optimization technique is available for the "asymmetric" architecture of the TR based C-RAN, i.e., much of the complexity is moved to the BBU side while the TDs can be of very low complexity in both downlink and uplink transmissions. In the downlink transmission of a TR based system, the TDs detect the transmitted signal by single-tap detection, while in the uplink they directly transmit the symbols after simple amplification.

In this chapter, we aim to leverage all the available information and computing power at the BBUs to better manage the interference so that the transmissions in

the TR based C-RAN become more reliable and efficient. In the downlink, since the instantaneous channel impulse responses (CIRs) as well as the intended symbols of all the TDs are available at the BBUs, we propose algorithms that combine these information to optimally determine the power allocation and transmitting waveforms to minimize the mean square error (MSE) of the signal received by the TDs. In the uplink, since only the CIRs of all the TDs are available at the BBUs, we propose to utilize such information to optimize the receiver design as well as the transmitting power of all the TDs. All the proposed algorithms are guaranteed to converge. To illustrate the effectiveness of the proposed schemes, we conduct experiments to measure the multipath channel information in a real-world environment, based on which we show that the proposed schemes can significantly reduce the bit error rate (BER) of both downlink and uplink transmissions compared with using the basic TR waveforms. Moreover, since all these optimizations are performed in the BBUs, the asymmetric architecture of the TR communications are preserved, and the performance is improved without any change at the TD side.

The rest of the chapter is organized as follows: in section 4.1, both downlink and uplink transmission optimization problems are formulated; the downlink waveform design is optimized in section 4.2; the uplink detector and power control is optimized in section 4.3; numerical results are shown in section 4.4 and section 4.5 concludes this chapter.

4.1 System Models and Problem Formulations

In the time-reversal (TR) based cloud radio access network (C-RAN) [46] shown in Fig. 4.1, the terminal devices (TDs) periodically sends known sequences of waveforms to the remote radio heads (RRHs). The RRHs transmit the received baseband signal to the baseband units (BBUs), which then detects the channel impulse response (CIR) using the received signal. The CIR is considered as the transmitting waveform of the corresponding TD, and used by the BBUs for the downlink and uplink data transmissions.[1] In the downlink data transmission, the BBUs simply use the time-reversed version of the CIR as the symbol waveform to transmit the data symbols. After receiving the signal, the TD detects the transmitted symbols by looking at one sample of the received signal for each symbol. As a consequence, the complexity at the TD side can be very low while most of the computational burden is shifted to the BBUs. In the uplink data transmission, the TDs directly transmit the symbols through the multipath channel to the RRHs. The RRHs transmit the received signal through the front-haul links to the BBUs and the BBUs then convolve the received signal with the time-reversed version of the CIR of corresponding TDs to detect the symbols transmitted by the TDs. Although using basic TR waveform is simple and straightforward, it cannot achieve the opti-

[1] According to the analysis in [46], the time needed for transmitting the channel probing sequences takes approximately 0.1% of the total transmission time of a typical TD moving at walking speed. The system-wide overhead for obtaining the CIRs is approximately $N * 0.1\%$ where N is the total number of TDs that require frequent channel information update.

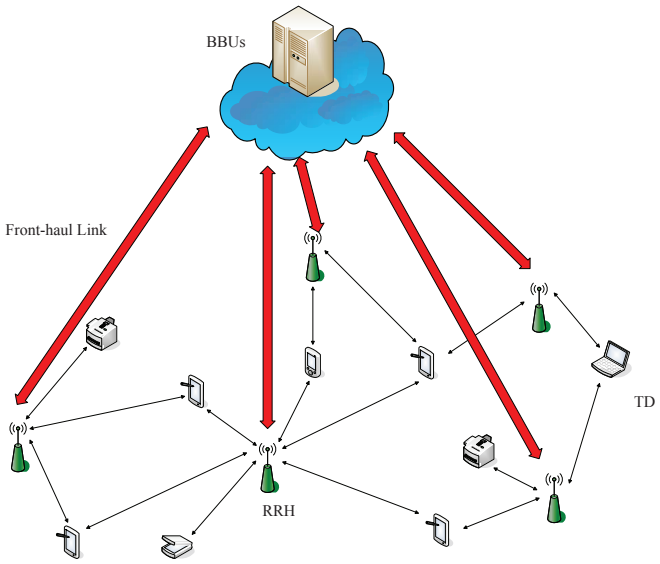

Figure 4.1: The System Model

mal performance, especially in the dense network where the inter-user interference (IUI) becomes the limiting factor. In this chapter, we focus on the waveform design problem to optimize both downlink and uplink data transmissions. The downlink and uplink waveform design problem will be formulated separately in the following.

4.1.1 Downlink Problem Formulation

We will first analyze the case that a single RRH serves multiple TDs. Let $h_{i,k}$ denote the multipath channel between the i-th RRH and the k-th TD, which is a vector of length L with L being the maximum channel length of all the N TDs. Let X_k and $g_{i,k}$ denote the information symbols and the transmit waveform for user k at RRH i. $g_{i,k}$ can be basic TR waveform or more advanced waveform. The length of $g_{i,k}$ is also L. In this chapter, we consider the frame-based transmission and reception schemes. The frame of symbols for user k is denoted by $X_k = [x_{k,1}, x_{k,2}, \cdots x_{k,F_k}]$

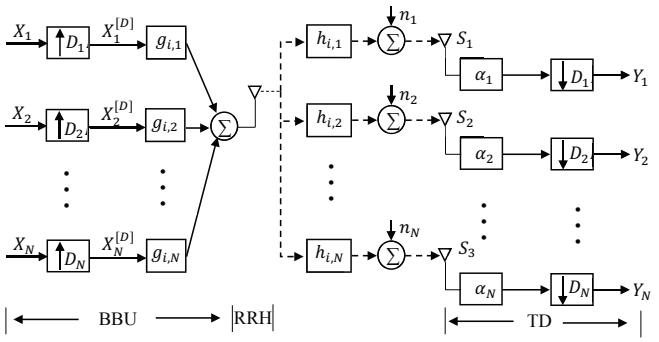

Figure 4.2: The Downlink Transmission Diagram

where F_k is the frame length of TD k. As shown Fig. 4.2, at RRH i, the X_k will be first upsampled by the backoff factor D_k for inter-symbol interference (ISI) alleviation. The upsampled symbol frame is denoted as $X_k^{[D_k]}$. After that, a blank sub-frame is appended to the end of the up-sampled signal to prevent the interference between frames. The length of the sub-frame is no less than L taps. Then, the entire frame is convolved with the downlink transmission signature $g_{i,k}$, after which the convoluted signal for all the TDs are summed up together and transmitted over the air to multiple TDs simultaneously.

The signal received at TD k can be represented as

$$S_k = h_{i,k} * \sum_{v=1}^{N} g_{i,v} * X_v^{[D_v]} + n_k, \tag{4.1}$$

where n_k is the noise vector with appropriate length. Without loss of generality, we assume $E[\|n_k[j]\|^2] = \sigma^2, \forall k, j$.

The k-th TD will first amplify the S_k with α_k and then down-sample it with the backoff factor D_k, obtaining the receiced sequence Y_k, based on which it will try

to detect X_k. The received sequence Y_k can be represented as

$$Y_k = \alpha_k M_k \cdot h_{i,k} * \sum_{v=1}^{N} g_{i,v} * X_v^{[D_v]} + \alpha_k M_k n_k, \tag{4.2}$$

where M_k is a masking matrix for TD k since only the sampled taps of the received signal are considered. More specifically,

$$M_k = [\mathbf{e}_L; \quad \mathbf{e}_{L+D_k}; \quad \cdots \quad \mathbf{e}_{L+(F_k-1)D_k}], \tag{4.3}$$

where $\mathbf{e}_i$ denotes the i-th row of the $(2L-1+(F_k-1)D_k) \times (2L-1+(F_k-1)D_k)$ identity matrix.

We define $H_{i,k}$ as the Toeplitz matrix of size $(2L-1) \times L$ with the first column being $[h_{i,k}^T \quad \mathbf{0}_{1\times(L-1)}]$, then Y_k can be further written as

$$Y_k = \alpha_k \cdot \tilde{B}_{i,k} g_i + \alpha_k \cdot M_k n_k, \tag{4.4}$$

where

$$g_i = \begin{pmatrix} g_{i,1} \\ g_{i,2} \\ \vdots \\ g_{i,N} \end{pmatrix} \tag{4.5}$$

is the aggregation of all the downlink transmission signature $g_{i,k}$'s of the RRH i. $\tilde{B}_{i,k}$ is the equivalent channel matrix combining both the channel information $h_{i,k}$'s and content information X_k's. More specifically,

$$\tilde{B}_{i,k} = M_k[\tilde{B}_{i,k}^{(1)} \quad \tilde{B}_{i,k}^{(2)} \quad \cdots \quad \tilde{B}_{i,k}^{(N)}], \tag{4.6}$$

where

$$\tilde{B}_{i,k}^{(t)} = \sum_{j=1}^{F_k} X_t[j] \cdot H_{i,k}^{(j)}, \tag{4.7}$$

and

$$H_{i,k}^{(j)} = \begin{pmatrix} \mathbf{0}_{(j-1)D_k \times L} \\ H_{i,k} \\ \mathbf{0}_{(F_k-j)D_k \times L} \end{pmatrix} \tag{4.8}$$

is the augmented matrix of $H_{i,k}$ with size $(2L-1+(F_k-1)D_k) \times L$.

In the TR communication system, due to the asymmetric architecture [16,17], all the computation complexity are migrated to the BBUs and the TDs have low complexity. In other words, the TDs are unable to perform sophisticated signal processing to detect the transmitted symbols. Due to this constraint, we aim to make the received signal Y_k close to X_k so that TD k could directly get the transmitted information based on the received signal.

To achieve this, some sophisticated processing are needed at the BBU side. It can be seen in (4.4) that we combine the channel information $h_{i,k}$'s and the content information X_k's in the matrix $\tilde{B}_{i,k}$, which are readily available at the BBUs, and the BBUs can instantaneously compute the $\tilde{B}_{i,k}$'s and utilize them to optimize the downlink data transmission. Since all the TDs simultaneously work at the same spectrum, each TD suffers from the inter-symbol interference (ISI) and the inter-user interference (IUI), which are significantly affected by the design of g_i. We aim to find the optimal g_i and $\alpha = [\alpha_1, \alpha_2, \quad \cdots \quad \alpha_N]$ to minimize the mean square error (MSE) of the received signal without violating the transmitting power constraints.

More specifically, the optimization problem becomes

$$\begin{aligned} \min_{\alpha, g_i} \quad & \sum_{k=1}^{N} E[\|Y_k - X_k\|^2] \\ \text{s.t.} \quad & g_i' g_i \leq P_{max}^{(dl)}, \end{aligned} \tag{4.9}$$

where $P_{max}^{(dl)}$ is the maximum transmitting power allowed for each RRH in the downlink transmission.

4.1.2 Uplink Problem Formulation

In the uplink of the TR based C-RAN system, All the TDs simultaneously transmit the information through the RRHs to the BBUs. The BBUs collect the information received by all the RRHs and then detect the transmitted symbols by processing the received signal. We will first analyze the case that a single RRH serves multiple TDs. Similar to the downlink case, the uplink will also be using the frame based transmission. The frame of symbols of TD k is denoted by $X_k = [x_{k,1}, x_{k,2}, \cdots x_{k,F_k}]$ where F_k is the frame length of TD k. As shown in Fig. 4.3, at TD k, the X_k will be first upsampled by the backoff factor D_k for ISI alleviation. After that, a blank sub-frame is appended to the end of the up-sampled signal to prevent the interference between frames. The length of the sub-frame is no less than L taps. Then, the entire frame is amplified element-wisely by $\beta_k = [\beta_{k,1}, \beta_{k,2}, \cdots, \beta_{k,F_k}]$ and then transmitted over the air to the RRH, i.e., the symbol $x_{k,j}$ is amplified by $\beta_{k,j}$. The signal received at the i-th RRH is the summation of the frame transmitted by each TD convoluted with its corresponding multipath channel. Similar to the

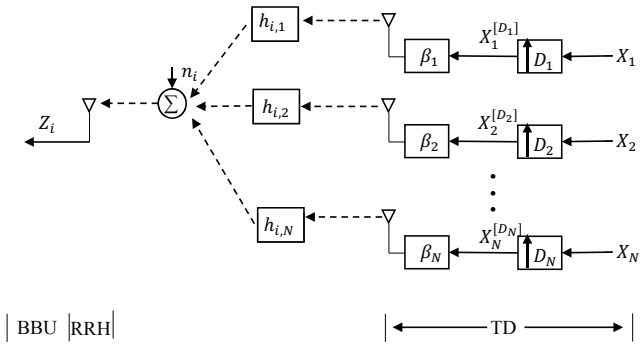

Figure 4.3: The Uplink Transmission Diagram

downlink case, we use matrix notations to represent the received signal, which is

$$Z_i = R_i \beta X + n_i, \tag{4.10}$$

where

$$X = \begin{pmatrix} X_1 \\ X_2 \\ \vdots \\ X_N \end{pmatrix} \tag{4.11}$$

is the aggregation of the frames of all the TDs,

$$R_i = \begin{pmatrix} R_{i,1} & R_{i,2} & \cdots & R_{i,N} \end{pmatrix}, \tag{4.12}$$

and β is a diagonal matrix with the diagonal elements being $\beta_{1,1}, \cdots \beta_{1,F_1}, \beta_{2,1}, \cdots \beta_{2,F_2}$, $\cdots$, $\beta_{N,1}, \cdots \beta_{N,F_N}$. $R_{i,j}$ is the Toeplitz matrix of size $(D_j \cdot (F_j - 1) + L) \times F_j$ with the j-th column being $[\mathbf{0}_{(j-1)*D_j}; h_{i,j}^T; \mathbf{0}_{(F_j - j)\times D_j}]$.

It can be seen that the channel information $h_{i,k}$'s are combined in R_i, which are readily available at the BBUs in the uplink. Moreover, the BBUs are equipped with all the computation power so that they have the ability to process the received

signal in sophisticated ways to extract the information transmitted by the TDs. In this chapter, we aim to design the linear minimum mean square error (LMMSE) detector W_i to detect the symbols transmitted by the TDs. Moreover, the BBUs need also determine the power control factor $\beta_{k,j}$'s in order to avoid the strong-weak effect. The problem can be formulated as

$$\begin{aligned} \min_{\beta, W_i} \quad & E[\|W_i Z_i - X\|^2] \\ \text{s.t.} \quad & \beta_{k,j}^2 E[\|x_{k,j}\|^2] \leq P_{max}^{(ul)}, \qquad \forall k, j, \end{aligned} \tag{4.13}$$

where $P_{max}^{(ul)}$ is the maximum transmitting power allowed for each TD in the uplink transmission.

4.2 Downlink Waveform Design

In this section, we solve the problem (4.9) formulated in section 4.1 to optimize the downlink data transmission. We will start with the single RRH multiple TD case. Since the problem in (4.9) is a non-convex problem, we propose to use iterative algorithms to solve it. Through designing the algorithm, we find that under a special single TD case, a closed form optimal waveform design can be derived. Eventually, we extend the problem to the coordinated waveform design such that multiple RRHs can work together to focus the signal at the intended locations.

4.2.1 Single RRH Waveform Design and Power Allocation

In this subsection, we will analyze the waveform design problem in the case that a single RRH serves multiple TDs. The MSE of TD k can be expressed as

$$\begin{aligned} MSE_k &= E[\|\alpha_k \tilde{B}_{i,k} g_i + \alpha_k M_k n_k - X_k\|^2] \\ &= \|\alpha_k\|^2 g_i' \tilde{B}_{i,k}' \tilde{B}_{i,k} g_i - \alpha_k' g_i' \tilde{B}_{i,k}' X_k - \alpha_k X_k' \tilde{B}_{i,k} g_i + \|\alpha_k\|^2 F_k \sigma^2 + X_k' X_k \end{aligned} \tag{4.14}$$

The total MSE can be represented as

$$\begin{aligned} \sum_{k=1}^{N} MSE_k = g_i' (\sum_{k=1}^{N} \|\alpha_k\|^2 \tilde{B}_{i,k}' \tilde{B}_{i,k}) g_i - g_i' (\sum_{k=1}^{N} \alpha_k' \tilde{B}_{i,k}' X_k) \\ - (\sum_{k=1}^{N} \alpha_k X_k' \tilde{B}_{i,k}) g_i + \sum_{k=1}^{N} X_k' X_k + \sum_{k=1}^{N} \|\alpha_k\|^2 F_k \sigma^2 \end{aligned} \tag{4.15}$$

The problem in (4.9) becomes

$$\begin{aligned} \min_{\alpha, g_i} \quad & g_i' (\sum_{k=1}^{N} \|\alpha_k\|^2 \tilde{B}_{i,k}' \tilde{B}_{i,k}) g_i - g_i' (\sum_{k=1}^{N} \alpha_k' \tilde{B}_{i,k}' X_k) - (\sum_{k=1}^{N} \alpha_k X_k' \tilde{B}_{i,k}) g_i + \sum_{k=1}^{N} \|\alpha_k\|^2 F_k \sigma^2 \\ \text{s.t.} \quad & g_i' g_i \leq P_{max}^{(dl)}, \end{aligned} \tag{4.16}$$

which is a non-convex optimization problem. Since each TD's optimal $g_{i,k}$ and α_k depend on those of other TDs, the closed form global optimal solution is difficult to find. In the following, we provide two algorithms that are guaranteed to converge to a local optimal point.

4.2.1.1 Alternating Optimization Algorithm

In this subsection, we will introduce the alternating optimization algorithm, where we alternatively optimize one of g_i and α given the other.

The Lagrangian of the problem in (4.16) can be written as

$$L(\alpha, g_i, \lambda) = g_i'(\sum_{k=1}^{N} \|\alpha_k\|^2 \tilde{B}_{i,k}' \tilde{B}_{i,k}) g_i - g_i'(\sum_{k=1}^{N} \alpha_k' \tilde{B}_{i,k}' X_k) - (\sum_{k=1}^{N} \alpha_k X_k' \tilde{B}_{i,k}) g_i + \sum_{k=1}^{N} \|\alpha_k\|^2 F_k \sigma^2 + \lambda(g_i' g_i - P_{max}^{(dl)}). \quad (4.17)$$

Given g_i, optimizing α is an unconstrained optimization problem, which can be solved by

$$\frac{\partial L}{\partial \alpha_k} = 0 \Rightarrow \alpha_k = (F_k \sigma^2 + g_i' \tilde{B}_{i,k}' \tilde{B}_{i,k} g_i)^{-1} g_i' \tilde{B}_{i,k}' X_k'. \quad (4.18)$$

Next, we will derive how to optimize g_i given α. We have

$$\frac{\partial L}{\partial g_i} = 0 \Rightarrow g_i(\sum_{k=1}^{N} \|\alpha_k\|^2 \tilde{B}_{i,k}' \tilde{B}_{i,k}) - \sum_{k=1}^{N} \alpha_k X_k' \tilde{B}_{i,k} + \lambda g_i' = 0. \quad (4.19)$$

By solving (4.18) and (4.19), we can have

$$\lambda = \frac{\sum_{k=1}^{N} \|\alpha_k\|^2 F_k \sigma^2}{P_{max}^{(dl)}}. \quad (4.20)$$

Substituting (4.20) into (4.19), we can have

$$g_i = (\sum_{k=1}^{N} \|\alpha_k\|^2 \tilde{B}_{i,k}' \tilde{B}_{i,k} + \frac{\sum_{k=1}^{N} \|\alpha_k\|^2 F_k \sigma^2}{P_{max}^{(dl)}} \mathbf{I})^{-1} (\sum_{k=1}^{N} \alpha_k' \tilde{B}_{i,k}' X_k). \quad (4.21)$$

The alternating optimization algorithm can be summarized in Algorithm 1.

In the alternating optimization algorithm, the MSE is non-increasing each time we update α or g_i. As a result, the MSE is non-increasing as the iteration goes on. Since the MSE in (4.16) is lower bounded, the proposed algorithm is guaranteed to converge.

Although the problem in (4.16) is non-convex, an interesting observation is that when there is only one TD, by solving the Lagrangian, we find that the necessary conditions lead to a unique solution, which is the optimal solution for (4.16).

Algorithm 1 Alternating Optimization Algorithm

1 Initialize $\alpha_k = 1,\ \forall k$

2 **loop:**

3 Calculate g_i according to (4.21)

4 Calculate α_k's according to (4.18)

5 **until** g_i and α_k's converge or the maximum number of iterations is reached

---

Specifically, from (4.18) we have

$$\|\alpha_k\|^2 g_i' \tilde{B}_{i,k}' \tilde{B}_{i,k} g_i + \|\alpha_k\|^2 F_k \sigma^2 = \alpha_k X_k' \tilde{B}_{i,k} g_i. \tag{4.22}$$

From (4.19) we have

$$\|\alpha_k\|^2 g_i' \tilde{B}_{i,k}' \tilde{B}_{i,k} g_i + \lambda g_i' g_i = \alpha_k X_k' \tilde{B}_{i,k} g_i. \tag{4.23}$$

By comparing (4.22) and (4.23), we can have $\|\alpha_k\|^2 F_k \sigma^2 = \lambda g_i' g_i$. Obviously, $\lambda = 0 \Rightarrow \alpha_k = 0$, which is not an optimal solution. If $\lambda \neq 0$, we have

$$g_i' g_i = P_{max}^{(dl)} \tag{4.24}$$

by complementary slackness [53]. Therefore, $\lambda = \frac{\|\alpha_k\|^2 F_k \sigma^2}{P_{max}^{(dl)}}$. Substituting the solution of λ into (4.19), we can obtain

$$g_i = \alpha_k' (\|\alpha_k\|^2 \tilde{B}_{i,k}' \tilde{B}_{i,k} + \frac{\|\alpha_k\|^2 F_k \sigma^2}{P_{max}^{(dl)}} \mathbf{I})^{-1} \tilde{B}_{i,k}' X_k, \tag{4.25}$$

where $\mathbf{I}$ is an identity matrix. By substituting (4.25) into (4.24), we have

$$\alpha_k = \sqrt{\frac{X_k' \tilde{B}_{i,k} (\tilde{B}_{i,k}' \tilde{B}_{i,k} + \frac{F_k \sigma^2}{P_{max}^{(dl)}} \mathbf{I})^{-2} \tilde{B}_{i,k}' X_k}{P_{max}^{(dl)}}}. \tag{4.26}$$

Substituting (4.26) into (4.25), we can obtain the optimal waveform for the single user. The resulting MSE in the single user case can be expressed as

$$MSE^{SU} = X_k' \tilde{B}_{i,k} (\tilde{B}_{i,k}' \tilde{B}_{i,k} + \frac{F_k \sigma^2}{P_{max}^{(dl)}} \mathbf{I})^{-2} \tilde{B}_{i,k}' X_k (1 + \frac{F_k \sigma^2}{P_{max}^{(dl)}}) - X_k' \tilde{B}_{i,k} (\tilde{B}_{i,k}' \tilde{B}_{i,k} + \frac{F_k \sigma^2}{P_{max}^{(dl)}} \mathbf{I})^{-1} \tilde{B}_{i,k}' X_k + X_k' X_k. \quad (4.27)$$

We observe that in this problem, the optimal solution satisfies $g_i' g_i = P_{max}^{(dl)}$. In other words, when only one single TD is served by the RRH, the RRH always uses full power for the downlink transmission. This conclusion can be verified in another way. If there are certain g_i and α_k such that $g_i' g_i < P_{max}^{(dl)}$, then we can always scale up g_i until it reaches $P_{max}^{(dl)}$, and scale down α_k accordingly to keep the first term in (4.4) the same while reducing the power of the second term, which is the power of the noise. As a result, the impairment caused by noise is alleviated and the MSE can be reduced.

4.2.1.2 Gradient Algorithm

In addition to the alternating optimization algorithm, we also propose another algorithm to find the optimal waveform.

From (4.18), we are able to calculate the optimal α_k given g_i. By plugging (4.18) into (4.14), the MSE of the k-th TD can be expressed as

$$MSE_k = X_k' X_k - \frac{g_i' \tilde{B}_{i,k}' X_k X_k' \tilde{B}_{i,k} g_i}{g_i' \tilde{B}_{i,k}' \tilde{B}_{i,k} g_i + F_k \sigma^2}. \quad (4.28)$$

The total MSE of all the TDs can be represented as

$$\sum_{k=1}^{N} MSE_k = \sum_{k=1}^{N} (X_k' X_k - \frac{g_i' \tilde{B}_{i,k}' X_k X_k' \tilde{B}_{i,k} g_i}{g_i' \tilde{B}_{i,k}' \tilde{B}_{i,k} g_i + F_k \sigma^2}). \quad (4.29)$$

The gradient can be calculated as

$$\begin{aligned}\nabla g_i \triangleq & \quad \frac{\partial}{\partial g_i}(\sum_{k=1}^{N} MSE_k) \\ = & \sum_{k=1}^{N}[\frac{2\tilde{B}'_{i,k}\tilde{B}_{i,k}g_i(g_i'\tilde{B}'_{i,k}X_kX'_k\tilde{B}_{i,k}g_i)}{(g_i'\tilde{B}'_{i,k}\tilde{B}_{i,k}g_i+F_k\sigma^2)^2} - \frac{2\tilde{B}'_{i,k}X_kX'_k\tilde{B}_{i,k}g_i}{g_i'\tilde{B}'_{i,k}\tilde{B}_{i,k}g_i+F_k\sigma^2}]. \end{aligned} \tag{4.30}$$

Once the gradient is calculated, we use it to update the waveform in order to minimize the MSE. Moreover, we project it to the constraint set $g_i'g_i = P_{max}^{(dl)}$ by normalization to comply with the transmitting power constraint. Specifically,

$$g_i^{new} = g_i - \delta_n \cdot \nabla g_i \tag{4.31}$$

$$g_i^{new,p} = \frac{\sqrt{P_{max}^{(dl)}}}{\|g_i^{new}\|} \cdot g_i^{new}, \tag{4.32}$$

where the first equation is to determine the shape of the new waveform by line search. We choose the step size for the n-th iteration in line search as $\delta_n = \frac{1}{n}$ for its good convergence behavior [53]. The second equation is to project the waveform into the space satisfying the transmitting power constraint. The gradient optimization algorithm can be summarized in Algorithm 2.

In this algorithm, g_i is updated in step 7 only when the MSE is reduced by the update. Therefore, the MSE is non-increasing in this algorithm. Since the MSE is lower bounded, the gradient algorithm is guaranteed to converge.

4.2.2 Extension to multi-RRH Joint Waveform Design and Power Allocation

In this subsection, we will extend the gradient algorithm to the multiple RRH case so that multiple RRHs are able to jointly determine the waveform for the

Algorithm 2 Gradient Optimization Algorithm

1 Initialize g_i as the basic TR waveform

2 **loop:**

3 Calculate ∇g according to (4.30)

4 Set $n = 1$

5 Update $g_i^{new,p}$ according to (4.31) and (4.32)

6 **if** $MSE_{new} < MSE_{current}$

7 $g_i = g_i^{new,p}$

8 **else**

9 $n = n + 1$, go to step 5

10 **until** g_i and α_k's converge or the maximum number of iterations is reached

downlink transmission so as to better focus the signal at the intended TDs.

First, we extend the problem in (4.9) to the multiple RRH case. When multiple RRHs work together to serve the TDs distributed in the area, each TD simultaneously receives and combines the signal transmitted by all the serving RRHs. Suppose there are totally M RRHs serving N TDs in the area. The signal received by TD k can be represented as

$$\begin{aligned} Y_k &= \alpha_k \sum_{i=1}^{M} \tilde{B}_{i,k} g_i + \alpha_k \cdot M_k n_k \\ &= \alpha_k \cdot \tilde{B}_k g + \alpha_k \cdot M_k n_k, \end{aligned} \tag{4.33}$$

where

$$g = \begin{pmatrix} g_1 \\ g_2 \\ \vdots \\ g_M \end{pmatrix} \tag{4.34}$$

is the aggregation of all the downlink transmission signature g_i's of the RRH i, and

$$\tilde{B}_k = [\tilde{B}_{1,k} \quad \tilde{B}_{2,k} \quad \cdots \quad \tilde{B}_{M,k}]. \tag{4.35}$$

Since the transmitting power at each of the RRHs cannot exceed $P_{max}^{(dl)}$, the problem in (4.9) becomes

$$\begin{aligned} \min_{\alpha,g} \quad & g'(\sum_{k=1}^{N} \|\alpha_k\|^2 \tilde{B}'_{i,k} \tilde{B}_k) g - g'(\sum_{k=1}^{N} \alpha'_k \tilde{B}'_k X_k) - (\sum_{k=1}^{N} \alpha_k X'_k \tilde{B}_k) g + \sum_{k=1}^{N} \|\alpha_k\|^2 F_k \sigma^2 \\ \text{s.t.} \quad & g'_i g_i \leq P_{max}^{(dl)}, \ \forall i. \end{aligned} \tag{4.36}$$

The gradient optimization algorithm proposed earlier can be modified to work in the multiple RRH case. Since each single RRH has only limited transmitting power, the projection in (4.32) is modified by normalizing the maximum transmitting power of all the RRHs to $P_{max}^{(dl)}$, while the transmitting power of all the other RRHs are scaled down accordingly. Specifically, the projection step is

$$g^{new,p} = \frac{\sqrt{P_{max}^{(dl)}}}{\max_i \|g_i\|} \cdot g_{new}. \tag{4.37}$$

By solving problem (4.36), all the RRHs work together to determine the optimal g without violating the transmitting power constraint at each of the RRHs. As a result, the transmitted signal are better focused at the intended receivers with little leakage to the surroundings. It will be shown later in the numerical results that, compared with the single RRH case, multiple RRHs not only bring in extra power, but also additional degree of freedom so that the signal can be focused at the intended locations more sharply.

4.3 Uplink Joint Power Control and Detector Design

In this section, we try to solve the problem (4.13) formulated in section 4.1. We will first analyze the single RRH case where RRH i determines the transmitting power of all the TDs and then processes the received signal to extract the uplink information. Then we extend it to the multiple RRH case where the BBUs can leverage the signal collected by more than one RRHs.

4.3.1 Single RRH Power Control and Detector Design

Suppose the RRH i collects the uplink signal transmitted by N TDs and forward it to the BBUs for further processing. The MSE in (4.13) can be written as

$$E[\|W_i Z_i - X\|^2] = E[\|W_i R_i \beta X + W_i n_i - X\|^2]. \tag{4.38}$$

In this chapter, we use the LMMSE detector to detect X. By [54], the LMMSE detector can be written as

$$W_i = \Sigma_x \beta' R_i' (R_i \beta \Sigma_x \beta' R_i' + \Sigma_e)^{-1}, \tag{4.39}$$

where

$$\begin{aligned} \Sigma_x &= E[XX'] \\ \Sigma_e &= E[n_i n_i']. \end{aligned} \tag{4.40}$$

It can be seen that if β is available, the LMMSE detector can be determined. The MSE can be written as

$$MSE^{(ul)} = trace[(\beta' R_i' \Sigma_e^{-1} R_i \beta + \Sigma_x^{-1})^{-1}], \tag{4.41}$$

which is affected by β. Moreover, β is also limited by the transmitting power constraints of the TDs. Since the R_i, Σ_x and Σ_e are available at the BBUs, the BBUs are able to optimize over β in order to further minimize the MSE, and signal them to the TDs through the control/feedback links. The problem becomes

$$\begin{aligned} \min_{\beta} \quad & trace[(\beta' R_i' \Sigma_e^{-1} R_i \beta + \Sigma_x^{-1})^{-1}] \\ \text{s.t.} \quad & \beta_{k,j} \leq \sqrt{\frac{P_{max}^{(ul)}}{E[\|x_{k,j}\|^2]}}, \qquad \forall k, j, \end{aligned} \tag{4.42}$$

which is a non-convex problem. Since the global optimal solution is hard to find, in the following, we use a gradient algorithm to find the optimal β to minimize the MSE while satisfying the transmission power constraint of each TD.

Let $A \triangleq \Sigma_e^{-\frac{1}{2}} R_i$. Note that β is a diagonal matrix. By [55], we have

$$\nabla\beta(s,s) \triangleq \frac{\partial MSE^{(ul)}}{\partial\beta(s,s)} = -trace[(\beta' A' A\beta + \Sigma_x)^{-2}(\psi_s' A' A\beta + \beta' A' A\psi_s)], \quad (4.43)$$

where ψ_s is a matrix the same size with β. All elements in ψ_s are zeros except that $\psi_s(s,s) = 1$. We define $\nabla\beta$ to be the diagonal matrix the same size with β, and the i-th item in the diagonal is $\nabla\beta(i,i)$, i.e.,

$$\nabla\beta = \begin{pmatrix} \nabla\beta(1,1) & 0 & \cdots & 0 \\ 0 & \nabla\beta(2,2) & \ddots & 0 \\ \vdots & \ddots & \ddots & \vdots \\ 0 & \cdots & 0 & \nabla\beta(U,U) \end{pmatrix}, \quad (4.44)$$

where $U = \sum_{i=1}^{N} F_i$.

After we obtain the gradient for each $\beta(s,s)$, we update each $\beta(s,s)$ by line search and projection similar to the downlink gradient algorithm. Specifically,

$$\beta^{new} = \beta - \delta_n \cdot \nabla\beta, \quad (4.45)$$

$$\beta^{proj} = \frac{\sqrt{P_{max}^{(ul)}}}{\max_s(\beta^{new}(s,s)\sqrt{\Sigma_x(s,s)})}\beta^{new}, \quad (4.46)$$

where we choose $\delta_n = \frac{1}{n}$. The algorithm can be summarized in Algorithm 3.

In this algorithm, β is updated in step 7 only when the MSE is reduced by the update. Therefore, the MSE is non-increasing in this algorithm. Since the MSE is lower bounded, the gradient algorithm is guaranteed to converge.

Algorithm 3 Gradient Optimization Algorithm for Optimal Power Control in Uplink

1 Initialize $\beta(s,s) = \sqrt{\frac{P_{max}^{(ul)}}{\Sigma_x(s,s)}},\ \forall s$

2 **loop:**

3 Calculate $\nabla\beta$ according to (4.43) and (4.44)

4 Set $n = 1$

5 Update β^{proj} according to (4.45) and (4.46)

6 **if** $MSE_{new} < MSE_{current}$

7 $\beta = \beta^{proj}$

8 **else**

9 $n = n + 1$, go to step 5

10 **until** β converges or the maximum number of iterations is reached

4.3.2 Extension to the Multiple RRH Joint Power Control and Detector Design

In the above, we proposed the joint LMMSE detector design and power control algorithm in the single RRH case so that the BBUs can determine the optimal transmitting power utilized by each TD and then use the baseband signal collected by RRH i to extract the information transmitted by all the TDs. In the C-RAN setting, usually more than one RRHs are available in a specific area. Compared to the single RRH case, extra RRHs can provide additional information about the signal transmitted by the TDs, which can be utilized to improve the accuracy in detecting the transmitted symbols. In this subsection, we extend the LMMSE detector design and power control algorithm to the multiple RRH case.

In the multiple RRH case, we assume the M RRHs simultaneously observe the transmitted signal from the N TDs and forward the collected signal to the BBUs for processing. The BBUs collect the aggregation of the signal received by all the RRHs, which can be represented as

$$Z = R\beta X + n, \tag{4.47}$$

where $Z = [Z_1^T, Z_2^T, \cdots Z_M^T]^T$, $R = [R_1^T, R_2^T, \cdots R_M^T]^T$, $n = [n_1^T, n_2^T, \cdots n_M^T]^T$.

The LMMSE detector design in (4.39) and the gradient power control algorithm can be readily extended to the multiple RRH case by replacing R_i by R and n_i by n, respectively.

4.4 Experimental Results

In this section, we will use some numerical results to illustrate the effectiveness of the proposed waveform design algorithms. We start with the experiment settings in which we collect the multipath channels. After that, we will show the BER and MSE performance of the proposed algorithms under various conditions.

4.4.1 Experiment Setting

The experimental setting is the same as that described in section 2.6 of this dissertation where 4800 independent channel measurements from the indoor environment are obtained. The following numerical results are based on these channel measurements.

4.4.2 Single RRH Waveform Design

In this subsection, we show the numerical results obtained by using the single RRH waveform design algorithms proposed in section 4.2 and section 4.3.

In Fig. 4.4 and Fig. 4.5, we show the BER performance of the single RRH single TD waveform design algorithm. The curve labeled "WD" stands for the BER performance of the sum rate maximization waveform design algorithm proposed in [19], the curves labeled "Content-aware WD" stand for the performance of the algorithms proposed in this chapter since the content information is used in the waveform design, and the curve labeled "TR" stands for the BER performance using basic TR waveforms in [16]. As shown in the figures, as $\frac{P_{max}^{(dl)}}{\sigma^2}$ increases, the

BER of the basic TR fails to go down since it is dominated by the interference. The BER decreases as $\frac{P_{max}^{(dl)}}{\sigma^2}$ increases for the algorithms proposed in this chapter and in [19]. Moreover, the algorithm proposed in this chapter always outperforms that in [19]. However, the performance gap between those two algorithms shrinks when D increases, since the interference is less severe with larger D. Moreover, we show in Fig. 4.6 that the theoretical MSE calculated by (4.27) matches the theoretical values well.

Next, we evaluate the proposed design in the single RRH multiple TD setting. In Fig. 4.7 and Fig. 4.8, we show the BER performance of the proposed algorithm in the single AP and multiple TD settings. Similar to the single TD case, the BER of the basic TR goes down very slowly as $\frac{P_{max}^{(dl)}}{\sigma^2}$ increases due to the saturation of interference. The proposed algorithm always outperforms the waveform design in [19]. The performance gap is larger than the single TD case since the interference is more severe than the single TD case. Moreover, it is illustrated that the performance of the alternating algorithm is close to that of the gradient algorithm.

4.4.3 Multiple RRH Waveform Design

In Fig. 4.11, we show the BER performance of the algorithm in section 4.2.2 for the multiple RRH settings. The BER of the basic TR waveform goes down very slowly with the increase of $\frac{P_{max}^{(dl)}}{\sigma^2}$. On the other hand, in the proposed content-aware waveform design schemes, multiple RRHs work together to determine the transmitting power and waveform and thus achieve good interference management.

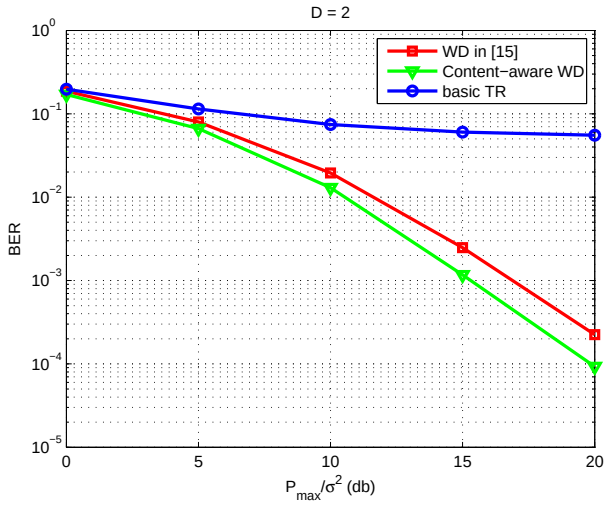

Figure 4.4: The BER of the single RRH single TD (D=2)

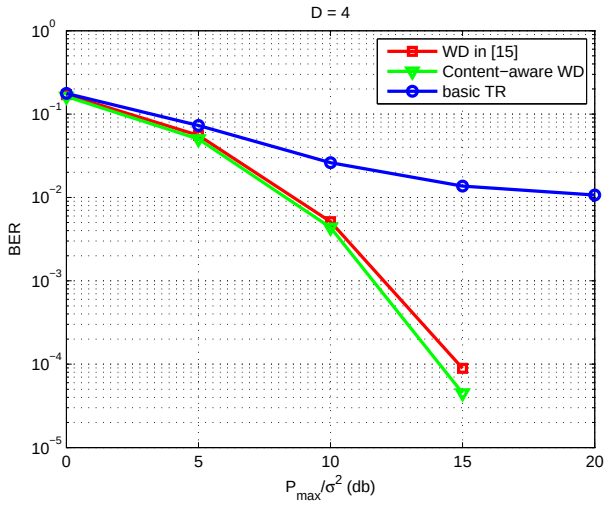

Figure 4.5: The BER of the single RRH single TD (D=4)

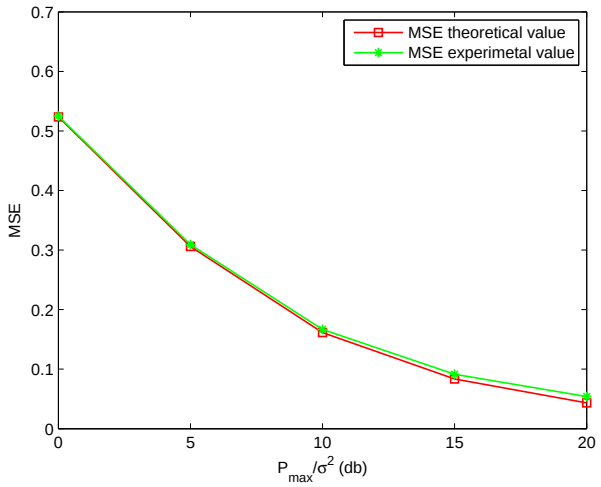

Figure 4.6: The Theoretical and Experimental MSE of a Single TD

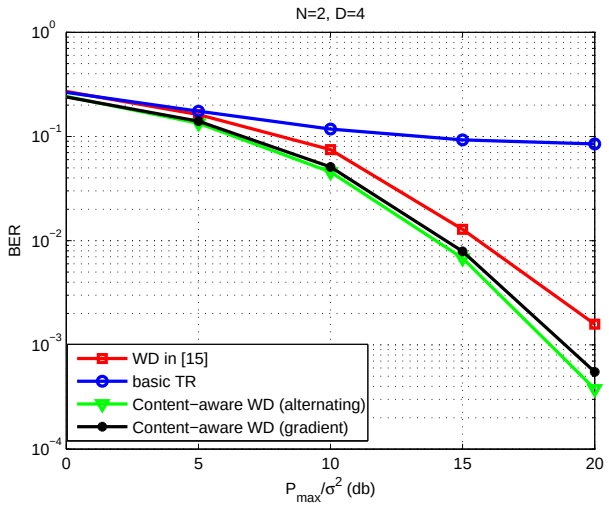

Figure 4.7: The BER of the single RRH with two TDs (D=4)

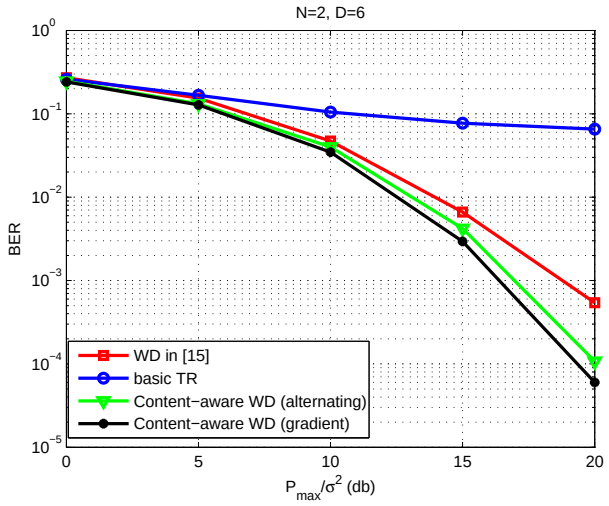

Figure 4.8: The BER of the single RRH with two TDs (D=6)

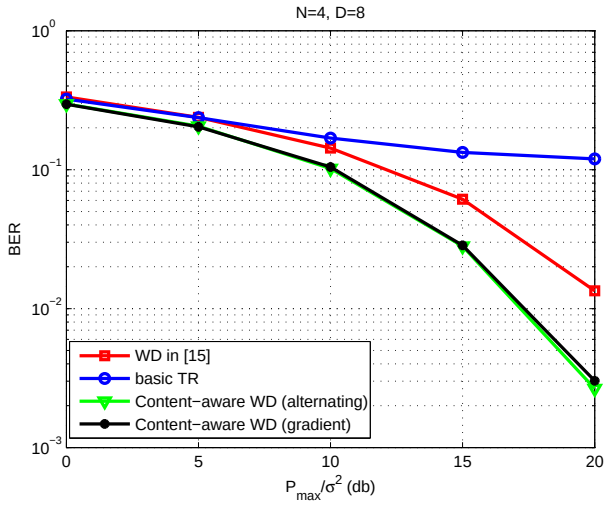

Figure 4.9: The BER of the single RRH with Four TDs (D=8)

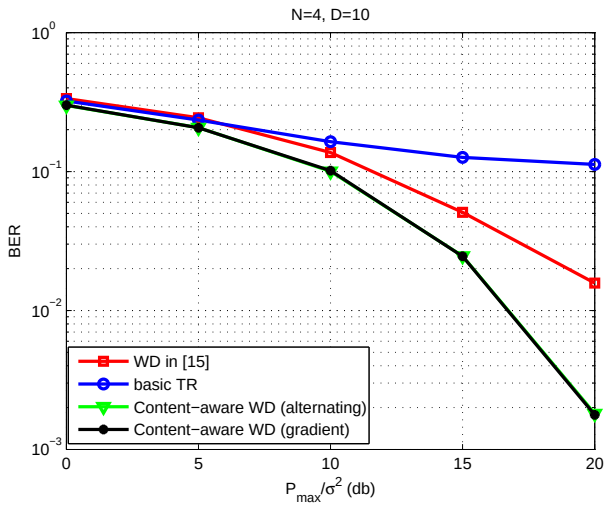

Figure 4.10: The BER of the single RRH with Four TDs (D=10)

As a result, the extra RRHs not only brings in more transmitting power, but also the additional degree of freedom that can be utilized to better focus the signal at the intended locations. As shown in Fig. 4.12, the average BER of the TDs decrease with more RRHs installed.

For the uplink case, we show the BER performance of the proposed algorithm in the multiple RRH setting. The curves labeled "LMMSE" stand for the performance of the proposed LMMSE estimator design, and the curves labeled "TR" stand for the performance of the basic TR waveforms in [17]. As shown in Fig. 4.13, The BER of the basic TR waveform goes down very slowly as $\frac{P_{max}^{(ul)}}{\sigma^2}$ increases. On the other hand, by using the proposed algorithm, the observations from multiple RRHs are gathered and processed to detect the symbols transmitted by the TDs. Additional RRHs provide extra observations of the symbols transmitted by the TDs, which can be utilized to improve the accuracy of the detection. As shown in Fig. 4.14, the average BER of the TD decreases with the more RRHs installed.

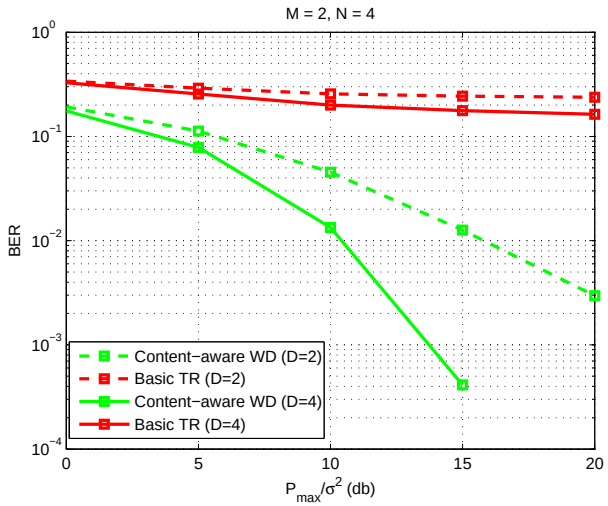

Figure 4.11: The BER Performance of Downlink Transmission in a Multiple RRH Case

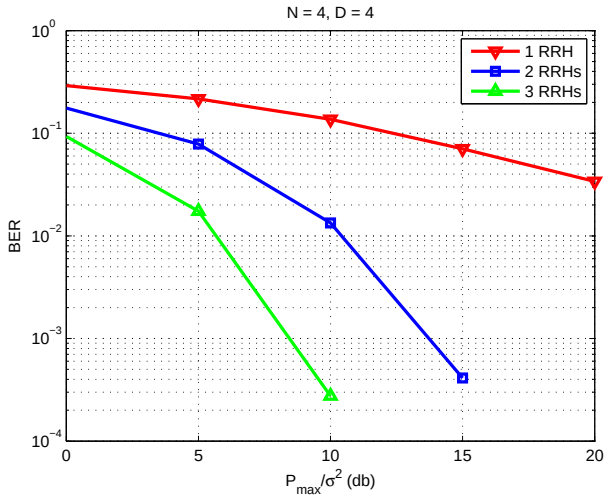

Figure 4.12: The Improvement of BER by Adding RRHs in Downlink Transmission

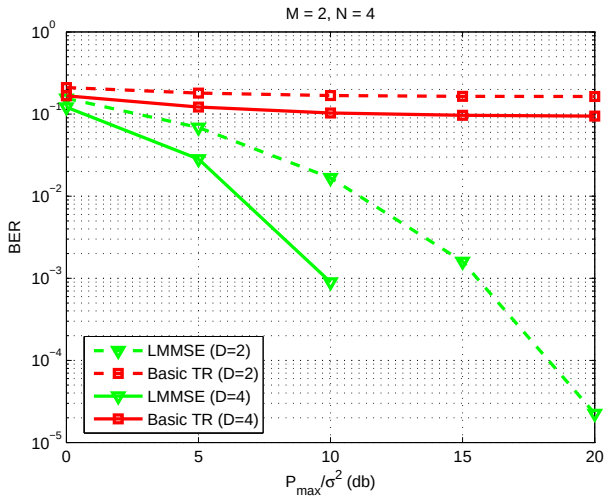

Figure 4.13: The BER Performance of Uplink Transmission in a Multiple RRH Case

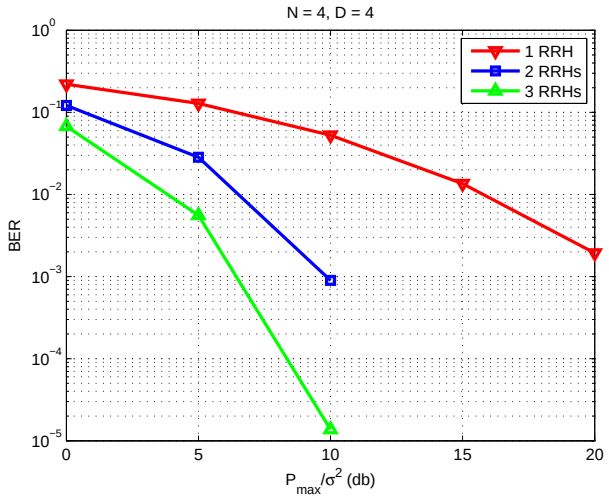

Figure 4.14: The Improvement of BER by Adding RRHs in Uplink Transmission

4.5 Conclusion

In this chapter, we studied the optimization on the downlink and uplink transmission in TR based C-RAN. The content/channel information and the computing power in the BBU pool is utilized to optimize the waveform design in the downlink and receiver design in the uplink. The asymmetric architecture of TR communication is preserved in the optimization and no change in the terminal device (TD) is needed. In this way, the performance of the TR based C-RAN can be improved while keeping the low cost of the TDs. We built a TR radio prototype to measure the wireless channel in the real-world environment, with which we illustrated that the proposed algorithms can significantly improve the downlink and uplink transmission reliability over basic TR waveforms and traditional waveform design schemes.

Chapter 5: Compressive Quantization for Multi-Antenna Cloud Radio Access Network

In the previous sections, a time-reversal (TR) based cloud radio access network (C-RAN) is proposed where the "tunneling effects" are discovered, by which the traffic load in the front-haul link is alleviated. In this chapter, we generalize from this idea and propose the compressive quantization scheme that applies to the uplink of a multi-antenna C-RAN so that massive antennas can be utilized.

In recent years, massive MIMO has drawn the attention of researchers. Following the same idea of leveraging the spatial multiplexing gain as the traditional MIMO, the massive MIMO utilizes a much larger number of antennas, and some interesting features have been discovered, such as the improved spectral efficiency and energy efficiency which can be achieved by MRC in the uplink or MRT in the downlink [56, 57]. However, despite the advantages, the massive MIMO is limited by a few bottlenecks. For example, due to the limited separation between antennas, the channels are always correlated, which undermines the advantages made possible with massive antennas [58, 59].

The C-RAN has the same initiative of utilizing extra antennas with the massive MIMO. We notice that if the total number of antennas is large, the C-RAN works like

a virtual massive MIMO, and many nice properties of massive MIMO will apply. For example, the massive antennas help focus the energy into smaller region [60], such that more terminal devices (TDs) can be accommodated efficiently. These features are essential to the next generation of wireless networks. However, in the C-RAN, the amount of traffic in the front-haul is proportional to the number of antennas utilized by the remote radio head (RRH). Therefore, due to the limited front-haul capacities, each RRH always uses a single antenna in the current literature, and the total number of antennas that can be utilized is limited, which hinders the C-RAN from achieving the nice properties of using massive antennas.

Recently, motivated by the advantages of massive antennas, the multi-antenna C-RAN is investigated [61]. Since the amount of baseband signal data in the front-haul link is proportional to the number of antennas used by the RRH, a spatial filtering method is designed in [62] to compress the baseband signal in the uplink. However, the design of the spatial filter is performed at the baseband units (BBUs) due to the limited computation capability of RRHs, which creates a lot of overhead in the already-tight front-haul links. Moreover, the compression of the baseband signal using the spatial filter involves massive multiplication operations, which increases the cost of each RRH.

Recall that in the TR based C-RAN proposed in Chapter 3 of this dissertation, the baseband signals of multiple devices can be combined and transmitted in the front-haul links since they are naturally separated by the location-specific signatures. In the multi-antenna C-RAN, similar separation is also available due to the fact that the total number of antennas is large, and the channel impulse response from the

large number of antennas can serve as the signature for each TD. In this chapter, we aim to leverage this feature to design low cost but effective baseband signal processing schemes which can facilitate the C-RAN tackle the front-haul capacity challenge caused by using multi-antenna RRHs. Instead of elaborately designed compressor, quantizer and decoder, we propose a novel baseband signal compressive quantization at the RRH side coupled with the weight vectors designed at the BBU side. The compressive quantization consists of two phases: the delay-and-add and the quantization. The delay-and-add simply buffers the baseband signals of multiple time instants and sums the delayed versions of them, which is then quantized and transmitted to the BBUs through the front-haul link. By the delay-and-add, the raw baseband signals from multiple time instants are embedded in a vector with lower dimension compared with the direct concatenation, and thus more bits can be allocated to each value in the quantization. As a result, the quantization noise is mitigated. On the other hand, due to the overlapping of baseband signals from multiple time instants, extra interference is created. Unlike the quantization noise, the interference has its own structure, and is easy to mitigate and cancel out with the rich spatial diversity provided by the massive antennas. In other words, different from general baseband signal compression algorithms, the compressive quantization is tailored for the multi-antenna C-RAN where massive antennas are available. In the BBU side, the LMMSE and MRC detectors are designed to detect the symbols from the signal processed by the RRHs using compressive quantization. To fully utilize the computation power of the BBUs, a parallel interference cancellation algorithm is proposed to further reduce the influence of interference. Moreover, we

extend the proposed scheme to an OFDM based multi-antenna C-RAN and find that the proposed scheme helps the OFDM based multi-antenna C-RAN utilize larger bandwidth with limited front-haul capacity. Numerical results in various settings illustrate the effectiveness of the proposed schemes.

The chapter is organized as follows: in section 5.1, the system model is introduced. We propose and analyze the compressive quantization scheme as well as the corresponding symbol detection schemes in section 5.2. In section 5.3, the proposed scheme is applied to the OFDM based multi-antenna C-RAN. Numerical results are shown in section 5.4 and section 5.5 concludes the chapter.

5.1 System Model

We consider the uplink communication of the cloud radio access network (C-RAN). As shown in Fig. 5.1, a group of N terminal devices (TDs) are distributed in an area and they work in the same band. Each TD transmits the signal, which is received by M remote radio heads (RRHs) distributed in the same area. All the RRHs periodically report the received baseband signal to the baseband unit (BBU) pool through front-haul links with limited capacity. Without loss of generality, we assume the i-th RRH is equipped with Q_i antennas where $Q_i > 1$, and each TD is equipped with single antenna.

In this chapter, we assume that the channel state information (CSI) is instantly available at the BBUs through channel estimation prior to the uplink transmission. The channel impulse response between the i-th RRH and the j-th TD is $\mathbf{h}_{i,j} =$

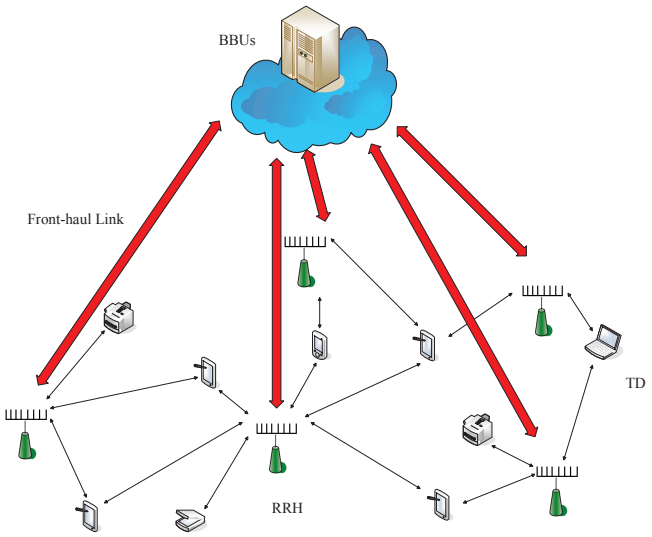

Figure 5.1: The System Model

$[h_{i,j}^{(1)}, h_{i,j}^{(2)}, \cdots, h_{i,j}^{(Q_i)}]^T$ where $h_{i,j}^{(m)}$ is the channel impulse response between the m-th antenna of RRH i and TD j.

In the uplink transmission, all the RRHs periodically report the received baseband signal to BBUs and the BBUs are responsible for detecting the symbols transmitted by the TDs using the received signal. The signal received by the ith RRH at time instant t can be represented as

$$\mathbf{y}_{i,t} = \mathbf{H}_i \mathbf{x}_t + \mathbf{n}_{i,t} \tag{5.1}$$

where $\mathbf{x}_t \in \mathbb{C}^{N\times 1}$ is the vector containing the intended symbols of all the TDs at time t, $\mathbf{n}_{i,t} \in \mathbb{C}^{Q_i\times 1}$ is the additive white gaussian noise (AWGN) received by RRH i at time t, and

$$\mathbf{H}_i = [\mathbf{h}_{i,1}, \mathbf{h}_{i,2}, \cdots, \mathbf{h}_{i,N}]\,. \tag{5.2}$$

As shown in (5.1), the dimension of the baseband signal $\mathbf{y}_{i,t}$ increases as more antennas are used at each RRH. The baseband signals transmitted directly through

the front-haul links will suffer from severe quantization noise. Let the capacity of the front-hual link be C_i bits per second, and the wireless bandwidth be J Hz. We analyze the quantization noise under uniform quantization. The average number of bits allocated to an individual value in $\mathbf{y}_{i,t}$ is

$$B_i = \frac{C_i}{J \cdot Q_i}. \tag{5.3}$$

Typically, the quantization noise $\mathbf{q}_i[k]$ can be approximated as a complex random variable whose real and imaginary parts are uniformly distributed in the range $(-\frac{L_i}{2}, \frac{L_i}{2})$ where $L_i = \frac{2K_i}{2^{b_i}-1}$ is the quantization level [42] of the baseband signal of i-th RRH, $b_i = B_i/2$ is the number of bits used to represent the real/imaginary part of $\mathbf{y}_{i,t}[k]$, and $[-K_i, K_i]$ is the dynamic range of the real/imaginary part of $\mathbf{y}_{i,t}[k]$.

By [42], the power of the quantization noise can be written as

$$E[\|q_i[k]\|^2] = \frac{(L_i)^2}{12} + \frac{(L_i)^2}{12} = \frac{(L_i)^2}{6}. \tag{5.4}$$

It can be seen from (5.3) and (5.4) that with limited front-haul capacity, the number of bits allocated to each individual value of $\mathbf{y}_{i,t}[k]$ decreases as Q_i increases, and in consequence the quantization noise power increases. In other words, under direct quantization, the limited front-haul capacity is the main obstacle in transmitting the $\mathbf{y}_{i,t}$'s to the BBUs. In the next section, we will introduce the compressive quantization scheme which is able to quantize $\mathbf{y}_{i,t}$'s more efficiently so that the signal fits the front-haul capacity.

5.2 Compressive Quantization and Symbol Detection

To tackle the aforementioned quantization noise problem, in this section, we propose the distributed baseband signal compressive quantization as well as the corresponding symbol detection schemes. We will first introduce the compressive quantization which happens in the RRH, and then the corresponding weight vectors that can be used to detect the symbols from the compressive quantized baseband signal. Finally, we propose a parallel interference cancellation algorithm which further improves the symbol detection accuracy.

5.2.1 Compressive Quantization

The frame based compressive quantization scheme consists of the delay-and-add phase and the quantization phase. Let F denote the frame length. In the delay-and-add phase, the $\mathbf{y}_{i,t}$'s obtained in $t = 1, 2, \cdots, F$ are buffered. As shown in Fig. 5.2, instead of quantizing and transmitting $\mathbf{y}_{i,t}$ to the BBUs at each time instant, each $\mathbf{y}_{i,t}$ is delayed for D_i time instants from the previous one. The vector $\mathbf{z}_i$ is the summation of the delayed versions of $\mathbf{y}_{i,t}$'s. More specifically, $\mathbf{z}_i$ can be written as

$$\mathbf{z}_i[k] = \sum_{t=1}^{F} \tilde{\mathbf{y}}_{i,t}[k] \tag{5.5}$$

where

$$\tilde{\mathbf{y}}_{i,t}[k] = \begin{cases} \mathbf{y}_{i,t}[k - (t-1) \cdot D_i], & \text{if } (t-1) \cdot D_i + 1 \leq k \leq (t-1) \cdot D_i + Q_i \\ 0, & \text{otherwise} \end{cases} \tag{5.6}$$

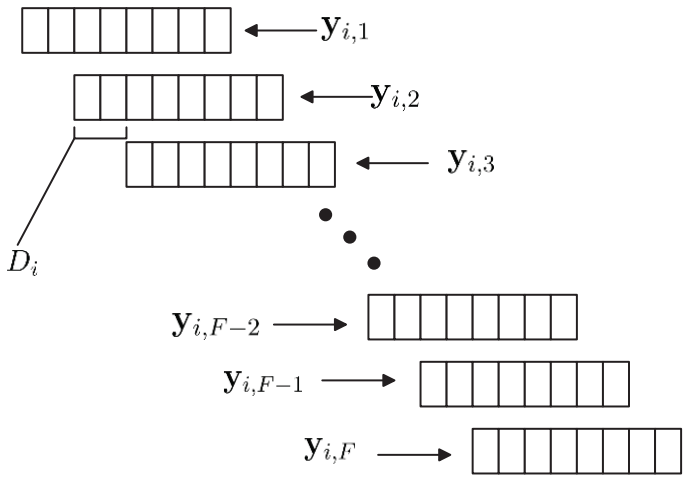

Figure 5.2: An example of the delay-and-add phase with $Q_i = 8$, $D_i = 2$

To model the proposed compressive quantization scheme, we introduce the equivalent channel $\mathbf{H}_i^{(eq)}$ as

$$\mathbf{H}_i^{(eq)} = \left[\tilde{\mathbf{H}}_i^{(1)}, \tilde{\mathbf{H}}_i^{(2)}, \cdots, \tilde{\mathbf{H}}_i^{(F)}\right] \tag{5.7}$$

where

$$\tilde{\mathbf{H}}_i^{(r)} = \begin{pmatrix} \mathbf{0}_{(r-1)D_i \times N} \\ H_{i,k} \\ \mathbf{0}_{(F-r)D_i \times N} \end{pmatrix}. \tag{5.8}$$

The overlapped baseband signal $\mathbf{z}_i$ can be written as

$$\mathbf{z}_i = \mathbf{H}_i^{(eq)} \mathbf{x}^{(eq)} + \mathbf{n}_i^{(eq)} \tag{5.9}$$

where $\mathbf{x}^{(eq)} = [\mathbf{x}_1^T, \mathbf{x}_2^T, \cdots, \mathbf{x}_F^T]^T$ and $\mathbf{n}_i^{(eq)} = \mathbf{A} \cdot [\mathbf{n}_{i,1}^T, \mathbf{n}_{i,2}^T, \cdots, \mathbf{n}_{i,F}^T]^T$. The noise transformation matrix $\mathbf{A} \in \mathbb{R}^{(Q_i + (F-1)D_i) \times (Q_i F)}$ can be written as

$$\mathbf{A} = [\mathbf{a}_1, \mathbf{a}_2, \cdots, \mathbf{a}_F] \tag{5.10}$$

and

$$\mathbf{a}_k = \begin{pmatrix} \mathbf{0}_{(k-1)D_i \times Q_i} \\ \mathbf{I}_{Q_i \times Q_i} \\ \mathbf{0}_{(F-k)D_i \times Q_i} \end{pmatrix}. \tag{5.11}$$

The quantization phase follows the delay-and-add phase. Uniform quantization is applied to each element in $\mathbf{z}_i$. More specifically, the quantized signal $\tilde{\mathbf{z}}_i$ can be represented as

$$\begin{aligned} \tilde{\mathbf{z}}_i &= \mathbf{z}_i + \mathbf{q}_i^{(CQ)} \\ &= \mathbf{H}_i^{(eq)} \mathbf{x}^{(eq)} + \mathbf{n}_i^{(eq)} + \mathbf{q}_i^{(CQ)} \end{aligned} \tag{5.12}$$

where $\mathbf{q}_i^{(CQ)}$ is the quantization noise caused by compressive quantization. In the following, we will show the quantization noise is reduced by the proposed method.

The total length of vector $\mathbf{z}_i$ containing the information of $\mathbf{y}_{i,t}$'s is $Q_i + (F-1) \cdot D_i$. Compared with the aggregation of $\mathbf{y}_{i,t}$'s of the length $Q_i \cdot F$, the dimension of the vector is much reduced. For instance, as in the example shown in Fig. 5.2 where $Q_i = 8$ and $D_i = 2$, the number of components is reduced to nearly $\frac{1}{4}$ of the original value. As a result, with limited front-haul capacity, more bits can be allocated to each individual component. More specifically, similar to (5.3), we have

$$B_i^{(CQ)} = \frac{F \cdot C_i}{J \cdot (Q_i + (F-1) \cdot D_i)}. \tag{5.13}$$

By (5.9), $\mathbf{z}_i[k]$ is a summation of multiple independent variables and can be approximated as a complex Gaussian random variable by the law of large numbers. Similar to (5.4), the quantization noise power under the compressive quantization

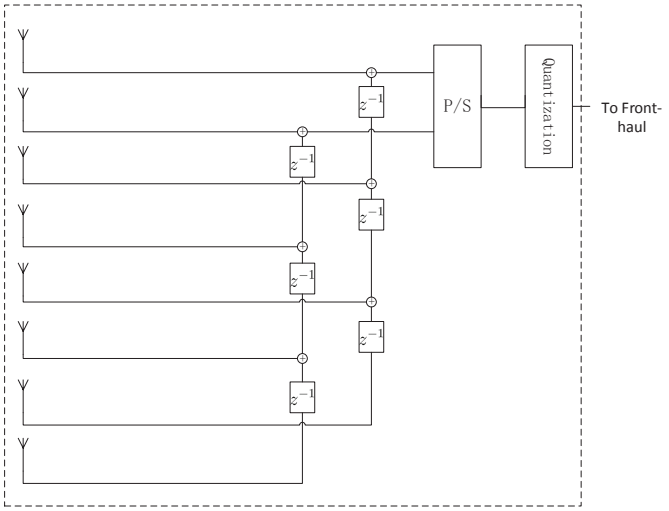

Figure 5.3: An example of the DSP circuit for compressive quantization with $Q_i = 8$, $D_i = 2$

can be written as

$$E[\|\mathbf{q}_i^{(CQ)}[k]\|^2] = \frac{(L_i^{(CQ)})^2}{12} + \frac{(L_i^{(CQ)})^2}{12} = \frac{(L_i^{(CQ)})^2}{6} \tag{5.14}$$

where

$$L_i^{(CQ)} = \frac{2K_i^{(CQ)}}{2^{B_i^{(CQ)}}} \tag{5.15}$$

is the quantization level under the compressive quantization and $K_i^{(CQ)}$ is the dynamic range of $\mathbf{z}_i[k]$.

In fact, $\mathbf{z}_i[k]$ is formed by the summation of $\frac{Q_i}{D_i}$ independent components. While $K_i^{(CQ)}$ increases linearly with $\frac{1}{D_i}$, $B_i^{(CQ)}$ also increases linearly with $\frac{1}{D_i}$ by (5.13). In other words, the numerator of (5.15) increases linearly while the denominator increases exponentially. As a result, the $L_i^{(CQ)}$ decreases with $\frac{1}{D_i}$ and the quantization noise power is reduced as well by (5.14).

In summary, in the proposed compressive quantization scheme, the baseband

signals from multiple time instants are first reduced into a lower dimension vector using the delay-and-add and then quantized. Because of the reduction in dimension, more bits can be allocated to each individual value in quantization, and the quantization noise power is reduced. On the other hand, due to the reduction of dimension, the independent baseband signals of multiple time instants are overlapped together, which creates some additional interference and makes the detection of the symbols more difficult. The parameter D_i in the proposed scheme can be tuned to balance the quantization noise power and the interference power. Since the length of $\mathbf{z}_i$ is $Q_i + (F-1) \cdot D_i$, with smaller D_i, the raw baseband signals are densely overlapped together, which creates much interference while significantly reduces the quantization noise power. With larger D_i, the reduction in quantization noise power is not so aggressive, while the extra interference created by the compressive quantization is also mild. In next subsection, we will propose weight vector designs to detect the symbols from the compressive quantized baseband signals.

Before we introduce the weight vectors that are used in the BBUs to detect the symbols, it is worth analyzing the complexity of the compressive quantization in the RRHs. By (5.5), the delay-and-add does not require the channel information, which reduces the communication overhead between the BBUs and the RRHs since the channel information is obtained in the BBUs. This is a desirable feature in the C-RAN since the front-haul link capacity is usually the bottleneck limiting the performance of the system. Moreover, as an example shown in Fig. 5.3, the processing in the RRHs only involves buffering and adding without multiplying, which can be easily implemented using low cost hardware. It enables the RRH to compress

the baseband signal from multiple antennas without complicated processing, which preserves the advantages of the C-RAN system that the RRHs are cheap and can be deployed with low cost.

5.2.2 The Weight Vector Design

As introduced in last subsection, each RRH processes the baseband signal using compressive quantization and transmits them to the BBUs via the front-haul links with limited capacity. The BBUs collect the baseband signals transmitted by each RRH and detect the intended symbol of each TD. In this subsection, two weight vector designs are proposed to detect the intended symbols from the compressive quantized baseband signals.

The aggregate of the baseband signal from all the RRHs collected at the BBUs can be written as

$$\begin{aligned}\tilde{\mathbf{z}} &= [\tilde{\mathbf{z}}_1^T, \tilde{\mathbf{z}}_2^T, \cdots, \tilde{\mathbf{z}}_M^T]^T \\ &= \mathbf{H}^{(eq)}\mathbf{x}^{(eq)} + \mathbf{n}^{(eq)} + \mathbf{q}^{(CQ)}\end{aligned} \tag{5.16}$$

where $\mathbf{H}^{(eq)} = [(\mathbf{H}_1^{(eq)})^T, (\mathbf{H}_2^{(eq)})^T, \cdots, (\mathbf{H}_M^{(eq)})^T]^T$, $\mathbf{n}^{(eq)} = [(\mathbf{n}_1^{(eq)})^T, (\mathbf{n}_2^{(eq)})^T, \cdots, (\mathbf{n}_M^{(eq)})^T]^T$, $\mathbf{q}^{(CQ)} = [(\mathbf{q}_1^{(CQ)})^T, (\mathbf{q}_2^{(CQ)})^T, \cdots, (\mathbf{q}_M^{(CQ)})^T]^T$.

Without loss of generality, in the rest of the chapter, we assume that $D_i = D$ for $i \in \{1, 2, \cdots, N\}$, while the analysis can be easily extended to the case that the RRHs use different D_i's. The BBUs use weight vectors to combine the elements of $\mathbf{z}$ so as to optimally detect the transmitted symbols of all the TDs. In this chapter, we first determine the optimal weight vectors $\mathbf{W}_{LMMSE}$ to minimize the mean square

error (MSE) of the detection. The problem can be formulated as

$$\min_{\mathbf{W}} \quad \sum_{k=1}^{N} E[\|\hat{\mathbf{x}}^{(eq)} - \mathbf{x}^{(eq)}\|^2] \tag{5.17}$$

where $\hat{\mathbf{x}}^{(eq)} = \mathbf{W}\tilde{\mathbf{z}}$. The solution to (5.17) can be written as [54]

$$\mathbf{W}^{(LMMSE)} = [\mathbf{\Sigma}_x - \mathbf{\Sigma}_x(\mathbf{H}^{(eq)})'\mathbf{\Sigma}_e^{-1}\mathbf{H}^{(eq)}(\mathbf{\Sigma}_x^{-1} + (\mathbf{H}^{(eq)})'\mathbf{\Sigma}_e^{-1}\mathbf{H}^{(eq)})^{-1}](\mathbf{H}^{(eq)})'\mathbf{\Sigma}_e^{-1} \tag{5.18}$$

where $\mathbf{\Sigma}_x = E[\mathbf{x}^{(eq)} \cdot (\mathbf{x}^{(eq)})']$, $\mathbf{\Sigma}_e = E[(\mathbf{n}^{(eq)} + \mathbf{q}^{(CQ)}) \cdot (\mathbf{n}^{(eq)} + \mathbf{q}^{(CQ)})']$. Since $\mathbf{n}^{(eq)}$ and $\mathbf{q}^{(CQ)}$ are independent, $\mathbf{\Sigma}_e = E[(\mathbf{n}^{(eq)}) \cdot (\mathbf{n}^{(eq)})'] + E[\mathbf{q}^{(CQ)} \cdot (\mathbf{q}^{(CQ)})']$.

The error covariance matrix for estimating $\mathbf{x}^{(eq)}$ using $\mathbf{W}^{(LMMSE)}$ can be written as

$$\mathbf{\Sigma_d} = \mathbf{\Sigma}_x - \mathbf{\Sigma}_x(\mathbf{H}^{(eq)})'(\mathbf{H}^{(eq)}\mathbf{\Sigma_x}(\mathbf{H}^{(eq)})' + \mathbf{\Sigma}_e)^{-1}\mathbf{H}^{(eq)}\mathbf{\Sigma}_x. \tag{5.19}$$

By (5.18), the calculation of $\mathbf{W}^{(LMMSE)}$ becomes difficult as the number of antennas increases. Under this condition, similar to that in the massive MIMO, some simple weight vector design such as maximum-radio combining (MRC) is effective. The MRC weight vector design is

$$\mathbf{W}^{(MRC)} = \mathbf{\Lambda} \cdot (\mathbf{H}^{(eq)})' \tag{5.20}$$

where $\mathbf{\Lambda}$ is a diagonal matrix with $\mathbf{\Lambda}_{i,i} = \frac{1}{(\mathbf{h}_i^{(eq)})' \cdot \mathbf{h}_i^{(eq)}}$ and $\mathbf{h}_i^{(eq)}$ is the i-th column of $\mathbf{H}^{(eq)}$.

To gain a better understanding of the performance of the symbol detection, let $\mathbf{x}[s]$ denote the symbol transmitted by the TD i at time j, i.e., $s = (j-1)*F+i$.

The $\hat{\mathbf{x}}^{(eq)}[s]$ can be written as

$$\begin{aligned}
\hat{\mathbf{x}}^{(eq)}[s] &= \mathbf{w}_s^H \tilde{\mathbf{z}} \\
&= \mathbf{w}_s^H \left(\mathbf{H}^{(eq)} \mathbf{x}^{(eq)} + \mathbf{n}^{(eq)} + \mathbf{q} \right) \\
&= \mathbf{w}_s^H \mathbf{h}_s^{(eq)} \mathbf{x}^{(eq)}[s] + \mathbf{w}_s^H \sum_{\substack{k=1 \\ k \neq s}}^{N*F} \mathbf{h}_k^{(eq)} \mathbf{x}^{(eq)}[k] + \mathbf{w}_s^H \left(\mathbf{n}^{(eq)} + \mathbf{q} \right) \\
&= \mathbf{w}_s^H \mathbf{h}_s^{(eq)} \mathbf{x}^{(eq)}[s] + \mathbf{w}_s^H \left(\sum_{k=1}^{(i-1)*F} \mathbf{h}_k^{(eq)} \mathbf{x}^{(eq)}[k] + \sum_{k=i*F+1}^{N*F} \mathbf{h}_k^{(eq)} \mathbf{x}^{(eq)}[k] \right) \\
&\quad + \mathbf{w}_s^H \sum_{\substack{k=(i-1)F+1 \\ k \neq s}}^{i*F} \mathbf{h}_k^{(eq)} \mathbf{x}^{(eq)}[k] + \mathbf{w}_s^H \left(\mathbf{n}^{(eq)} + \mathbf{q} \right)
\end{aligned} \tag{5.21}$$

where $\mathbf{w}_s^H$ is the s-th row of $\mathbf{W}$, which can be either $\mathbf{W}^{(LMMSE)}$ or $\mathbf{W}^{(MRC)}$. The first term in the last equality of (5.21) is the intended signal, the second term is inter-transmission interference (ITI) that caused by the transmission of other time instants, the third term is the inter-user interference (IUI) that caused by the symbols transmitted by other TDs at the same time instant, and the last term is noise which is the sum of the received AWGN and the quantization noise.

The signal power can be written as

$$\begin{aligned}
P_{sig} &= E_X[\|\mathbf{w}_s^H \mathbf{h}_s^{(eq)} \mathbf{x}^{(eq)}[s]\|^2] \\
&= \alpha_s \|\mathbf{w}_s^H \mathbf{h}_s^{(eq)}\|^2
\end{aligned} \tag{5.22}$$

where $\alpha_s = E[\|\mathbf{x}^{(eq)}[s]\|^2]$ is the power of $\mathbf{x}^{(eq)}[s]$. In this chapter, we assume that the transmitting power of all the symbols α_s's are predetermined before the transmission and the information is available in the BBUs.

Accordingly, the power of the ITI and the IUI can be written as

$$P_{iti} = E_X[\left\|\mathbf{w}_s^H \left(\sum_{k=1}^{(i-1)*F} \mathbf{h}_k^{(eq)} \mathbf{x}^{(eq)}[k] + \sum_{k=i*F+1}^{N*F} \mathbf{h}_k^{(eq)} \mathbf{x}^{(eq)}[k] \right) \right\|^2]$$
$$= \sum_{k=1}^{(i-1)*F} \alpha_k \|\mathbf{w}_s^H \mathbf{h}_k^{(eq)}\|^2 + \sum_{k=i*F+1}^{N*F} \alpha_k \|\mathbf{w}_s^H \mathbf{h}_k^{(eq)}\|^2 \tag{5.23}$$

and

$$P_{iui} = E_X[\left\|\mathbf{w}_s^H \sum_{\substack{k=(i-1)F+1 \\ k\neq s}}^{i*F} \mathbf{h}_k^{(eq)} \mathbf{x}^{(eq)}[k] \right\|^2]$$
$$= \sum_{\substack{k=(i-1)F+1 \\ k\neq s}}^{i*F} \alpha_k \|\mathbf{w}_s^H \mathbf{h}_k^{(eq)}\|^2. \tag{5.24}$$

The power of the noise can be written as

$$P_{noise} = E[\|\mathbf{w}_s^H (\mathbf{n}^{(eq)} + \mathbf{q})\|^2]$$
$$= \mathbf{w}_s^H \sigma_e \mathbf{w}_s. \tag{5.25}$$

By combining (5.22) to (5.25), the SINR of the symbol $\mathbf{x}^{(eq)}[s]$ can be written as

$$SINR = \frac{P_{sig}}{P_{iti} + P_{iui} + P_{noise}}. \tag{5.26}$$

From the analysis above, compared with the signal detection using $\mathbf{y}_i$'s, we can see extra interference ITI in (5.23) is created by overlapping the baseband signal of multiple time instants, which makes the detection of the symbol $\mathbf{x}^{(eq)}[s]$ more difficult than using the original baseband signal. On the other hand, by applying the compressive quantization, each individual value in $\mathbf{z}_i$ is allocated more bits, and in consequence the quantization noise power in (5.4) is reduced. Therefore, the

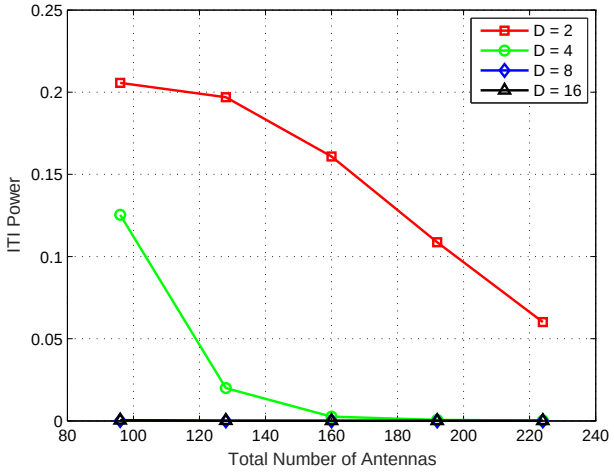

Figure 5.4: The ITI power decreases as more antennas are available

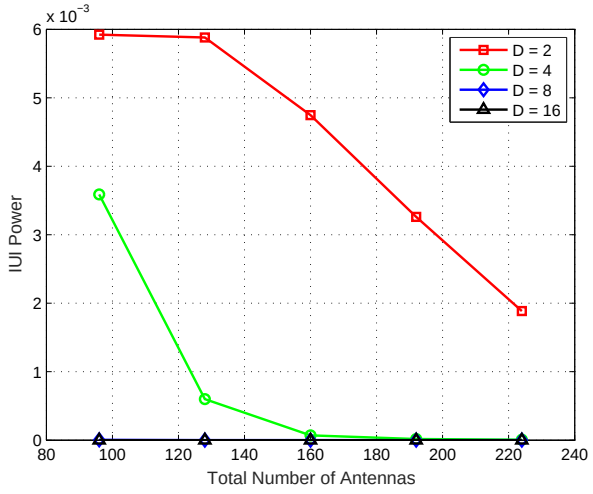

Figure 5.5: The IUI power decreases as more antennas are available

compressive quantization scheme reduces the quantization noise power at the cost of introducing extra interference power.

In this chapter, since all the RRHs are equipped with multiple antennas, the total number of antennas can be quite large, and the C-RAN system is in essence a virtual massive MIMO. In a massive MIMO system, it had been shown that when more antennas are available, the channel information vectors of multiple users are near orthogonal to each other, and the interference power diminishes [56, 57]. This phenomenon is also observed here. As shown in Fig. 5.4 and Fig. 5.5 where $Q_i = 16$ for $i = 1, 2, \cdots, M$, we increase the total number of antennas by deploying more RRHs. Both the ITI power and IUI power diminishes for different D's using the LMMSE weight vectors. Moreover, since Q_i and $B_i^{(CQ)}$ does not change for each RRH, the quantization noise power does not increase according to (5.14) and (5.15). As a result, the SINR in (5.26) is improved. In other words, the proposed compressive quantization scheme transforms the quantization power into interference power, which can be tackled in the BBUs by the corresponding weight vectors, especially when there are massive antennas available.

5.2.3 The Parallel Interference Cancellation

In last subsection, we introduce the weight vectors to detect the symbols transmitted by the TDs from the compressive quantized baseband signals. The weight vectors are constrained in the linear domain. In this subsection, we go one step beyond by using the parallel interference cancellation method to further mitigate

the interference, which is in the non-linear domain.

Unlike the AWGN and the quantization noise, the interference terms in (5.23) and (5.24) have their own structures, which can be further explored to improve the accuracy of the detection. Since the channel information $\mathbf{H}^{(eq)}$ is available in the BBUs, the ITI and IUI can be reconstructed and isolated from the intended signal if the relevant transmitted symbols are available. More specifically, the symbols initially detected by using the weight vectors are used to generate the approximate interference terms in (5.23) and (5.24), which are then subtracted from the original baseband signal in (5.21). After that, the updated estimator is employed to detect each symbol. In the following, the steps for the parallel interference cancellation scheme will be introduced. Without loss of generality, we assume that transmitted symbols are modulated using QPSK, while the proposed algorithm can be easily extended to other modulations.

The initially detected symbol $\bar{\mathbf{x}}^{(eq)}[s]$ can be written as

$$\bar{\mathbf{x}}^{(eq)}[s] = \mathtt{sign}(Re(\hat{\mathbf{x}}^{(eq)}[s])) + \mathtt{sign}(Im(\hat{\mathbf{x}}^{(eq)}[s])) * j \tag{5.27}$$

where $\hat{\mathbf{x}}^{(eq)}$ is obtained using either LMMSE or MRC weight vectors.

Next, we generate the ITI and IUI cancellation vectors for symbol $\mathbf{x}[s]$.

$$ITI[s] = \left(\sum_{k=1}^{(i-1)*F} \mathbf{h}_k^{(eq)} \bar{\mathbf{x}}^{(eq)}[k] + \sum_{k=i*F+1}^{N*F} \mathbf{h}_k^{(eq)} \bar{\mathbf{x}}^{(eq)}[k] \right) \tag{5.28}$$

$$IUI[s] = \sum_{\substack{k=(i-1)F+1 \\ k \neq s}}^{i*F} \mathbf{h}_k^{(eq)} \bar{\mathbf{x}}^{(eq)}[k] \tag{5.29}$$

Since the ITI and IUI cancellation vectors only depend on the initial detected symbols $\bar{\mathbf{x}}^{(eq)}$, the calculation can be done in parallel for each symbol $\mathbf{x}[s]$. When the ITI and IUI cancellation vectors are available, they are subtracted from the orignal baseband signal, which can be written as

$$\tilde{\mathbf{z}}^{(IC)}[s] = \tilde{\mathbf{z}}[s] - ITI[s] - IUI[s]. \tag{5.30}$$

When $\tilde{\mathbf{z}}^{(IC)}$ is obtained, the ITI and IUI are eliminated from the original baseband signal[1] $\tilde{\mathbf{z}}$, and we can use the simple MRC weight vector [63] to update the corresponding transmitted symbols. The updated estimated symbol $\hat{\mathbf{x}}^{(eq,IC)}[s]$ is calculated as

$$\hat{\mathbf{x}}^{(eq,IC)}[s] = \mathbf{m}_s' \tilde{\mathbf{z}}^{(IC)} \tag{5.31}$$

where $\mathbf{m}_s = \mathbf{h}_s^{(eq)}$ is the weight vector for symbol $\mathbf{x}^{(eq)}[s]$. The detected symbols are updated using $\hat{\mathbf{x}}^{(eq,IC)}$. More specifically,

$$\bar{\mathbf{x}}^{(eq,IC)}[s] = \texttt{sign}(Re(\hat{\mathbf{x}}^{(eq,IC)}[s])) + \texttt{sign}(Im(\hat{\mathbf{x}}^{(eq,IC)}[s])) * j. \tag{5.32}$$

The steps for the parallel interference cancellation based symbol updating are summarized in Algorithm 4.

With this algorithm, we can further leverage the advantages of the C-RAN architecture to improve the detection accuracy of each symbol: the BBUs are empowered by high performance computing, and holds the necessary information that enables us to perform the algorithm.

[1]There are residue IUI and ISI power due to the errors in determining $\bar{\mathbf{x}}^{(eq)}$, which can be ignored if the original BER is not too high.

Algorithm 4 Parallel Interference Cancellation Based Symbol Updating

1 Make the initial decision using (5.27)

2 Generate the approximate IUI and ISI terms using (5.28) and (5.29)

3 Subtract the IUI and ISI terms from the original baseband signal using (5.30)

4 Update the symbols using (5.31) and (5.32)

Looking at the overall compressive quantization and detection process, we can see it is tailored for the C-RAN architecture. In the compressive quantization which happens at the RRH side, the processing is as simple as possible so that the advantage of low deployment cost of the C-RAN architecture is preserved. The entire process is effective with all the complicated signal processing in the BBUs where high performance computing power and the necessary information are readily available.

5.3 Extension to The OFDM Based C-RAN

In the above, we have proposed the compressive quantization algorithm which applies to the single tap channel. Due to the rapid growth of demand for wireless communications, larger bandwidth are being utilized. Typically, with larger bandwidth, the traffic load in the front-haul link will increase due to higher sampling rate. In this section, we apply the proposed algorithm to the uplink of OFDM based C-RAN, which significantly reduces the traffic load in the front-haul links caused by increasing the bandwidth.

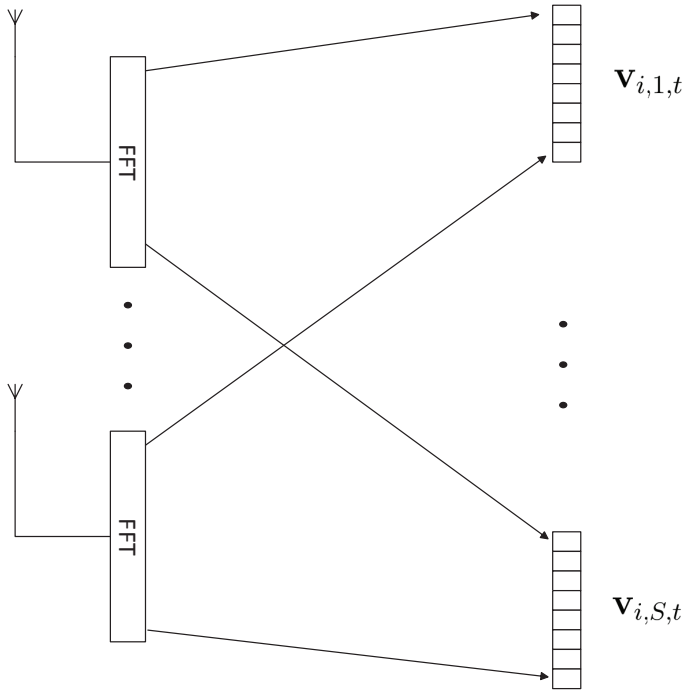

Figure 5.6: An example of re-organizing the baseband signal with $Q_i = 8$

We consider the uplink of OFDM based multi-antenna C-RAN where the TDs use OFDMA [64] to access the wireless medium. Assume that all the TDs are equipped with a single antenna while RRH i is equipped with Q_i antennas where $Q_i > 1$. All the RRHs work in the same spectrum. Each TD maps the symbols to the allocated subcarriers before adding the cyclic prefix and transmitting them. Without loss of generality, we assume that the transmitted signal is received by all the RRHs.

At the RRH side, for the baseband signal received by each antenna, the cyclic prefix is removed and the FFT is periodically performed. We define a cycle as the time between two consecutive FFTs. As shown in Fig. 5.6, after the FFT, the baseband signal of the same subcarrier from all the antennas are collected in

$\mathbf{v}_{i,c,t} = [\mathbf{v}_{i,c,t}[1], \mathbf{v}_{i,c,t}[2], \cdots, \mathbf{v}_{i,c,t}[Q_i]]^T$ where $\mathbf{v}_{i,c,t}[k]$ denotes the component in the subcarrier c of the k-th antenna of RRH i at the t-th cycle.

By the special property of OFDM in transforming multipath channel into a number of equivalent interference-free subchannels [65], $\mathbf{v}_{i,c,t}[k]$ can be written as

$$\mathbf{v}_{i,c,t} = \begin{bmatrix} \mathbf{g}_{i,c,t}[1] \\ \mathbf{g}_{i,c,t}[2] \\ \vdots \\ \mathbf{g}_{i,c,t}[Q_i] \end{bmatrix} x_c + \mathbf{n}_{i,c,t} \triangleq \mathbf{g}_{i,c,t} x_c + \mathbf{n}_{i,c,t} \tag{5.33}$$

where x_c is the value transmitted in the subcarrier c, $\mathbf{g}_{i,c}[k]$ is the equivalent channel impulse response on subcarrier c between the k-th antenna of RRH i and the TD which the subcarrier is allocated to at cycle t. $\mathbf{n}_{i,c,t}$ is the noise at RRH i in subcarrier c at cycle t. It is shown that an equivalent channel is established in the subcarrier c.

As the system utilizes larger bandwidth, there are more subcarriers and thus more $\mathbf{v}_{i,c,t}$'s are obtained at each cycle. Directly transmitting them through the limited capacity front-haul to the BBUs becomes difficult. To tackle this problem, we apply the proposed compressive quantization and detection scheme to the system. Instead of transmitting the baseband signal $\mathbf{v}_{i,c,t}$'s separately, we partition them into multiple groups and apply the compressive quantization to the baseband signals within each group. More specifically, let β_r denote the set of subcarriers in group r and the cardinality of β_r is N_r, then we can calculate the baseband signal $\mathbf{u}_{i,t}^r$ for

the group r of the i-th RRH at cycle t, which can be written as

$$\begin{aligned}
\mathbf{u}_{i,t}^{r} &= \sum_{c\in\beta_r} \mathbf{v}_{i,c,t} \\
&= \sum_{c\in\beta_r} \mathbf{g}_{i,c,t} x_c + \sum_{c\in\beta_r} \mathbf{n}_{i,c,t} \\
&= [\mathbf{g}_{i,1,t}\mathbf{g}_{i,2,t}\cdots\mathbf{g}_{i,N_r,t}] \begin{bmatrix} x_1 \\ x_2 \\ \vdots \\ x_{N_r} \end{bmatrix} + \sum_{c\in\beta_r} \mathbf{n}_{i,c,t} \\
&\triangleq \mathbf{G}_{i,t}\mathbf{x}_t + \mathbf{n}_{i,t}. \qquad (5.34)
\end{aligned}$$

Since (5.34) is equivalent to (5.1), the proposed compressive quantization scheme can be applied to each group, and all the subcarrier components can be recovered at the BBUs by performing the weight vectors and the parallel interference cancellation schemes for each group.

By applying the compressive quantization, the baseband signals are reduced in both frequency and time domain. Compared with directly transmitting the baseband signals through the front-haul links, the baseband signals corresponding to different subcarriers do not need to be transmitted separately. As a result, the traffic load in the front-haul links caused by adopting larger bandwidth is less severe.

To illustrate this effect, we analyze the front-haul traffic load for the proposed method. For RRH i, since the baseband signal for each group is transmitted separately, we just analyze the baseband signal for one group. Assume the bandwidth utilized in the system is J Hz, which is corresponding to S subcarriers. Then the

rate of each baseband component $\mathbf{v}_{i,c,t}^r$ is $\frac{J}{S}$ Hz, i.e., the separation between $\mathbf{u}_{i,t}^r$ and $\mathbf{u}_{i,t+1}^r$ is $\frac{S}{J}$ seconds. Assume U_i bits are used for each individual value of the signal reduced using delay-and-add, the group r of RRH i requires $(Q_i + (F-1)D_i)U_i$ bits in $\frac{SF}{J}$ seconds. Therefore, the traffic load in the front-link is

$$\begin{aligned} C_i &= \frac{(Q_i + (F-1)D_i)U_i}{\frac{SF}{J}} \\ &= \frac{(Q_i + (F-1)D_i)U_i}{F} \cdot \frac{J}{S} \\ &\approx D_i U_i \cdot \frac{J}{S} \end{aligned} \tag{5.35}$$

where the approximation is due to the fact that the frame length F is always much larger than Q_i.

Typically, the number of subcarriers S increases with the utilized bandwidth J and $\frac{J}{S}$ keeps constant. Therefore, if D_i keeps constant, the traffic load in the front-haul link only depends on U_i. If U_i also keeps constant, the traffic load in the front-haul link keeps constant independent of the bandwidth J adopted. In fact, when larger bandwidth is used, there are more subcarriers in each group. As a result, more raw baseband signal components are added together and the dynamic range increases. Larger U_i is required for each value and the traffic load in the front-haul link grows accordingly. However, as will be shown in section 5.4, U_i only increases slightly as J increase to maintain good performance. Therefore, the proposed compressive quantization scheme facilitates the usage of larger bandwidth in the OFDM based multi-antenna C-RAN system.

5.4 Numerical Results

In this section, we use numerical results to illustrate the effectiveness of the proposed scheme. We first evaluate the performance of the proposed compressive quantization scheme under the single tap channel model. It is shown that the proposed scheme is better than existing schemes in tackling the front-haul link capacity deficit. The performance gap between LMMSE and MRC weight vectors are also investigated. It is shown that the gap decreases with more antennas available or by performing the proposed parallel interference cancellation scheme. We further evaluate the performance of the proposed scheme to the OFDM based C-RAN under multipath channel. It is shown that the proposed scheme can facilitate the C-RAN utilize larger bandwidth with limited front-haul capacity.

5.4.1 Performance of The Proposed Scheme Under Single-Tap Channel

Suppose there are N TDs and M RRHs distributed in an area where each TD is equipped with a single antenna, while each RRH is equipped with multiple antennas and has limited front-haul capacity. All the TDs and RRHs work in the same spectrum. All the TDs simultaneously transmit the signal through the wireless medium to all the RRHs. Each RRH receives a mixture of the signal transmitted by all the TDs. The baseband signal is processed at each RRH using the proposed compressive quantization scheme before it is transmitted through the front-haul

links to the BBUs where the LMMSE weight vector proposed in (5.18) is applied to detect the symbols transmitted by all the TDs.

In the first experiment, the bandwidth is 10 MHz, and the signal to noise ratio (SNR) is 10 db[2], the number of TDs is $N = 30$. We fix $Q_i = 16$ and vary the number of RRHs so as to change the total number of antennas T. We run the experiment over multiple channel realizations where the $h_{i,j}^{(k)}$'s are drawn from independent complex Gaussian distributions and calculate the average SINR and MSE. In Fig. 5.7 through 5.12, we show the average SINR and MSE of each single TD using LMMSE weight vectors under various per front-haul link capacities.

We use $D_i = D, \forall i$ in this experiment and change the parameter D so as to adjust the interference power and the quantization noise. It is shown that for each of the D, the SINR of each TD improves as more antennas are available where the interference power is mitigated. Moreover, the theoretical values of MSE in (5.19) match well with the experimental values.

We continue to look at Fig. 5.7 through 5.12. The performance of the proposed compressive quantization scheme is compared with the spatial filtering method in [62]. It is shown that the proposed compressive quantization scheme outperforms the spatial filtering method when the front-haul link capacity is low. The reason is that the compressive quantization scheme provides the flexibility in transforming the

[2]Typically, the AWGN is composed of the environmental noise, the device thermal noise and the quantization noise caused by the ADC. In this work, even with 8-bit commodity ADC, the quantization noise power is approximately $\frac{1}{10000}$ of the signal power. Therefore, the 10 db SNR is compatible with commodity ADC.

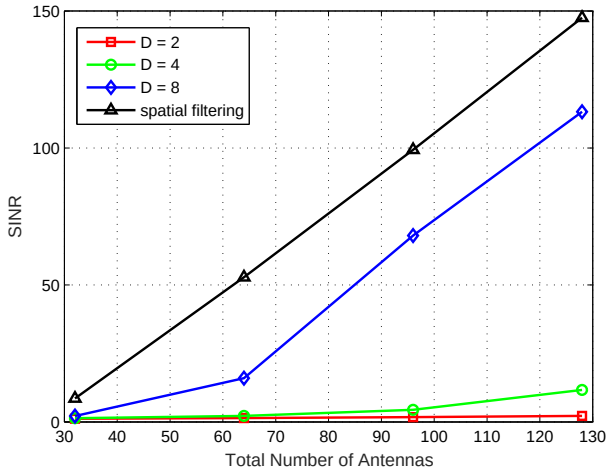

Figure 5.7: Average SINR of C = 1.2 Gb/s

quantization noise power into interference power to suit for low capacity front-haul links. The tradeoff between the quantization noise power and the interference power can be adjusted by changing the parameter D. By Fig. 5.2, smaller D will create stronger interference power since the signals are densely overlapped, and reduces the quantization noise power significantly. On the other hand, larger D will create less interference power while mitigates the quantization noise power moderately. In the spatial filtering method, no such flexibility is provided since the baseband signals of multiple time instants are transmitted separately. The ability to tackle low capacity front-haul links is limited.

We further apply the interference cancellation method proposed in section 5.2.3 to the multi-RRH uplink system. All the 30 TDs use QPSK as the modulation. As shown in Fig. 5.13 through 5.15, the interference cancellation scheme improves the BER when the original BER is not too high. Moreover, it is observed that the improvement of BER is more significant in the compressive quantization

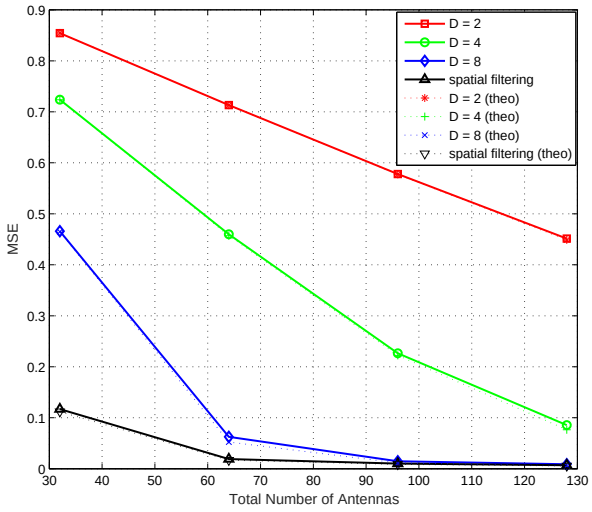

Figure 5.8: Average MSE of C = 1.2 Gb/s

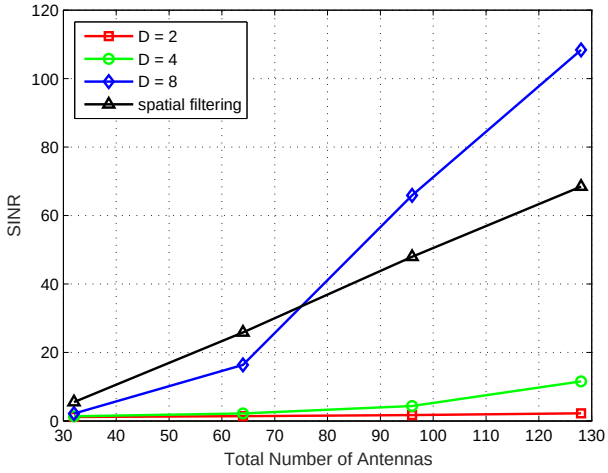

Figure 5.9: Average SINR of C = 1.0 Gb/s

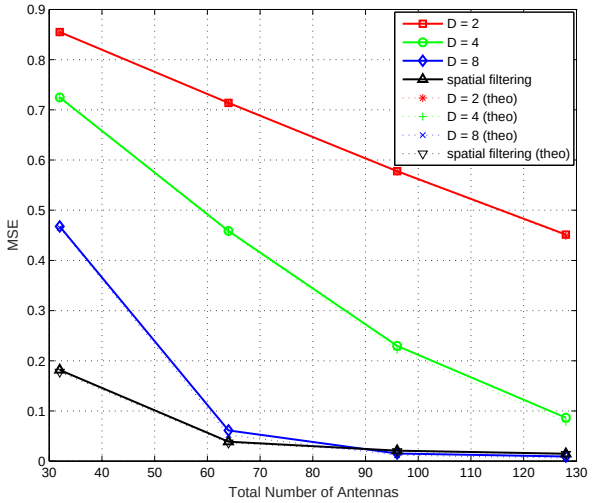

Figure 5.10: Average MSE of C = 1.0 Gb/s

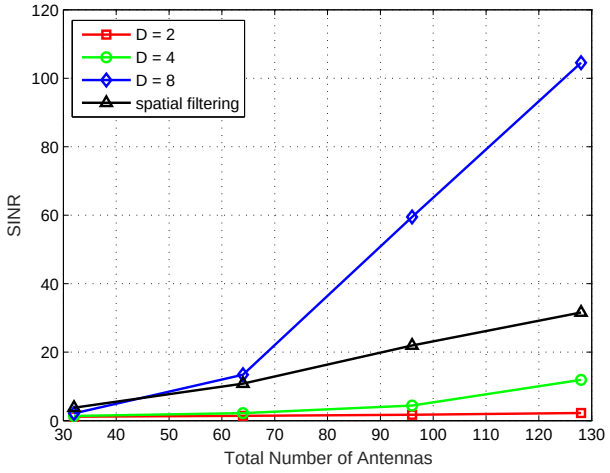

Figure 5.11: Average SINR of C = 0.8 Gb/s

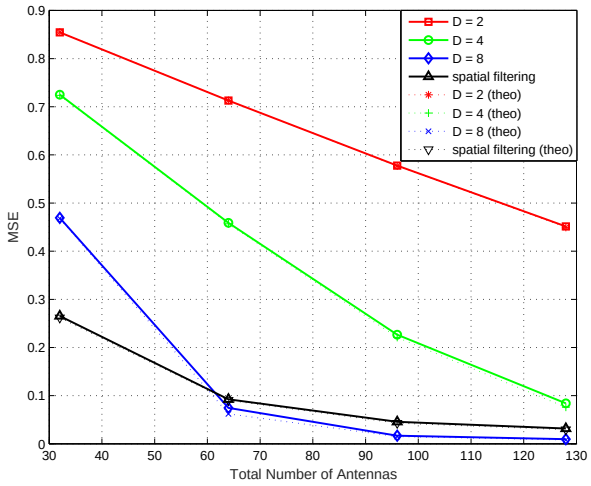

Figure 5.12: Average MSE of C = 0.8 Gb/s

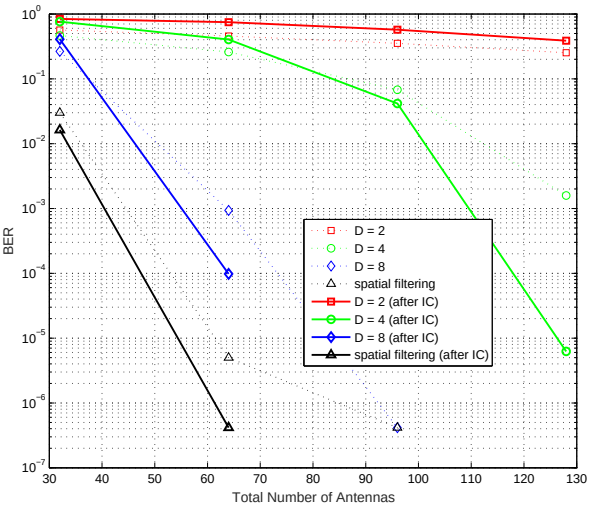

Figure 5.13: The BER performance of C = 1.0 Gb/s

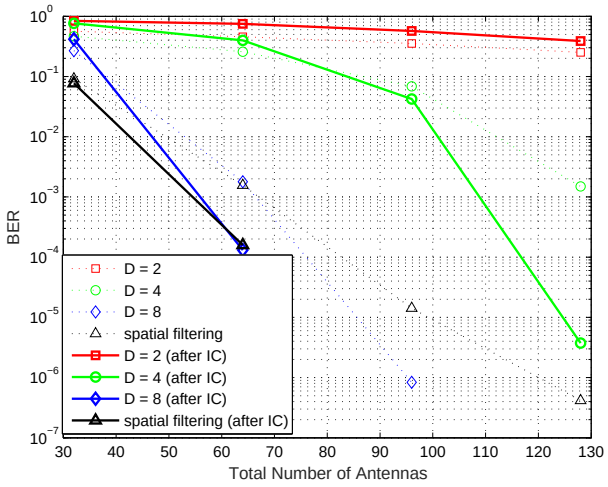

Figure 5.14: The BER performance of C = 800 Mb/s

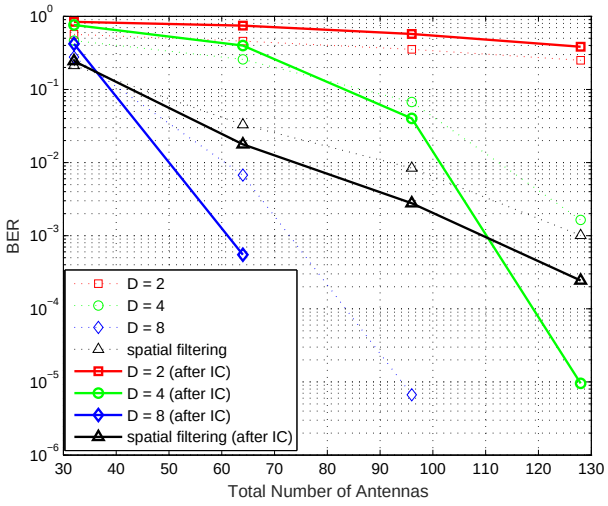

Figure 5.15: The BER performance of C = 600 Mb/s

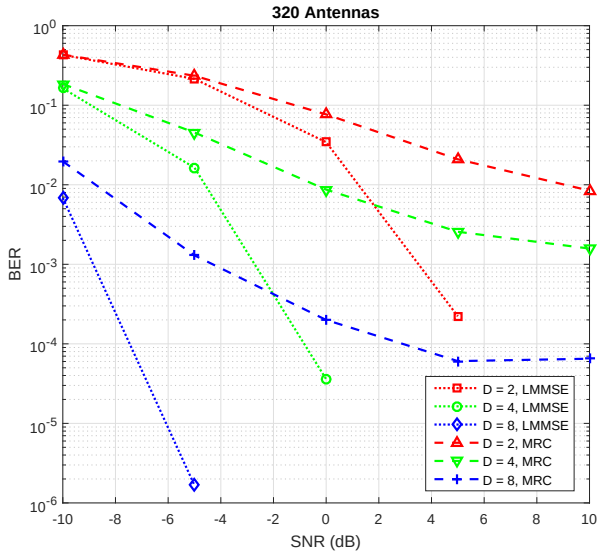

Figure 5.16: The BER performance of 320 antennas without PIC

scheme than in the spatial filtering scheme in [62]. The reason is that the compressive quantization scheme transforms the quantization noise power into interference power. Unlike the quantization noise, the interference has its own structure and can be further suppressed by the interference cancellation scheme.

It can be seen from (5.18) that as the total number of antennas increases, the calculation of $\mathbf{W}^{(LMMSE)}$ becomes difficult. On the other hand, when there are significantly more antennas than users, the entire system becomes a virtual massive MIMO and the basic MRC weight vectors become effective. As the performance gap between the LMMSE and MRC weight vectors have been observed in [66] and [67], we compare the performance of the LMMSE and MRC weight vectors in the proposed system under the condition $Q_i = 16$ an $N = 10$. The front-haul capacity $C = 0.6Gb/s$ is used. The symbols are modulated using QPSK.

As shown in Fig. 5.16 and Fig. 5.17, the performances of the LMMSE weight

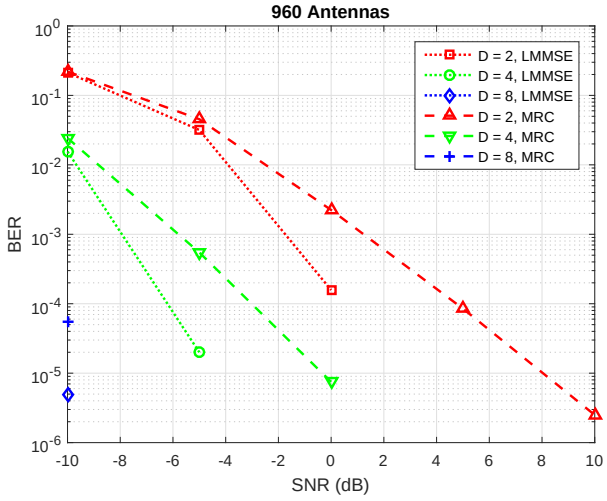

Figure 5.17: The BER performance of 960 antennas without PIC

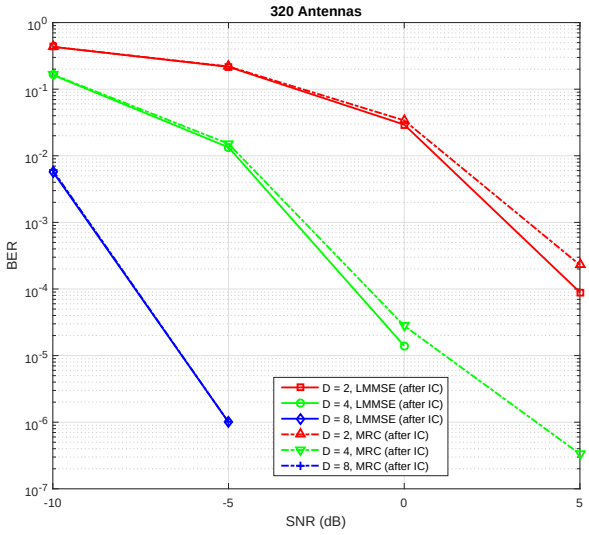

Figure 5.18: The BER performance of 320 antennas with PIC

vectors and the MRC weight vectors get close as more antennas are available. In other words, with massive antennas, while calculating $\mathbf{W}^{(LMMSE)}$ becomes difficult, it can be replaced by $\mathbf{W}^{(MRC)}$ that is much easier to obtain.

Another way to bypass the difficulty in calculating $\mathbf{W}^{(LMMSE)}$ is to use the proposed parallel interference cancellation (PIC) scheme. By comparing Fig. 5.16 and Fig. 5.18, the system performance is improved by performing PIC for both LMMSE and MRC weight vectors without changing the number of antennas. Moreover, the performance gap is reduced after the PIC. The reason is that the PIC cancels much of the interference which the MRC weight vectors are not able to deal with as well as the LMMSE weight vectors do.

5.4.2 Application to The OFDM Based Multi-Antenna C-RAN Under Multipath Channel

Next, we apply the proposed scheme to the OFDM based broadband uplink system. In this experiment, each RRH is equipped with 8 antennas. The bandwidth of the system is 20 MHz, which is corresponding to 1200 subcarriers. We group the 1200 subcarriers into 40 groups with 30 subcarriers in each group. The bits are allocated equally among all groups. Within each group, the baseband signals within each group are processed using the compressive quantization proposed in section 5.3 and the LMMSE weight vectors are used in the BBUs. In Table 5.1, the EVM [68] performance under different modulations and front-haul capacities are presented. It is shown that even with the 40 Mb/s front-haul link capacity which

is relatively low, the EVM performance is satisfactory. In contrast, typically, at 20 MHz bandwidth, even the single-antenna RRH has to use fiber optics with multiple Gb/s capacity to have satisfactory performance [69]. It is due to the fact that the baseband signals from multiple subcarriers and multiple time instants are combined together and transmitted in the front-haul links, which alleviates a lot of traffic load in the front-haul links. This phenomenon is similar to the "time-reversal tunneling effect" observed in [70] where the unique spatial and temporal focusing effects of time-reversal communication make it possible to detect the symbols transmitted by multiple TDs from the blended baseband signals. In this system, the spatial diversity provided by the large number of available antennas help the BBUs effectively detect the symbols transmitted by the TDs from the compressive quantized baseband signal.

To further illustrate the advantage of the compressive quantization scheme, we compare the growth of the front-haul traffic load in the front-haul links. In this experiment, instead of using fixed bandwidth, we gradually change the bandwitdh from 5 MHz to 20 MHz. Let $\phi^{(CQ)}(J)$ and $\phi^{(CPRI)}(J)$ denote the traffic load in each front-haul link for bandwidth J using compressive quantization and the CPRI compression [71] under the condition that the EVM is below 5% with QPSK modulation. We plot the normalized traffic load for each compression scheme where $\epsilon^{(CQ)}(J) = \frac{\phi^{(CQ)}(J)}{\phi^{(CQ)}(J)|_{J=5MHz}}$ and $\epsilon^{(CPRI)}(J) = \frac{\phi^{(CPRI)}(J)}{\phi^{(CPRI)}(J)|_{J=5MHz}}$. As shown in Fig. 5.19, the traffic load for the system using compressive quantization grows slower than that using the CPRI compression. The reason is that the compressive quantization scheme allows the baseband signals in multiple subcarriers to be combined

together and transmitted.

Table 5.1: the EVM of the compressive quantization scheme applied to the OFDM based C-RAN

	$T = 80$	$T = 112$	$T = 128$
QPSK, C = 0.02	19.64	12.31	10.75
QPSK, C = 0.03	9.99	5.47	4.63
QPSK, C = 0.04	7.71	5.84	3.49
16QAM, C = 0.02	19.72	12.40	10.80
16QAM, C = 0.03	9.14	6.89	4.38
16QAM, C = 0.04	7.65	5.61	4.22
64QAM, C = 0.02	19.72	12.26	10.80
64QAM, C = 0.03	9.29	6.63	4.65
64QAM, C = 0.04	8.08	4.65	4.54

5.5 Conclusion

In this chapter, inspired by the TR based C-RAN proposed in Chapter 3, we propose the compressive quantization and symbol detection scheme for the uplink of multi-antenna cloud radio access network (C-RAN) to tackle the limited front-haul capacity challenge. The proposed scheme is tailored for the C-RAN architecture in that the complexity of the compressive quantization which happens in the remote radio head (RRH) is low and can be implemented using basic buffering and adding

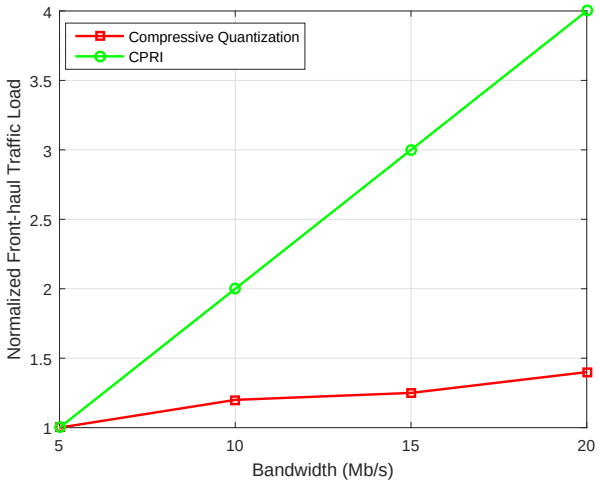

Figure 5.19: The comparison of traffic load in front-haul link between CPRI and compressive quantization

operations, due to which the low deployment cost feature of the C-RAN is preserved and massive antennas can be utilized by deploying multiple RRHs. With the spatial diversity provided by the massive antennas, the baseband units (BBUs) are able to efficiently detect the symbols transmitted by the terminal devices (TDs) from the compressive quantized baseband signal. Numerical results show that the proposed scheme is efficient for the multi-antenna C-RAN in tackling the front-haul capacity deficit challenge. We further extend the proposed scheme to the OFDM based multi-antenna C-RAN. It is also shown that the proposed scheme can facilitate the OFDM based C-RAN utilize larger bandwidth with limited front-haul capacity.

Chapter 6: Conclusion and Future Work

6.1 Conclusion

In this dissertation, we have addressed the scalable cloud radio access networks (C-RAN) in the following aspects:

First, we investigated the scalability issues in the existing wireless networks and proposed a time-reversal (TR) based network by utilizing the natural focusing effects of TR based communications. The performance of the proposed system was evaluated in the open access and closed access models. Since the interference is automatically mitigated without coordination among access points (APs), the proposed system can be easily extended to serve massive terminal devices (TDs) in the open access model. In the closed access model, the performance degradation caused by neighboring devices is graceful. Moreover, it is shown that the packet delay in the proposed system is lower than that in the IEEE 802.11 system under the massive device setting. Through this work, we realize the advantage of TR communications in providing scalable wireless networking solutions.

Second, we proposed a time-reversal (TR) based cloud radio access network (C-RAN) architecture. Both the downlink and uplink working schemes were designed and analyzed. Through analysis, we discovered the TR "tunneling effects" in

the proposed C-RAN architecture, i.e., the baseband signals for multiple terminal devices (TDs) can be efficiently combined and transmitted in the front-haul link to alleviate the traffic load. We built a TR radio prototype to measure the wireless channel in the real-world environment, with which we illustrated the tunneling effects in both downlink and uplink of the proposed C-RAN architecture. It is observed that for both downlink and uplink, the sum spectral efficiency of multiple TDs increases with the number of TDs in the system while the front-haul data rate keeps almost constant.

Third, we investigated the optimization on the downlink and uplink transmissions in TR based C-RAN. The content/channel information and the computing power in the baseband unit (BBU) pool are utilized to optimize the waveforming in the downlink and the uplink. The asymmetric architecture of TR communication is preserved in the optimization and no change in the terminal device (TD) is needed. In this way, the performance of the TR based C-RAN can be improved while keeping the low cost of the TDs. We illustrated that the proposed algorithms can significantly improve the downlink and uplink transmission reliability over basic TR waveforms and traditional waveforming schemes.

Lastly, generalizing from the TR-based C-RAN, we proposed the compressive quantization and symbol detection scheme for the uplink of a multi-antenna C-RAN to tackle the limited front-haul capacity challenge. The proposed scheme is tailored for the C-RAN architecture in that the complexity of the compressive quantization which happens in the remote radio head (RRH) is low and can be implemented using basic buffering and adding operations, due to which the low deployment cost

feature of the C-RAN is preserved and massive antennas can be utilized by deploying multiple RRHs. With the spatial diversity provided by the massive antennas, the BBUs are able to efficiently detect the symbols transmitted by the terminal devices (TDs) from the compressive quantized baseband signal. It was illustrated that the proposed scheme is efficient for the multi-antenna C-RAN in tackling the front-haul capacity deficit challenge. We further extended the proposed scheme to the OFDM based multi-antenna C-RAN. It was also shown that the proposed scheme can facilitate the OFDM based C-RAN utilize larger bandwidth with limited front-haul capacity.

6.2 Future Work

In this dissertation, the scalable C-RAN problems are formulated from the perspective that all the devices are homogeneous. In the future, the massive wireless devices can be quite different from one another in many aspects. For example, different types of devices can have different requirements on the quality of service. They can also have different power constraints due to the variation in power source. The bandwidth that can be utilized by each device can be different since higher rate analog to digital converter (ADC) and digital to analog converter (DAC) are necessary to leverage larger bandwidth, which might not be possible for every device. In the future work, it is important to study the scalability of the C-RAN considering heterogeneous devices.

In the problems studied in this dissertation, the main focus is on the transmis-

sion phase where precise and instantaneous channel information is available from the prior channel acquisition phase. However, in a network with massive devices, it might be difficult to obtain the channel information of all the devices within limited time. Moreover, the obtained channel information is always contaminated by different types of noise and interference. The lack of precise channel information will affect the performance of transmission phase. Therefore, in the future research on the scalability of wireless network, the channel acquisition phase deserves more investigation. It is interesting to jointly design the channel acquisition and transmission schemes where the transmission phase is aware of the inaccuracy in the channel information and can formulate optimization problems to minimize its influence.

Bibliography

[1] Qualcomm. 1000x mobile data challenge. Technical report, November 2013.

[2] ChinaMobile. C-ran: The road towards green ran. *White Paper*, October 2011.

[3] M. Webb, Zhaojun Li, P. Bucknell, T. Moulsley, and S. Vadgama. Future evolution in wireless network architectures: Towards a 'cloud of antennas'. In *Vehicular Technology Conference (VTC Fall), 2012 IEEE*, pages 1–5, Sept 2012.

[4] Chih-Lin I, Jinri Huang, Ran Duan, Chunfeng Cui, J.X. Jiang, and Lei Li. Recent progress on c-ran centralization and cloudification. *IEEE Access*, 2:1030–1039, 2014.

[5] Y.D. Beyene, R. Jantti, and K. Ruttik. Cloud-ran architecture for indoor das. *IEEE Access*, 2:1205–1212, 2014.

[6] A Ghosh, R. Ratasuk, B. Mondal, N. Mangalvedhe, and T. Thomas. Lte-advanced: next-generation wireless broadband technology [invited paper]. *Wireless Communications, IEEE*, 17(3):10–22, June 2010.

[7] J. Lorca and L. Cucala. Lossless compression technique for the fronthaul of lte/lte-advanced cloud-ran architectures. In *2013 IEEE 14th International Symposium and Workshops on a World of Wireless, Mobile and Multimedia Networks (WoWMoM)*, pages 1–9, June 2013.

[8] Rui Wang, Honglin Hu, and Xiumei Yang. Potentials and challenges of c-ran supporting multi-rats toward 5g mobile networks. *IEEE Access*, 2:1187–1195, 2014.

[9] Binbin Dai and Wei Yu. Sparse beamforming and user-centric clustering for downlink cloud radio access network. *IEEE Access*, 2:1326–1339, 2014.

[10] R. Zakhour and D. Gesbert. Optimized data sharing in multicell mimo with finite backhaul capacity. *IEEE Transactions on Signal Processing*, 59(12):6102–6111, Dec 2011.

[11] Yuhan Zhou and Wei Yu. Optimized backhaul compression for uplink cloud radio access network. *IEEE Journal on Selected Areas in Communications*, 32(6):1295–1307, June 2014.

[12] Xiongbin Rao and V.K.N. Lau. Distributed fronthaul compression and joint signal recovery in cloud-ran. *IEEE Transactions on Signal Processing*, 63(4):1056–1065, Feb 2015.

[13] Seok-Hwan Park, O. Simeone, O. Sahin, and S. Shamai. Inter-cluster design of precoding and fronthaul compression for cloud radio access networks. *IEEE Wireless Communications Letters*, 3(4):369–372, Aug 2014.

[14] O. Simeone, O. Somekh, H. V. Poor, and S. Shamai. Downlink multicell processing with limited-backhaul capacity. *EURASIP Journal on Advances in Signal Processing*, 2009:3:1–3:10, February 2009.

[15] Beibei Wang, Yongle Wu, Feng Han, Yu-Han Yang, and K. J. R. Liu. Green wireless communications: A time-reversal paradigm. *Selected Areas in Communications, IEEE Journal on*, 29(8):1698–1710, September 2011.

[16] Feng Han, Yu-Han Yang, Beibei Wang, Yongle Wu, and K. J. Ray Liu. Time-reversal division multiple access over multi-path channels. *Communications, IEEE Transactions on*, 60(7):1953–1965, July 2012.

[17] Feng Han and K. J. Ray Liu. A multiuser trdma uplink system with 2d parallel interference cancellation. *Communications, IEEE Transactions on*, 62(3):1011–1022, March 2014.

[18] Hang Ma, Feng Han, and K. J. R. Liu. Interference-mitigating broadband secondary user downlink system: A time-reversal solution. In *Global Communications Conference (GLOBECOM), 2013 IEEE*, pages 884–889, Dec 2013.

[19] Yu-Han Yang, Beibei Wang, W.S. Lin, and K. J. R. Liu. Near-optimal waveform design for sum rate optimization in time-reversal multiuser downlink systems. *Wireless Communications, IEEE Transactions on*, 12(1):346–357, January 2013.

[20] Y. Chen, F. Han, Y.-H. Yang, H. Ma, Y. Han, C. Jiang, H.-Q. Lai, D. Claffey, Z. Safar, and K. J. R. Liu. Time-reversal wireless paradigm for green internet of things: An overview. *Internet of Things Journal, IEEE*, 1(1):81–98, Feb 2014.

[21] Juan Ramiro and Khalid Hamied. *Self-Organizing Networks (SON): Self-Planning, Self-Optimization and Self-Healing for GSM, UMTS and LTE*. John Wiley & Sons, 2011.

[22] Iperf - the tcp/udp bandwidth measurement tool.

[23] Mesut Ali Ergin, Kishore Ramachandran, and Marco Gruteser. An experimental study of inter-cell interference effects on system performance in unplanned wireless lan deployments. *Computer Networks*, 52(14):2728–2744, 2008.

[24] Jing Zhu, B. Metzler, Xingang Guo, and Y. Liu. Adaptive csma for scalable network capacity in high-density wlan: A hardware prototyping approach. In *INFOCOM 2006. 25th IEEE International Conference on Computer Communications. Proceedings*, pages 1–10, April 2006.

[25] M.K. Panda and A. Kumar. Modeling multi-cell ieee 802.11 wlans with application to channel assignment. In *Modeling and Optimization in Mobile, Ad Hoc, and Wireless Networks, 2009. WiOPT 2009. 7th International Symposium on*, pages 1–10, June 2009.

[26] Andrea Goldsmith. *Wireless communications*. Cambridge university press, 2005.

[27] Radha Krishna Ganti. *A STOCHASTIC GEOMETRY APPROACH TO THE INTERFERENCE AND OUTAGE CHARACTERIZATION OF LARGE WIRELESS NETWORKS*. Phd dissertation, University of Notre Dame, Indiana, 2009.

[28] G. de la Roche, A. Valcarce, D. Lopez-Perez, and Jie Zhang. Access control mechanisms for femtocells. *Communications Magazine, IEEE*, 48(1):33–39, January 2010.

[29] Ping Xia, V. Chandrasekhar, and J.G. Andrews. Open vs. closed access femtocells in the uplink. *Wireless Communications, IEEE Transactions on*, 9(12):3798–3809, December 2010.

[30] J.G. Andrews, H. Claussen, M. Dohler, S. Rangan, and M.C. Reed. Femtocells: Past, present, and future. *Selected Areas in Communications, IEEE Journal on*, 30(3):497–508, April 2012.

[31] S. Mukherjee. Distribution of downlink sinr in heterogeneous cellular networks. *Selected Areas in Communications, IEEE Journal on*, 30(3):575–585, April 2012.

[32] J.G. Andrews, F. Baccelli, and R.K. Ganti. A tractable approach to coverage and rate in cellular networks. *Communications, IEEE Transactions on*, 59(11):3122–3134, November 2011.

[33] Jacques Janssen and Raimondo Manca. *Applied semi-Markov processes*. Springer, 2006.

[34] Saeed S Ghassemzadeh, Rittwik Jana, Christopher W Rice, William Turin, and Vahid Tarokh. A statistical path loss model for in-home uwb channels. In *Ultra Wideband Systems and Technologies, 2002. Digest of Papers. 2002 IEEE Conference on*, pages 59–64. IEEE, 2002.

[35] David Cheung and Cliff Prettie. A path loss comparison between the 5 ghz unii band (802.11 a) and the 2.4 ghz ism band (802.11 b). *Intel Labs Report*, 2002.

[36] T. Melodia and IF. Akyildiz. Cross-layer qos-aware communication for ultra wide band wireless multimedia sensor networks. *Selected Areas in Communications, IEEE Journal on*, 28(5):653–663, June 2010.

[37] P. Chatzimisios, AC. Boucouvalas, and V. Vitsas. Ieee 802.11 packet delay-a finite retry limit analysis. In *Global Telecommunications Conference, 2003. GLOBECOM '03. IEEE*, volume 2, pages 950–954 Vol.2, Dec 2003.

[38] Z. H. Wu, Y. Han, Y. Chen, and K. J. R. Liu. A time-reversal paradigm for indoor positioning system. *IEEE Transactions on Vehicular Technology*, 64(4):1331–1339, April 2015.

[39] Marcel J.E. Golay. Complementary series. *IRE Transactions on Information Theory*, 7(2):82–87, April 1961.

[40] Zhung-Han Wu, Yi Han, Yan Chen, and K. J. Liu. A time-reversal paradigm for indoor positioning system. *IEEE Transactions on Vehicular Technology*, 64(4):1331–1339, 2015.

[41] Fanghua Weng, Changchuan Yin, and Tao Luo. Channel estimation for the downlink of 3gpp-lte systems. In *2010 2nd IEEE International Conference on Network Infrastructure and Digital Content*, pages 1042–1046, Sept 2010.

[42] B. Widrow and I. Kollár. *Quantization Noise: Roundoff Error in Digital Computation, Signal Processing, Control, and Communications*. Cambridge University Press, 2008.

[43] J.E. Gentle. *Computational Statistics*. Statistics and Computing. Springer, 2009.

[44] Jim Zyren and Wes McCoy. Overview of the 3gpp long term evolution physical layer. *Freescale Semiconductor Inc., white paper*, 2007.

[45] Yan Chen, Yu-Han Yang, Feng Han, and K. J. R. Liu. Time-reversal wideband communications. *IEEE Signal Processing Letters*, 20(12):1219–1222, Dec 2013.

[46] Hang Ma, Beibei Wang, Yan Chen, and K. J. R. Liu. Time-reversal tunneling effects for cloud radio access network. *Wireless Communications, IEEE Transactions on*, to appear.

[47] Eunchul Yoon, Sun-Yong Kim, and Unil Yun. A time-reversal-based transmission using predistortion for intersymbol interference alignment. *Communications, IEEE Transactions on*, 63(2):455–465, Feb 2015.

[48] Seok-Hwan Park, O. Simeone, O. Sahin, and S. Shamai. Joint precoding and multivariate backhaul compression for the downlink of cloud radio access networks. *Signal Processing, IEEE Transactions on*, 61(22):5646–5658, Nov 2013.

[49] Binbin Dai and Wei Yu. Sparse beamforming and user-centric clustering for downlink cloud radio access network. *Access, IEEE*, 2:1326–1339, 2014.

[50] Yuhan Zhou and Wei Yu. Optimized backhaul compression for uplink cloud radio access network. *Selected Areas in Communications, IEEE Journal on*, 32(6):1295–1307, June 2014.

[51] Yuanming Shi, Jun Zhang, and K.B. Letaief. Group sparse beamforming for green cloud-ran. *Wireless Communications, IEEE Transactions on*, 13(5):2809–2823, May 2014.

[52] Shixin Luo, Rui Zhang, and Teng Joon Lim. Downlink and uplink energy minimization through user association and beamforming in c-ran. *Wireless Communications, IEEE Transactions on*, 14(1):494–508, Jan 2015.

[53] Stephen Boyd and Lieven Vandenberghe. *Convex optimization*. Cambridge university press, 2004.

[54] Bruce Hajek. An exploration of random processes for engineers. *Department of Electrical and Computer Engineering at the University of Illinois at Urbana-Champaign, Urbana, Illinois*, 2009.

[55] Kaare Brandt Petersen, Michael Syskind Pedersen, et al. The matrix cookbook. *Technical University of Denmark*, 450:7–15, 2008.

[56] T. L. Marzetta. Noncooperative cellular wireless with unlimited numbers of base station antennas. *IEEE Transactions on Wireless Communications*, 9(11):3590–3600, November 2010.

[57] H. Q. Ngo, E. G. Larsson, and T. L. Marzetta. Energy and spectral efficiency of very large multiuser mimo systems. *IEEE Transactions on Communications*, 61(4):1436–1449, April 2013.

[58] J. Hoydis, S. ten Brink, and M. Debbah. Massive mimo in the ul/dl of cellular networks: How many antennas do we need? *IEEE Journal on Selected Areas in Communications*, 31(2):160–171, February 2013.

[59] A. L. Moustakas, S. H. Simon, and A. M. Sengupta. Mimo capacity through correlated channels in the presence of correlated interferers and noise: a (not so) large n analysis. *IEEE Transactions on Information Theory*, 49(10):2545–2561, Oct 2003.

[60] E. Larsson, O. Edfors, F. Tufvesson, and T. Marzetta. Massive mimo for next generation wireless systems. *Communications Magazine, IEEE*, 52(2):186–195, February 2014.

[61] S. Park, C. B. Chae, and S. Bahk. Before/after precoding massive mimo systems for cloud radio access networks. *Journal of Communications and Networks*, 15(4):398–406, Aug 2013.

[62] L. Liu and R. Zhang. Optimized uplink transmission in multi-antenna c-ran with spatial compression and forward. *IEEE Transactions on Signal Processing*, 63(19):5083–5095, Oct 2015.

[63] K. J. R. Liu, Ahmed K. Sadek, Weifeng Su, and Andres Kwasinski. *Cooperative Communications and Networking*. Cambridge University Press, 2009.

[64] M. Morelli. Timing and frequency synchronization for the uplink of an ofdma system. *IEEE Transactions on Communications*, 52(2):296–306, Feb 2004.

[65] Ove Edfors, Magnus Sandell, Jan-Jaap Van De Beek, Sarah Kate Wilson, and Per Ola Börjesson. Ofdm channel estimation by singular value decomposition. *Communications, IEEE Transactions on*, 46(7):931–939, 1998.

[66] K. T. Truong and R. W. Heath. The viability of distributed antennas for massive mimo systems. In *2013 Asilomar Conference on Signals, Systems and Computers*, pages 1318–1323, Nov 2013.

[67] Felipe AP de Figueiredo, Joao Paulo Miranda, Fabricio L Figueiredo, and Fabbryccio ACM Cardoso. Uplink performance evaluation of massive mu-mimo systems. *arXiv preprint arXiv:1503.02192*, 2015.

[68] Rishad Ahmed Shafik, Md Shahriar Rahman, and AHM Islam. On the extended relationships among evm, ber and snr as performance metrics. In *Electrical and Computer Engineering, 2006. ICECE'06. International Conference on*, pages 408–411. IEEE, 2006.

[69] J. Lorca and L. Cucala. Lossless compression technique for the fronthaul of lte/lte-advanced cloud-ran architectures. In *World of Wireless, Mobile and Multimedia Networks (WoWMoM), 2013 IEEE 14th International Symposium and Workshops on a*, pages 1–9, June 2013.

[70] H. Ma, B. Wang, Y. Chen, and K. J. R. Liu. Time-reversal tunneling effects for cloud radio access network. *IEEE Transactions on Wireless Communications*, PP(99):1–1, 2016.

[71] Bin Guo, Wei Cao, An Tao, and D. Samardzija. Lte/lte-a signal compression on the cpri interface. *Bell Labs Technical Journal*, 18(2):117–133, Sept 2013.